

**UCLA**

**UCLA Electronic Theses and Dissertations**

**Title**

Small Molecule Calcium Modulators Enhance Antisense-Targeted Exon Skipping on the DMD Gene

**Permalink**

<https://escholarship.org/uc/item/3qv0w03d>

**Author**

Kendall, Genevieve Claire

**Publication Date**

2013

Peer reviewed|Thesis/dissertation

UNIVERSITY OF CALIFORNIA

Los Angeles

Small Molecule Calcium Modulators Enhance Antisense-Targeted  
Exon Skipping on the *DMD* Gene

A dissertation submitted in partial satisfaction of the  
requirements for the degree of Doctor of Philosophy  
in Molecular Biology

by

Genevieve Claire Kendall

2013

@ Copyright by

Genevieve Claire Kendall

2013

## ABSTRACT OF THE DISSERTATION

### Small Molecule Calcium Modulators Enhance Antisense-Targeted Exon Skipping on the *DMD* Gene

by

Genevieve Claire Kendall

Doctor of Philosophy in Molecular Biology

University of California, Los Angeles, 2013

Professor Stanley F. Nelson, Chair

Duchenne muscular dystrophy (DMD) is a progressive muscle wasting disease caused by mutations in the X-linked *DMD* gene. These mutations result in a loss of expression of the dystrophin protein, which provides structural support to the muscle cell membrane and protects it from contraction induced damage. Without dystrophin, a cyclical process of skeletal muscle degeneration and regeneration occurs until it is ultimately replaced with adipose cells and fibrotic tissue, rendering it non-functional. The most critical dystrophin domains are the N-terminus, which binds to cytoplasmic filamentous actin and connects it to the extracellular matrix through C-terminus binding to  $\beta$ -dystroglycan, and by extension the associated dystrophin-glycoprotein complex. An allelic disease, Becker muscular dystrophy, is caused by in-frame mutations within the dispensable central domain and manifests as a less severe phenotype.

The most promising DMD therapy is antisense oligonucleotide approaches in which single exons adjacent to the mutation are targeted for pre-mRNA removal by the splicing

machinery to restore the mRNA reading frame. This has been successful in cell culture, animal models, and now has shown promise in clinical trials. However, rescued dystrophin protein levels remain variable suggesting the need for improvements in exon skipping efficiencies. We performed a high-throughput screen to identify and repurpose FDA approved drugs that potentiate this antisense exon skipping strategy. We found that one drug, dantrolene, enhanced exon skipping, rescued dystrophin protein levels, and improved overall function in a DMD mouse model. In reprogrammed patient myotubes, dantrolene, and other Ryanodine Receptor (RyR1) antagonists increased *DMD* exon 51 skipping, suggesting the RyR1 calcium channel as the relevant molecular target. An independent high-throughput screen found a cohort of small molecules with similar 2-D structures that enhanced *DMD* exon 51 skipping and shared a known protein target, calmodulin. Identified AO potentiating small molecules bind and inhibit either calcium channels (RyR1) or calcium regulatory proteins (Calmodulin) suggesting the importance of Ca<sup>2+</sup> regulation and its impact on Ca<sup>2+</sup>-binding proteins in directing exon skipping activity

Antisense-based exon skipping is highly sequence specific and benefits from the availability of diverse genetic mutations for the evaluation of potential therapies or molecular mechanisms. We have collected and derived 49 DMD patient fibroblasts and have reprogrammed a subset into muscle cells as a resource for the research community. In summary, we have established a research environment facilitating the discovery of novel therapies for the treatment of DMD, and have identified Ca<sup>2+</sup> modulation as a key regulator of antisense mediated splicing activity.

The dissertation of Genevieve Claire Kendall is approved.

Douglas L. Black

April D. Pyle

Melissa J. Spencer

M. Carrie Miceli

Stanley F. Nelson, Committee Chair

University of California, Los Angeles

2013

*Dedicated to my loving and supportive parents and family.*

## TABLE OF CONTENTS

Abstract of the Dissertation.....	ii
List of Figures.....	viii
List of Tables.....	xi
List of Acronyms.....	xii
Acknowledgements.....	xv
Curriculum Vitae.....	xvii
Chapter 1: Introduction.....	1
References.....	10
Chapter 2: Generation of iDRM Myotubes from Duchenne Muscular Dystrophy Primary Fibroblasts.....	16
Figures.....	35
References.....	59
Chapter 3: Dantrolene Enhances Antisense-Mediated Exon Skipping in Human and Mouse Models of Duchenne Muscular Dystrophy.....	63
Figures.....	66
References.....	75

Chapter 4: High-throughput Chemical Genetics Identifies Structurally Similar Small Molecules that Enhance Antisense-Targeted <i>DMD</i> Exon Skipping.....	92
Figures.....	108
References.....	132
Chapter 5: Conclusions.....	136
Figure.....	144
References.....	146

## LIST OF FIGURES

Chapter 2		
Figure 1	Strategy for primary patient fibroblast banking, immortalization, and MyoD-ER(T) reprogramming into iDRMs.	35
Figure 2	Copy number variation in a subset of mutations represented in the cDMD cell bank.	37
Figure 3	Inducible MyoD overexpression and myogenesis in DMD patient iDRMs.	39
Figure 4	Tamoxifen exposure induces nuclear MyoD expression in DMD Patient iDRMs.	41
Figure 5	iDRM patient fibroblasts reprogrammed into myotubes selectively express terminal muscle markers after MyoD induction and fusion.	43
Figure 6	iDRMs as a clinical model for antisense based exon skipping strategies.	45
Figure S1	Copy number variation in a subset of cDMD patient fibroblasts.	47
Figure S2	Evaluation of lentiviral hTERT and GFP transduction efficiency in cDMD patient fibroblasts.	49
Figure S3	Genomic insertion of hTERT mRNA coding sequence in transduced cDMD fibroblasts.	51
Figure S4	Determination of puromycin selection concentration in mock and LV-Puro-MyoD-ER(T) transduced fibroblasts.	53
Figure S5	Impact of TERT overexpression on terminal myotube fusion.	55
Chapter 3		
Figure 1	High-throughput screening identifies dantrolene as a modulator of AO-mediated DMD exon 50 skipping.	66
Figure 2	Dantrolene synergizes with AO to promote DMD exon skipping in mouse and human DMD myotubes in culture.	67
Figure 3	Dantrolene synergizes with intramuscularly injected PMOE23 to restore sarcolemmal dystrophin protein expression in mdx mice.	68
Figure 4	Dantrolene synergizes with intramuscular PMOE23 to promote Dmd exon 23 skipping in mdx mice.	69

Figure 5	Dantrolene synergizes with intravascularly delivered PMOE23 to promote exon 23 skipping and rescue sarcolemmal dystrophin and DGC in <i>mdx</i> mice.	70
Figure 6	Dantrolene and PMOE23 treatment rescue sarcolemmal dystrophin protein in multiple skeletal muscles.	71
Figure 7	Dantrolene synergizes with intravascularly delivered PMOE23 to promote <i>Dmd</i> exon 23 skipping and improve muscle strength in <i>mdx</i> mice.	72
Figure 8	Ryanodine receptor antagonists enhance AO-directed DMD exon 51 skipping in a patient cell line.	73
Fig. S1	Confirmation of enhancement of exon skipping is demonstrated in 12- or 16-point titrations on the <i>DMD</i> exon 50 reporter cell line.	80
Fig. S2	Custom CGH array confirms deletion breakpoints in GM05017 used to create iDRM5017.	81
Fig. S3	DMD patient–derived iDRM5017 temporally express muscle markers at the RNA and protein level during the fusion process.	82
Fig. S4	Dantrolene rescues dystrophin protein in the TA muscle after intramuscular injection of PMOE23.	84
Fig. S5	Dantrolene synergizes with PMOE23 to promote systemic exon 23 skipping and dystrophin protein rescue in the <i>mdx</i> mouse.	86
Fig. S6	Representative Western blots demonstrate sarcolemmal dystrophin expression in the quadriceps, TA, and diaphragm after systemic PMOE23/dantrolene injection.	88
Chapter 4		
Figure 1	Correlation of AO uptake and exon skipping activity in iDRM5017.	108
Figure 2	High-throughput screening results and Z score determination.	110
Figure 3	2-D structural clustering analysis of the Prestwick small molecule library.	112
Figure 4	Menadione as a potentiator of antisense mediated exon skipping.	114
Figure 5	Two structurally similar compounds from Cluster 394 increase antisense based exon skipping activity.	116
Figure 6	Cluster 222, a calmodulin binding partner, modulates AO targeted exon skipping.	118

Figure 7	A calcium mediated model of Cluster 222 directed exon skipping activity.	120
Figure S1	Unlabeled AO uptake and exon skipping activity in iDRM5017.	122
Figure S2	Normalization of high-throughput screening data.	124
Figure S3	Distribution of Z scores is approximately normal.	126
Chapter 5		
Figure 1	A model for calcium regulation of exon skipping activity.	144

## LIST OF TABLES

Chapter 2		
Table 1	Available cDMD primary patient fibroblasts.	57
Table 2	cDMD genetic confirmation, TERT immortalization, and LV-MyoD-ER(T) reprogramming.	58
Chapter 3		
Table S1	Top 5% of compounds from the BioMol ± h50AON high-throughput screens.	89
Table S2	Treatment groups for the local administration of PMOE23 in combination with systemic dantrolene shown in Fig. 3.	91
Table S3	Treatment groups for the systemic administration of PMOE23 in combination with systemic dantrolene shown in Figs. 5 and 6 and figs. S5 and S6.	91
Chapter 4		
Table 1	Z scores from the high-throughput screen for the ‘Compound only’ screen, ‘Compound+AO’ screen, and the analysis of the ratio of ‘Compound+AO’ compared to ‘Compound only’.	128
Table S1	Compounds and their structurally similar ligands and protein targets identified from the Protein Data Bank.	130

## LIST OF ACRONYMS

2'OMe	2-O-Methyl
6MWT	Six minute walk test
AO	Antisense oligonucleotide
ATCC	American Type Culture Collection
ATF-1	Activating transcription factor 1
BMD	Becker muscular dystrophy
Ca <sup>2+</sup>	Calcium ion
CaM	Calmodulin
CAMKII	CaM dependent protein kinase two
CAMKIV	CaM dependent protein kinase four
CaRRE	CaMK IV-responsive RNA element
CAS	Chemical abstracts service
CDMD	Center for Duchenne Muscular Dystrophy
CGH	Comparative genomic hybridization
CREB	cAMP response element-binding protein
CREM $\tau$	cAMP responsive element modulator
DGC	Dystrophin glycoprotein complex
DMD	Duchenne muscular dystrophy
DMEM	Dulbecco's modified eagle medium
DMSO	Dimethyl sulfoxide
EGR1	Early growth response protein 1
ER(T)	Estrogen receptor - tamoxifen sensitive
ESE	Exonic splicing enhancer
ETS-1	V-ets avian erythroblastosis virus E26 oncogene homolog 1

FBS	Fetal bovine serum
FDA	Food and Drug Administration
FOS	FBJ murine osteosarcoma viral oncogene homolog
GAPDH	Glyceraldehyde 3-phosphate dehydrogenase
GFP	Green fluorescent protein
HBSS	Hank's balanced salt solution
HDAC4	Histone deacetylase 4
HTS	High-throughput screen
iDRM	Inducible directly reprogrammable myotubes
IRB	Institutional review board
LGMD2A	Limb girdle muscular dystrophy type 2A
LV	Lentivirus
MAPK	Mitogen activated protein kinase
<i>Mdx</i>	X-linked muscular dystrophy mouse
MEF2	Myocyte enhancer factor-2
MEK	Map kinase kinase
MFI	Mean fluorescence intensity
MRF4	Myogenic regulatory factor 4
<i>Myf5</i>	Myogenic factor 5
MyHC	Myosin heavy chain
MyoD	Myogenic differentiation antigen
MyoG	Myogenin
ND	Not determined
nM	Nanomolar
nNOS	Neuronal nitric oxide synthase
NS	Not significant

PBS	Phosphate buffered saline
PDB	Research Collaboratory for Structural Bioinformatics Protein Data Bank
PFA	Paraformaldehyde
PGC-1 $\alpha$	Peroxisome proliferator-activated receptor gamma coactivator 1-alpha
PKC	Protein kinase c
PMO	Morpholino antisense oligonucleotide
RyR1	Ryanodine Receptor Type 1
RyR2	Ryanodine Receptor Type 2
SDF	Structure-data file
SR	Sarcoplasmic reticulum
SRF	c-fos serum response element-binding transcription factor
TERT	Telomerase reverse transcriptase
TFP	Trifluoperazine dihydrochloride
WT	Wildtype
XLDC	X-linked dilated cardiomyopathy
$\mu\text{g}$	Microgram
$\mu\text{M}$	Micromolar

## ACKNOWLEDGEMENTS

Chapter 2 is an in preparation first-author manuscript, “Generation of iDRM myotubes from Duchenne muscular dystrophy primary fibroblasts.” I would like to acknowledge my co-authors Derek Wang, Dr. Richard Wang, Dr. Hane Lee, Paul Maurizio, Ascia Eskin, Dr. Kevin Squire, **Dr. Stanley Nelson**, and **Dr. M. Carrie Miceli**. The project directors are indicated in bold.

Chapter 3 is a published co-first author article presented with permission from the co-authors and Science Translational Medicine. The project directors are indicated in bold. The cover illustration is presented with permission from Science Translational Medicine.

Kendall GC, Mokhonova EI, Moran M, Sejbuk NE, Wang DW, Silva O, Wang RT, Martinez L, Lu QL, Damoiseaux R, **Spencer MJ**, **Nelson SF**, **Miceli MC**. (2012) Dantrolene enhances antisense-mediated exon skipping in human and mouse models of Duchenne muscular dystrophy. *Sci Transl Med* 4: 164ra160. doi: 10.1126/scitranslmed.3005054.

Cover Illustration Credit: G. Kendall/UCLA; Images: M.C. Miceli, S. Nelson, E. Mokhonova, M. Spencer. “Mouse on the Wire Cover”. *Sci. Transl. Med.* 4, (12 December 2012 online issue).

Chapter 4 is an in preparation first-author manuscript, “High-throughput chemical genetics identifies structurally similar small molecules that enhance antisense-targeted *DMD* exon skipping.” I would like to acknowledge my co-authors Derek Wang, Dr. Miriana Moran, Dr. Robert Damoiseaux, **Dr. Stanley Nelson** and **Dr. M. Carrie Miceli**. The project directors are indicated in bold.

I would like to thank the many people who have made this work possible:

My advisors, Dr. Stanley Nelson and Dr. Carrie Miceli, for their support, encouragement, and intellectual guidance during my graduate training.

The other members of my committee, Dr. Douglas Black, Dr. April Pyle, and Dr. Melissa Spencer, for their time, advice, and intellectual contributions to this work.

The members of the Nelson and Miceli laboratories, past and present, for their assistance and camaraderie. In particular for the work presented here I would like to thank Derek Wang, Dr. Richard Wang, Dr. Miriana Moran, Dr. Hane Lee, Ascia Eskin, Dr. Kevin Squire, Paul Maurizio, and Natalia Sejbuk. Dr. Oscar Silva and Jillian Crocetti have been both great friends and scientists. Thanks to Michael Yourshaw for the many lunch discussions ranging from scientific ideas to science fiction novels. I would also like to thank members of Dr. Melissa Spencer's laboratory including Dr. Ekaterina Mokhonova, Leo Martinez, Diana Becerra, and Jane Wen. Instrumental to this work has been the assistance of collaborators, including Dr. Qi Lu, Dr. Jeffrey Chamberlain, Dr. Jamie Marshall, and Dr. Rachelle Crosbie-Watson, who has been an invaluable role model.

I would like to thank the many friends that supported me throughout the years including Dr. Sanjeet Baidwan, Nicole and Josh Alderson, Tom, Susana, Iara and Lais Lacher, Dr. Elinne Becket, Dr. Rob Iafe, Dr. Jose Rodriguez, Nicole Walsh, Dr. Gabriela Monsalve, Dr. John Vincent, Dr. Faith Hall-Glen, Gabe Ferguson, and Dr. Sean Sherman.

Finally, I thank my parents and family for their love and support.

## CURRICULUM VITAE

Genevieve Claire Kendall

### Education

- 2003-2007 Bachelor of Science in Cellular and Molecular Biology, Highest Honors  
Minor Fields of Study: Chemistry and English  
Texas Tech University (TTU), Lubbock TX
- 2007-2013 Doctoral Studies in Molecular Biology  
University of California, Los Angeles (UCLA), Los Angeles CA

### Honors and Awards

- 2012 Center for Duchenne Muscular Dystrophy Excellence Award, 1st place poster
- 2011 UCSF Postdoctoral Bootcamp
- 2010 Pre-doctoral Trainee Fellowship Award from the Wellstone Muscular Dystrophy Research Center Training and Education Core \*Declined
- 2010 Best Poster Presentation Award from the Ottawa Conference on New Directions in Biology and Disease of Skeletal Muscle
- 2003-2007 Howard Hughes Undergraduate Research Fellowship, Texas Tech University
- 2007 Phi Beta Kappa
- 2007 Mortar Board National College Senior Honor Society
- 2006 Rushing Scholarship, Biology Department, Texas Tech University
- 2006 Richard L. Blanton Endowed Scholarship, HHMI, Texas Tech University
- 2006 Best Poster Presentation Award from the Texas Society of Mammalogists
- 2003 Honors College Scholarship, Texas Tech University

### Teaching Experience

- Fall 2008 & Winter 2010 Teaching Assistant, Introductory Genetics, University of California, Los Angeles.

### Service

- 2012-2013 Graduate student representative for the University of California system-wide Committee on Research Policy.
- 2011-2013 Graduate student representative for the UCLA Council on Research.

### Publications: Original Research

1. **G. C. Kendall**, E. I. Mokhonova, M. Moran, N. E. Sejbuk, D. W. Wang, O. Silva, R. T. Wang, L. Martinez, Q. L. Lu, R. Damoiseaux, M. J. Spencer, S. F. Nelson, M. C. Miceli, Dantrolene Enhances Antisense-Mediated Exon Skipping in Human and Mouse Models of Duchenne Muscular Dystrophy. *Sci. Transl. Med.* 4, 164ra160 (12 December 2012).

Featured in the following article:

J.S. Chamberlain, A Genetic Intervention Stands a Skip Away from Clinical Tests. *Science*. Vol. 338 no.6113 pp. 1431-1432 (14 December 2012).

### Publications: Illustrations

1. **G. C. Kendall**. Images: M.C. Miceli, S. Nelson, E. Mokhonova, M. Spencer. "Mouse on the Wire Cover". *Sci. Transl. Med.* 4, (12 December 2012 online issue).

### **Publications: Selected Abstracts**

1. **G. C. Kendall**, E. I. Mokhonova, M. Moran, N. E. Sejbuk, D. W. Wang, O. Silva, R. T. Wang, Q. L. Lu, R. Damoiseaux, M. J. Spencer, S. F. Nelson, M. C. Miceli. (2012) Dantrolene enhances antisense-mediated exon skipping in human and mouse models of Duchenne muscular dystrophy. Annual Center for Duchenne Muscular Dystrophy at UCLA Retreat, Los Angeles, California, November 29, 2012.
2. **G. C. Kendall**, E. I. Mokhonova, M. Moran, N. E. Sejbuk, D. W. Wang, O. Silva, R. T. Wang, Q. L. Lu, R. Damoiseaux, M. J. Spencer, S. F. Nelson, M. C. Miceli. (2011) Dantrolene enhances antisense-mediated exon skipping in human and mouse models of Duchenne muscular dystrophy. Annual Center for Duchenne Muscular Dystrophy at UCLA Retreat, Los Angeles, California, September 15, 2011.
3. **G. C. Kendall**, E. Mokhonova, M. Moran, P. Maurizio, M. Spencer, S. Nelson, M. C. Miceli. (2010) High Throughput Screening for the Identification of Small Molecules that Modulate Exon Skipping on the *DMD* Gene. Annual Center for Duchenne Muscular Dystrophy at UCLA Retreat, Los Angeles, California, September 16, 2010.
4. **G. C. Kendall**, E. Mokhonova, M. Moran, P. Maurizio, M. Spencer, S. Nelson, M. C. Miceli. (2010) High Throughput Screening for the Identification of Small Molecules that Modulate Exon Skipping on the *DMD* Gene. Ottawa Conference on New Directions in Biology and Disease of Skeletal Muscle, Ottawa, Canada, May 5-8, 2010.
5. **G. C. Kendall**, E. Mokhonova, M. Moran, P. Maurizio, M. Spencer, S. Nelson, M. C. Miceli. (2009) High Throughput Screening for the Identification of Compounds that Modulate Exon Skipping on *DMD*. Annual Molecular Biology Institute Retreat, Lake Arrowhead, California, October 16-18, 2009.
6. **G. C. Kendall**, S. Hooper, H. Meeks, S. Gaschak, J. Makluk, R. J. Baker. (2006) Karyotypic and Cytochrome b Variation in *Microtus* from Ukraine. American Society of Mammalogists, Amherst, MA, June 18-21, 2006.
7. **G. C. Kendall**, S. Hooper, H. Meeks, S. Gaschak, J. Makluk, R. J. Baker. (2006) Karyotypic and Cytochrome b Variation in *Microtus* from Ukraine. Texas Society of Mammalogists, Tarleton, TX, February 17-19, 2006.

## CHAPTER ONE

### Introduction

### *1.1 Duchenne muscular dystrophy: prevalence, genetic cause, and the resulting protein defect.*

Duchenne muscular dystrophy is a progressive muscle wasting disease caused by mutations in the X-linked *DMD* gene [1,2]. It is the most common inherited muscle disease in children, with an incidence of approximately 1/4,000 affected males worldwide [3]. The fraction of observed *DMD* mutations includes deletions (65%), duplications (12%), point mutations (22%), and deep intronic variants (1-2%) [4,5]. *DMD* mutations lead to a loss of expression of its gene product, dystrophin, which directly compromises sarcolemma stability [6-8]. Resulting consequences include a cyclical degeneration and regeneration process in which muscle satellite cells are continuously replacing damaged myofibers [9,10]. Skeletal muscle and the surrounding environment is further insulted by immune cells that scavenge necrotic tissue, adipose cells replacing dystrophic muscle, and fibrosis [11-14]. This culminates in an environment in which skeletal and cardiac muscle is progressively rendered non-functional, leading to respiratory or cardiac complications, and patient death by the third decade of life [15,16].

Dystrophin itself is a critical sarcolemma protein with multiple functions, most widely recognized as a structural protein that protects the integrity of the muscle cell membrane from contraction induced damage [8]. Dystrophin protects the sarcolemma by connecting the cytoplasmic interface to the extracellular environment: the N-terminal binds to cytoplasmic filamentous actin and the C-terminal binds to the transmembrane protein,  $\beta$ -dystroglycan, and by extension associates with proteins in the dystrophin-glycoprotein complex (DGC) [17,18]. The DGC consists of multiple proteins with distinct functions that localize to the sarcolemma, such as the sarcoglycans, dystrobrevin, dystroglycans, sarcospan, the syntrophins, and nNOS. Dystrophin expression is a requirement for correct localization of these DGC proteins, and in its absence the entire complex is disassembled [19-21]. In addition to providing structural support, dystrophin acts as a molecular scaffold, by both appropriately localizing protein chaperones and likely providing an interface for their interactions [22]. For example, dystrophin is critical for

the sarcolemmal localization of neuronal nitric oxide synthase (nNOS). Loss of sarcolemma nNOS expressions leads to functional muscle ischemia and further aggravates muscle disease, highlighting the importance of an intact dystrophin and DGC in normal muscle maintenance [23-25].

Both the N and C terminal domains facilitate the structural role of dystrophin, but the central domain, consisting of 24 spectrin repeats, does not appear to be as indispensable [17,18]. An allelic disorder, Becker muscular dystrophy (BMD), is typically caused by in-frame mutations within the spectrin repeats resulting in a milder disease phenotype. In BMD, although dystrophin is internally truncated the protein is partially functional. BMD affected individuals can be asymptomatic into their seventies, which has been observed with an in-frame *DMD* exon 45-55 deletion [26-28]. Strategies for DMD therapies have focused on the knowledge gained from BMD, by identifying the most critical domains of the dystrophin protein and inferring genotype-phenotype correlations. Thus a recapitulation of the BMD genetic state in DMD therapies would result in a less severe phenotype.

### *1.2 Development of therapies for DMD.*

Since the 1960s there has been an improvement in overall survival of DMD patients. The survival rate at the age of 25 has increased from 13.5% in DMD patients born in the 1960s to 49.2% in patients born in the 1980s [29]. This improvement in overall survival is due to improved interventions. One example is the introduction of nocturnal ventilation, which shifted the mean survival age from 14.4 years in the 1960's, to 25.3 years for those who were nocturnally ventilated since 1990 [30]. As a result, diaphragm failure related deaths have significantly declined [29].

The only pharmacological therapy that is widely implemented is the use of corticosteroids, which prolong ambulation for ~3 years [31-34]. The exact mechanism whereby

corticosteroids act is unknown, but it has been proposed to have a variety of effects ranging from anti-inflammatory/immunosuppressive effects to inhibition of muscle proteolysis and stabilization of the muscle membrane [35-38]. The drawback to the use of corticosteroids is that they have a range of adverse effects; including weight gain, cataracts, short stature, acne, excessive hair growth, gastrointestinal symptoms, and behavioral changes [34]. Accordingly, the search continues for therapies that cure the disease, extend life span, or improve the quality of life. Many new and promising therapies are under development for the treatment of DMD, including utrophin upregulation [39-41], viral micro-dystrophin gene delivery [42,43], stop codon read-through [44], stem cell replacement therapies [45], and exon skipping strategies [46-49], the latter of which will be discussed in detail in the next section.

### *1.3 Antisense oligonucleotide targeted exon skipping as a therapy for DMD.*

Antisense oligonucleotides (AOs) are nucleic acid analogs that are used in both laboratory and clinical settings mainly for gene-knockdown or splice-switching applications. Modified AO chemistries are necessary to avoid the body's natural defense mechanisms that degrade aberrant or foreign DNAs and RNAs. AO targeted exon skipping therapies for DMD use either 2-O-methyl (2'OMe) or morpholino (PMO) chemistries. Modifications for 2'OMe AOs include an additional methyl group on the second carbon of the ribose ring as well as phosphorothioate bonds. PMO AOs have a morpholine ring and an uncharged phosphorodiamidate linkage that may be responsible for the relative lack of observed toxicity in dose ranging clinical trials [50]. AOs induce exon skipping by uniquely binding 20-30 nucleotides typically located within splice acceptor, splice donor, or exonic splicing enhancer sites. Discrete binding of these complementary pre-mRNA sequences targets exons for removal during the splicing process and their exclusion from mature mRNA.

The strategy for using AOs as a potential treatment for DMD was suggested by the less severe allelic disorder, BMD. By skipping single exons adjacent to the mutation, AOs could

potentially revert out-of-frame *DMD* mutations into in-frame *DMD* mRNAs that result in translation of an internally truncated dystrophin protein. This protein is still partially functional and would be expected to result in a less severe phenotype. AOs efficiently induce exon skipping in a variety of mouse and human cell culture systems [51,52], in *DMD* mouse and dog models [53,54], in the humanized *DMD/mdx* mouse [55], and in clinical trials [46,47]. To date, the focus has been on single exon skipping, as this has proven the most feasible in pre-clinical validation. Candidate exons for the development of skipping therapies have been prioritized based on the number of patients that could be treated and include exons 51, 45, 53, 44, 52, and 50 [56].

Skipping of *DMD* exon 51 addresses the highest proportion of patients at ~13% [56]. Two companies have completed proof of concept studies with AOs targeting *DMD* exon 51 and are in the midst of Phase IIb or Phase III clinical trials, so far with promising results [46,47]. Prosensa Therapeutics and Glaxo Smith Kline have partnered to develop Drisapersen/Pro051, a 20mer 2'OMe AO that is directed against an exonic splicing enhancer (ESE) sequence in *DMD* exon 51. After local injection into the tibialis anterior muscle in four *DMD* patients, Drisapersen both enhanced *DMD* exon 51 skipping and rescued dystrophin protein expression to 3-12% of normal levels [49]. Following this success, dose ranging Phase I/II clinical trials were performed with 0.5-6mg/kg weekly doses, and after five weeks there was an increase in exon skipping and dystrophin protein levels, and 12 week extension data demonstrated functional improvement on the 6 minute walk test (6MWT) [47]. Sarepta Inc. has pursued a morpholino chemistry AO for the treatment of *DMD*. Specifically, their Eteplirsen/AVI-4658 AO targeting *DMD* exon 51 has an overlapping sequence with Drisapersen, but is a slightly longer 30mer. Eteplirsen has also shown promising pre-clinical results and tolerability in mice, and exon skipping and dystrophin protein rescue in a proof-of-concept and Phase I/II dose escalation studies in humans [46,48,57]. In Phase IIb long-term safety and efficacy studies involving 48 weekly 30 or 50

mg/kg treatments there was an increase in the amount of dystrophin protein with approximately 47% of positive muscle fibers. In April 2013 following 74 weeks of treatment Eteplirsen treated patients exhibited disease stabilization in the 6MWT, and overall had less than a 5% walking distance decline from baseline [58].

Limitations of antisense based therapies include variability in exon skipping efficiencies within the same muscle, across muscle types, and between patients and types of deletions [46,47,53]. For example, the heart has proven difficult to target, and results from *mdx* mice indicate current AO strategies likely will not produce functionally protective levels of dystrophin in the heart [53]. Also, exon 51 skipping is tailored to treat only a fraction of patients. Therefore, additional AOs are being evaluated that target *DMD* exons. The most widely applicable exon skipping strategy for DMD patients consists of a multi-exon skip between exons 45-55, which would treat 63% of all DMD patients [59]. In cell culture and in mouse models this multi-exon skip has proven feasible yet inefficient indicating that both single and multi-exon skip strategies would benefit from synergistic and independent molecular targets [60,61].

#### *1.4 Strategy for high-throughput screening and the re-purposing of off-label drugs for DMD.*

Our strategy was to identify small molecules that increase antisense-targeted exon skipping activity by focusing on high-throughput screening (HTS) of FDA approved drugs. The idea of re-purposing FDA approved drugs was attractive because of faster development times and reduced risks. FDA approved drugs have known toxicity profiles, and therefore can be moved into clinic more quickly than novel drugs, for which the current FDA approval process would take over 13 years [62]. The advantage of using high-throughput screening is its ability to identify compounds with significant biological activity, even in the absence of prior knowledge of the mechanism of action or the nature of the target [63,64].

Previous work and observations have suggested that approximately 20-30% of normal dystrophin levels are required to ameliorate the DMD phenotype [26,65,66]. These protein levels are likely not being achieved across all patients and muscles using the aforementioned antisense strategies that are in clinical trials, underscoring the need for molecular targets that can potentiate antisense based exon skipping activity. Thus, we screened the BioMol and FDA small molecule libraries in order to identify compounds that potentiated the exon skipping activity of an AO targeting human *DMD* exon 50. From the BioMol library we identified an FDA approved drug, dantrolene, that only enhanced exon skipping in the context of antisense treatment. Dantrolene is currently FDA approved for the treatment of malignant hyperthermia and muscle spasticity, and its mechanism of action includes binding the Ryanodine Receptor (RyR1), and inhibiting the release of calcium into the cytoplasm. After further testing we found that dantrolene increased exon skipping in both mouse and human cell culture models. A DMD mouse model, the *mdx* mouse, has a nonsense mutation in *Dmd* exon 23 and its mRNA reading frame can be rescued by skipping *Dmd* exon 23 [67]. We tested a combination therapy in the *mdx* mouse with weekly doses of antisense oligonucleotide and chronic dantrolene administration. Following this combined administration there was a significant increase in *Dmd* exon 23 skipping and dystrophin protein rescue in multiple skeletal muscles including the quadriceps, tibialis anterior, gastrocnemius, and diaphragm. This translated into a functional benefit as mice that were treated with the combination therapy had improved overall muscle strength, suggesting a potential repurposing success story with further development currently underway [51].

In a subsequent and independent screen of the FDA small molecule library we identified additional drugs that increased exon skipping activity only in the presence of antisense oligonucleotide. We performed a 2-D structural analysis of these compounds to identify active structures, and by extension, potential shared molecular targets [68]. Several structurally similar groups potentiated *DMD* exon 51 skipping in DMD patient cells, all with known, shared

molecular targets. Two structurally similar compounds with the highest exon skipping activity in a patient cell line both share a molecular target of calmodulin (CaM) binding and inhibition [69,70]. Active drugs from both screens, including dantrolene, ryanodine, S107, fluphenazine and trifluoperazine all bind and inhibit either calcium channels (RyR1) or calcium regulatory proteins (CaM) suggesting the importance of Ca<sup>2+</sup> regulation and its impact on Ca<sup>2+</sup>-binding proteins as a common theme in directing exon skipping activity [69-75].

### *1.5 Primary DMD patient cell models as tools to validate potential therapies and to better understand molecular pathogenesis.*

It is of particular importance to be able to test drugs in a model system that recapitulates the studied disease or phenotype. There are numerous mouse models for DMD that serve their purpose for *in vivo* efficacy and bio-distribution and toxicity of human AOs, but none of these models have the exact *DMD* human mutations. Also, the use of mouse models as a surrogate for all assays is problematic because antisense exon skipping methods are inherently sequence specific, necessitating the use of either humanized mice or human cell models. Therefore, we developed a patient cell bank that currently houses 49 dermal fibroblasts derived from DMD patient or unaffected and related individuals for use in the study of muscular dystrophies. This cell bank contains a variety of validated *DMD* deletions, insertions, and point mutations that can be used to evaluate exon skipping strategies or other therapies or hypotheses.

We have developed a standard operating procedure to expand, bank, detail the genomic mutation, and immortalize these fibroblasts for future use. Primary patient fibroblasts require reprogramming into a muscle cell lineage to study a muscle related disease. To address this we overexpressed an inducible muscle specific transcription factor, MyoD, and successfully optimized the reprogramming and fusion process to transform fibroblasts into multi-nucleated myotubes that express muscle specific genes and proteins in a temporally dependent manner [51,76-78]. These cells are termed inducible directly reprogrammable myotubes (iDRMs).

iDRMs, and their adaptation for *DMD* exon skipping assays, have played a crucial role in validating compounds identified from high-throughput screening in a *DMD* patient mutation specific context. This primary patient cell bank represents one of the largest single collections of *DMD* cells. We have made refinements to their immortalization, reprogramming, and fusion so that iDRMs are a reliable model used for study by UCLA researchers as well as nationally and internationally.

### 1.6 Overview of the chapters.

Chapter 2 of this thesis describes the generation of a *DMD* patient cell bank; including the detailed characterization of the genomic *DMD* mutation and the sequential process to bank patient fibroblasts. In addition, I describe improvements to the reprogramming protocol so that the 49 collected fibroblasts and iDRMs are more amenable to long-term use in cell culture. Chapter 3 focuses on the identification of an FDA approved drug, dantrolene, that enhances the activity of antisense-targeted exon skipping in both mouse and human *DMD* models and facilitates functional improvement in the *mdx* mouse model over a sustained treatment period. iDRMs and the reprogramming and fusion process described in Chapter 2 were used to validate dantrolene exon skipping activity in the context of a human *DMD* mutation. In addition, iDRMs were critical to the identification of exon skipping activity of other RyR1 antagonists, thus implicating RyR1 as the molecular target responsible for the observed effect. Chapter 4 discusses an independent high-throughput screen in which structurally similar small molecules increased antisense targeted *DMD* exon skipping activity. This chapter includes improvements to high-throughput screening analysis and structural comparison of small molecules within the FDA library, and identifies a structurally similar cluster that inhibits calmodulin activity and increases exon 51 skipping in iDRMs. Chapter 5 discusses the impact of the identification of small molecule potentiators of exon skipping, as well as the common theme of Ca<sup>2+</sup> regulation and its effects on Ca<sup>2+</sup>-binding proteins in directing exon skipping activity.

## References

1. Monaco AP, Bertelson CJ, Middlesworth W, Colletti CA, Aldridge J, et al. (1985) Detection of deletions spanning the Duchenne muscular dystrophy locus using a tightly linked DNA segment. *Nature* 316: 842-845.
2. Emery AE (2002) The muscular dystrophies. *Lancet* 359: 687-695.
3. Mendell JR, Shilling C, Leslie ND, Flanigan KM, al-Dahhak R, et al. (2012) Evidence-based path to newborn screening for Duchenne muscular dystrophy. *Ann Neurol* 71: 304-313.
4. Muntoni F, Torelli S, Ferlini A (2003) Dystrophin and mutations: one gene, several proteins, multiple phenotypes. *Lancet Neurol* 2: 731-740.
5. Abbs S, Tuffery-Giraud S, Bakker E, Ferlini A, Sejersen T, et al. (2010) Best practice guidelines on molecular diagnostics in Duchenne/Becker muscular dystrophies. *Neuromuscul Disord* 20: 422-427.
6. Hoffman EP, Brown RH, Jr., Kunkel LM (1987) Dystrophin: the protein product of the Duchenne muscular dystrophy locus. *Cell* 51: 919-928.
7. Bonilla E, Samitt CE, Miranda AF, Hays AP, Salviati G, et al. (1988) Duchenne muscular dystrophy: deficiency of dystrophin at the muscle cell surface. *Cell* 54: 447-452.
8. Petrof BJ, Shrager JB, Stedman HH, Kelly AM, Sweeney HL (1993) Dystrophin protects the sarcolemma from stresses developed during muscle contraction. *Proc Natl Acad Sci U S A* 90: 3710-3714.
9. Charge SB, Rudnicki MA (2004) Cellular and molecular regulation of muscle regeneration. *Physiol Rev* 84: 209-238.
10. Jejurikar SS, Kuzon WM, Jr. (2003) Satellite cell depletion in degenerative skeletal muscle. *Apoptosis* 8: 573-578.
11. Vetrone SA, Montecino-Rodriguez E, Kudryashova E, Kramerova I, Hoffman EP, et al. (2009) Osteopontin promotes fibrosis in dystrophic mouse muscle by modulating immune cell subsets and intramuscular TGF-beta. *J Clin Invest* 119: 1583-1594.
12. Spencer MJ, Tidball JG (2001) Do immune cells promote the pathology of dystrophin-deficient myopathies? *Neuromuscul Disord* 11: 556-564.
13. Leroy-Willig A, Willig TN, Henry-Feugeas MC, Frouin V, Marinier E, et al. (1997) Body composition determined with MR in patients with Duchenne muscular dystrophy, spinal muscular atrophy, and normal subjects. *Magn Reson Imaging* 15: 737-744.
14. Klingler W, Jurkat-Rott K, Lehmann-Horn F, Schleip R (2012) The role of fibrosis in Duchenne muscular dystrophy. *Acta Myol* 31: 184-195.
15. Kohler M, Clarenbach CF, Bahler C, Brack T, Russi EW, et al. (2009) Disability and survival in Duchenne muscular dystrophy. *J Neurol Neurosurg Psychiatry* 80: 320-325.

16. Ishikawa Y, Miura T, Ishikawa Y, Aoyagi T, Ogata H, et al. (2011) Duchenne muscular dystrophy: survival by cardio-respiratory interventions. *Neuromuscul Disord* 21: 47-51.
17. Rybakova IN, Patel JR, Ervasti JM (2000) The dystrophin complex forms a mechanically strong link between the sarcolemma and costameric actin. *J Cell Biol* 150: 1209-1214.
18. Ibraghimov-Beskrovnaya O, Ervasti JM, Leveille CJ, Slaughter CA, Sernett SW, et al. (1992) Primary structure of dystrophin-associated glycoproteins linking dystrophin to the extracellular matrix. *Nature* 355: 696-702.
19. Crosbie RH, Heighway J, Venzke DP, Lee JC, Campbell KP (1997) Sarcospan, the 25-kDa transmembrane component of the dystrophin-glycoprotein complex. *J Biol Chem* 272: 31221-31224.
20. Ervasti JM, Ohlendieck K, Kahl SD, Gaver MG, Campbell KP (1990) Deficiency of a glycoprotein component of the dystrophin complex in dystrophic muscle. *Nature* 345: 315-319.
21. Yoshida M, Ozawa E (1990) Glycoprotein complex anchoring dystrophin to sarcolemma. *J Biochem* 108: 748-752.
22. Brenman JE, Chao DS, Gee SH, McGee AW, Craven SE, et al. (1996) Interaction of nitric oxide synthase with the postsynaptic density protein PSD-95 and alpha1-syntrophin mediated by PDZ domains. *Cell* 84: 757-767.
23. Brenman JE, Chao DS, Xia H, Aldape K, Brecht DS (1995) Nitric oxide synthase complexed with dystrophin and absent from skeletal muscle sarcolemma in Duchenne muscular dystrophy. *Cell* 82: 743-752.
24. Lai Y, Thomas GD, Yue Y, Yang HT, Li D, et al. (2009) Dystrophins carrying spectrin-like repeats 16 and 17 anchor nNOS to the sarcolemma and enhance exercise performance in a mouse model of muscular dystrophy. *J Clin Invest* 119: 624-635.
25. Sander M, Chavoshan B, Harris SA, Iannaccone ST, Stull JT, et al. (2000) Functional muscle ischemia in neuronal nitric oxide synthase-deficient skeletal muscle of children with Duchenne muscular dystrophy. *Proc Natl Acad Sci U S A* 97: 13818-13823.
26. Anthony K, Cirak S, Torelli S, Tasca G, Feng L, et al. (2011) Dystrophin quantification and clinical correlations in Becker muscular dystrophy: implications for clinical trials. *Brain* 134: 3547-3559.
27. Helderma-van den Enden AT, Straathof CS, Aartsma-Rus A, den Dunnen JT, Verbist BM, et al. (2010) Becker muscular dystrophy patients with deletions around exon 51; a promising outlook for exon skipping therapy in Duchenne patients. *Neuromuscul Disord* 20: 251-254.
28. Ferreira V, Giliberto F, Muniz GM, Francipane L, Marzese DM, et al. (2009) Asymptomatic Becker muscular dystrophy in a family with a multiexon deletion. *Muscle Nerve* 39: 239-243.

29. Passamano L, Taglia A, Palladino A, Viggiano E, D'Ambrosio P, et al. (2012) Improvement of survival in Duchenne Muscular Dystrophy: retrospective analysis of 835 patients. *Acta Myol* 31: 121-125.
30. Eagle M, Baudouin SV, Chandler C, Giddings DR, Bullock R, et al. (2002) Survival in Duchenne muscular dystrophy: improvements in life expectancy since 1967 and the impact of home nocturnal ventilation. *Neuromuscul Disord* 12: 926-929.
31. Biggar WD, Harris VA, Eliasoph L, Alman B (2006) Long-term benefits of deflazacort treatment for boys with Duchenne muscular dystrophy in their second decade. *Neuromuscul Disord* 16: 249-255.
32. Fenichel GM, Florence JM, Pestronk A, Mendell JR, Moxley RT, 3rd, et al. (1991) Long-term benefit from prednisone therapy in Duchenne muscular dystrophy. *Neurology* 41: 1874-1877.
33. Mendell JR, Moxley RT, Griggs RC, Brooke MH, Fenichel GM, et al. (1989) Randomized, double-blind six-month trial of prednisone in Duchenne's muscular dystrophy. *N Engl J Med* 320: 1592-1597.
34. Balaban B, Matthews DJ, Clayton GH, Carry T (2005) Corticosteroid treatment and functional improvement in Duchenne muscular dystrophy: long-term effect. *Am J Phys Med Rehabil* 84: 843-850.
35. Elia M, Carter A, Bacon S, Winearls CG, Smith R (1981) Clinical usefulness of urinary 3-methylhistidine excretion in indicating muscle protein breakdown. *Br Med J (Clin Res Ed)* 282: 351-354.
36. Jacobs SC, Bootsma AL, Willems PW, Bar PR, Wokke JH (1996) Prednisone can protect against exercise-induced muscle damage. *J Neurol* 243: 410-416.
37. Kissel JT, Burrow KL, Rammohan KW, Mendell JR (1991) Mononuclear cell analysis of muscle biopsies in prednisone-treated and untreated Duchenne muscular dystrophy. CIDD Study Group. *Neurology* 41: 667-672.
38. Rifai Z, Welle S, Moxley RT, 3rd, Lorenson M, Griggs RC (1995) Effect of prednisone on protein metabolism in Duchenne dystrophy. *Am J Physiol* 268: E67-74.
39. Perkins KJ, Burton EA, Davies KE (2001) The role of basal and myogenic factors in the transcriptional activation of utrophin promoter A: implications for therapeutic up-regulation in Duchenne muscular dystrophy. *Nucleic Acids Res* 29: 4843-4850.
40. Tinsley J, Deconinck N, Fisher R, Kahn D, Phelps S, et al. (1998) Expression of full-length utrophin prevents muscular dystrophy in mdx mice. *Nat Med* 4: 1441-1444.
41. Tinsley JM, Fairclough RJ, Storer R, Wilkes FJ, Potter AC, et al. (2011) Daily treatment with SMTc1100, a novel small molecule utrophin upregulator, dramatically reduces the dystrophic symptoms in the mdx mouse. *PLoS One* 6: e19189.

42. Bowles DE, McPhee SW, Li C, Gray SJ, Samulski JJ, et al. (2012) Phase 1 gene therapy for Duchenne muscular dystrophy using a translational optimized AAV vector. *Mol Ther* 20: 443-455.
43. Mendell JR, Campbell K, Rodino-Klapac L, Sahenk Z, Shilling C, et al. (2010) Dystrophin immunity in Duchenne's muscular dystrophy. *N Engl J Med* 363: 1429-1437.
44. Welch EM, Barton ER, Zhuo J, Tomizawa Y, Friesen WJ, et al. (2007) PTC124 targets genetic disorders caused by nonsense mutations. *Nature* 447: 87-91.
45. Price FD, Kuroda K, Rudnicki MA (2007) Stem cell based therapies to treat muscular dystrophy. *Biochim Biophys Acta* 1772: 272-283.
46. Cirak S, Arechavala-Gomez V, Guglieri M, Feng L, Torelli S, et al. (2011) Exon skipping and dystrophin restoration in patients with Duchenne muscular dystrophy after systemic phosphorodiamidate morpholino oligomer treatment: an open-label, phase 2, dose-escalation study. *Lancet* 378: 595-605.
47. Goemans NM, Tulinius M, van den Akker JT, Burm BE, Ekhart PF, et al. (2011) Systemic administration of PRO051 in Duchenne's muscular dystrophy. *N Engl J Med* 364: 1513-1522.
48. Kinali M, Arechavala-Gomez V, Feng L, Cirak S, Hunt D, et al. (2009) Local restoration of dystrophin expression with the morpholino oligomer AVI-4658 in Duchenne muscular dystrophy: a single-blind, placebo-controlled, dose-escalation, proof-of-concept study. *Lancet Neurol* 8: 918-928.
49. van Deutekom JC, Janson AA, Ginjaar IB, Frankhuizen WS, Aartsma-Rus A, et al. (2007) Local dystrophin restoration with antisense oligonucleotide PRO051. *N Engl J Med* 357: 2677-2686.
50. Summerton J, Weller D (1997) Morpholino antisense oligomers: design, preparation, and properties. *Antisense Nucleic Acid Drug Dev* 7: 187-195.
51. Kendall GC, Mokhonova EI, Moran M, Sejbuk NE, Wang DW, et al. (2012) Dantrolene enhances antisense-mediated exon skipping in human and mouse models of Duchenne muscular dystrophy. *Sci Transl Med* 4: 164ra160.
52. Aartsma-Rus A, Janson AA, Kaman WE, Bremmer-Bout M, den Dunnen JT, et al. (2003) Therapeutic antisense-induced exon skipping in cultured muscle cells from six different DMD patients. *Hum Mol Genet* 12: 907-914.
53. Alter J, Lou F, Rabinowitz A, Yin H, Rosenfeld J, et al. (2006) Systemic delivery of morpholino oligonucleotide restores dystrophin expression bodywide and improves dystrophic pathology. *Nat Med* 12: 175-177.
54. Yokota T, Lu QL, Partridge T, Kobayashi M, Nakamura A, et al. (2009) Efficacy of systemic morpholino exon-skipping in Duchenne dystrophy dogs. *Ann Neurol* 65: 667-676.

55. Wu B, Benrashid E, Lu P, Cloer C, Zillmer A, et al. (2011) Targeted skipping of human dystrophin exons in transgenic mouse model systemically for antisense drug development. *PLoS One* 6: e19906.
56. Aartsma-Rus A, Fokkema I, Verschuuren J, Ginjaar I, van Deutekom J, et al. (2009) Theoretic applicability of antisense-mediated exon skipping for Duchenne muscular dystrophy mutations. *Hum Mutat* 30: 293-299.
57. Sazani P, Weller DL, Shrewsbury SB (2010) Safety pharmacology and genotoxicity evaluation of AVI-4658. *Int J Toxicol* 29: 143-156.
58. Mendell JR (2013) Results at 74 Weeks of a Phase IIb Extension Study of the Exon-Skipping Drug Eteplirsen in Patients with Duchenne Muscular Dystrophy (DMD). *Muscular Dystrophy Association Scientific Conference*. Washington DC.
59. Beroud C, Tuffery-Giraud S, Matsuo M, Hamroun D, Humbertclaude V, et al. (2007) Multiexon skipping leading to an artificial DMD protein lacking amino acids from exons 45 through 55 could rescue up to 63% of patients with Duchenne muscular dystrophy. *Hum Mutat* 28: 196-202.
60. Aoki Y, Yokota T, Nagata T, Nakamura A, Tanihata J, et al. (2012) Bodywide skipping of exons 45-55 in dystrophic mdx52 mice by systemic antisense delivery. *Proc Natl Acad Sci U S A* 109: 13763-13768.
61. van Vliet L, de Winter CL, van Deutekom JC, van Ommen GJ, Aartsma-Rus A (2008) Assessment of the feasibility of exon 45-55 multiexon skipping for Duchenne muscular dystrophy. *BMC Med Genet* 9: 105.
62. Paul SM, Mytelka DS, Dunwiddie CT, Persinger CC, Munos BH, et al. (2010) How to improve R&D productivity: the pharmaceutical industry's grand challenge. *Nat Rev Drug Discov* 9: 203-214.
63. Lemm JA, O'Boyle D, 2nd, Liu M, Nower PT, Colonna R, et al. (2010) Identification of hepatitis C virus NS5A inhibitors. *J Virol* 84: 482-491.
64. Cordek DG, Bechtel JT, Maynard AT, Kazmierski WM, Cameron CE (2011) Targeting the Ns5a Protein of Hcv: An Emerging Option. *Drugs Future* 36: 691-711.
65. Neri M, Torelli S, Brown S, Ugo I, Sabatelli P, et al. (2007) Dystrophin levels as low as 30% are sufficient to avoid muscular dystrophy in the human. *Neuromuscul Disord* 17: 913-918.
66. Phelps SF, Hauser MA, Cole NM, Rafael JA, Hinkle RT, et al. (1995) Expression of full-length and truncated dystrophin mini-genes in transgenic mdx mice. *Hum Mol Genet* 4: 1251-1258.
67. Sicinski P, Geng Y, Ryder-Cook AS, Barnard EA, Darlison MG, et al. (1989) The molecular basis of muscular dystrophy in the mdx mouse: a point mutation. *Science* 244: 1578-1580.

68. Johnson M, Maggioria G (1990) *Concepts and Applications of Molecular Similarity*. New York: John Wiley & Sons.
69. Cook WJ, Walter LJ, Walter MR (1994) Drug binding by calmodulin: crystal structure of a calmodulin-trifluoperazine complex. *Biochemistry* 33: 15259-15265.
70. Vandonselaar M, Hickie RA, Quail JW, Delbaere LT (1994) Trifluoperazine-induced conformational change in Ca(2+)-calmodulin. *Nat Struct Biol* 1: 795-801.
71. Andersson DC, Marks AR (2010) Fixing ryanodine receptor Ca leak - a novel therapeutic strategy for contractile failure in heart and skeletal muscle. *Drug Discov Today Dis Mech* 7: e151-e157.
72. Fill M, Copello JA (2002) Ryanodine receptor calcium release channels. *Physiol Rev* 82: 893-922.
73. Kobayashi S, Bannister ML, Gangopadhyay JP, Hamada T, Parness J, et al. (2005) Dantrolene stabilizes domain interactions within the ryanodine receptor. *J Biol Chem* 280: 6580-6587.
74. Rousseau E, Smith JS, Meissner G (1987) Ryanodine modifies conductance and gating behavior of single Ca<sup>2+</sup> release channel. *Am J Physiol* 253: C364-368.
75. Bellinger AM, Reiken S, Carlson C, Mongillo M, Liu X, et al. (2009) Hypernitrosylated ryanodine receptor calcium release channels are leaky in dystrophic muscle. *Nat Med* 15: 325-330.
76. Kimura E, Han JJ, Li S, Fall B, Ra J, et al. (2008) Cell-lineage regulated myogenesis for dystrophin replacement: a novel therapeutic approach for treatment of muscular dystrophy. *Hum Mol Genet* 17: 2507-2517.
77. Davis RL, Weintraub H, Lassar AB (1987) Expression of a single transfected cDNA converts fibroblasts to myoblasts. *Cell* 51: 987-1000.
78. Lassar AB, Paterson BM, Weintraub H (1986) Transfection of a DNA locus that mediates the conversion of 10T1/2 fibroblasts to myoblasts. *Cell* 47: 649-656.

## CHAPTER TWO

### Generation of iDRM Myotubes from Duchenne Muscular Dystrophy Primary Fibroblasts

## *Abstract*

We derived 49 dermal fibroblasts from muscular dystrophy patients and generated a subset of matching inducible directly reprogrammable myotubes (iDRMs) by overexpressing the muscle transcription factor, MyoD. We isolated dermal fibroblasts from Duchenne or Becker muscular dystrophy patient skin biopsies with diverse genetically confirmed causative mutations including deletions, insertions, and point substitutions in the *DMD* gene. For long-term use in cell culture, we first immortalized patient fibroblasts, and then stably reprogrammed them into iDRMs by inducing MyoD overexpression and fusion into multinucleated myotubes expressing muscle specific markers. We characterize the temporal expression of muscle specific genes and proteins during iDRM myogenesis, and describe the use of iDRMs in antisense-targeted *DMD* exon skipping strategies. Banked cells are available upon request to the research community. In some cases fibroblasts from unaffected maternal or paternal family members are available.

## *Introduction*

Duchenne muscular dystrophy (DMD) is a progressive muscle wasting disease caused by mutations in the X-linked *DMD* gene [1,2], which encodes the dystrophin protein. *DMD* mutations result in a loss of expression of dystrophin and its associated glycoprotein complex (DGC). Together, these components provide structural integrity to the sarcolemma, and when absent, expose the sarcolemma to contraction-induced damage [3-5]. Although *DMD* was one of the first human disease genes to be positionally cloned 27 years ago, glucocorticoid treatment is the only standard pharmacological intervention well demonstrated to slow disease progression and prolong ambulation [6,7]. Patients typically die in their third decade of life due to respiratory or cardiac complications [7,8], underscoring the need for effective therapies.

Emerging therapies aim to directly target the underlying genetic abnormality or ameliorate secondary pathologic processes in DMD. These include, but are not limited to, a

compensatory upregulation of utrophin [9-11], antisense based exon-skipping strategies [12-15], premature stop codon read through [16], viral mini-dystrophin gene expression [17,18], or stem cell replacement therapies [19]. However, there are insufficient DMD patient primary cell resources available for study [20,21]. The availability of diverse mutation sub-types is especially critical for the development and testing of personalized therapies, such as antisense based exon skipping strategies or stop codon read-through.

Our reprogramming strategy includes the overexpression of *TERT*, an approach we have used in 17 primary fibroblasts to extend their replicative capacity in culture [22-25]. Another inherent limitation of primary fibroblasts is that this cell lineage does not directly recapitulate the muscle cell phenotype. Previous work has shown that fibroblasts can be directly reprogrammed into the muscle lineage through the overexpression of myogenic differentiation antigen (MyoD), a strategy we have applied in 9 immortalized fibroblasts [26-28]. MyoD is the founding member of the muscle regulatory factor (MRF) transcription factor family, also including Myf5, MyoG, and MRF4, which are critical for muscle cell commitment or terminal differentiation [29]. MyoD and/or Myf5 are expressed early in muscle cell commitment and determination, whereas MyoG and MRF4 are necessary for terminal fusion into multinucleated myotubes [30-34].

Since its discovery in 1986, and subsequent identification of MyoD muscle reprogramming properties, focus has turned to improved MyoD conversion of fibroblasts into myotubes as a strategy to study muscle disease and potential therapies [27,28]. For instance, antisense based clinical trials screen DMD patients for aberrant splicing events in fibroblasts reprogrammed by constitutive adenoviral MyoD overexpression [12-15]. In this case, fibroblasts irreversibly withdraw from the cell cycle [35], inspiring the creation of alternative vectors in which MyoD can be selectively activated to convert mouse or human fibroblasts into myotubes [36,37]. Recently, a MyoD fusion protein was described in which a portion of the tamoxifen-

sensitive mutated estrogen receptor is inserted within the *Myod1* coding sequence. Functionally, the MyoD-ER(T) fusion protein is only active after tamoxifen addition, and subsequent dimerization and translocation into the nucleus. This MyoD-ER(T) vector has been previously described for the reprogramming of mouse fibroblasts into muscle myotubes, and was further characterized for its potential in viral based dystrophin genetic correction, and subsequent cell replacement therapies in a DMD mouse model [37]. We expand on these methods by creating a chemically selectable MyoD-ER(T) vector that allows for the enrichment of transduced cells, and improvements in fusion and stability in culture.

Ultimately, a cell repository with control and patient samples containing multiple *DMD* mutations is a powerful resource to study the molecular mechanisms underlying the DMD disease phenotype as well as the efficacy of potential therapies. We present a comprehensive cell resource that includes 49 available primary fibroblasts, and standard operating procedures for their collection, isolation, *DMD* mutation confirmation or identification, immortalization, and subsequent reprogramming into muscle myotubes (Fig. 1). We have further refined the fibroblast reprogramming protocol by creating and validating an improved selectable MyoD-ER(T) vector. In addition, we detail a fusion protocol including a defined media, timing, and expected morphological changes for the conversion of iDRMs into terminally differentiated myotubes. Finally, we address the applicability of using iDRMs to characterize antisense-targeted *DMD* exon skipping activity.

## *Materials and Methods*

### Collection, isolation, and propagation of dermal fibroblasts

Skin punches were obtained under IRB approved protocol (#11-001087) with informed patient consent, by coring a 3mm diameter small piece of skin from the arm. The entire skin punch was placed in sterile Dulbecco's modified Eagle's medium (DMEM; phenol red free, Invitrogen) + 1%

penicillin/streptomycin (Invitrogen) and either shipped overnight to UCLA on icepacks, or processed immediately. No difference was observed between overnight shipping or immediate processing with regard to fibroblast isolation and viability. Isolation of dermal fibroblasts follows Karumbayaram *et al* 2012 with a few modifications [38]. Briefly, biopsies were rinsed twice in 5mL of Hank's Balanced Salt Solution (HBSS; phenol red free, Invitrogen), and then directly transferred into an uncoated 6 well plate (Corning). Biopsies were minced into 1-mm pieces with sterile scalpels in the presence of 3mL of a 2% animal-origin-free collagenase (Worthington) in HBSS solution. After a 90min incubation at 37°C, 5mL of fibroblast growth media (DMEM (+phenol red, high glucose) + 15% Fetal Bovine Serum (FBS) + 1% Non-essential amino acids + 1% pen/strep) was added, and tissue pelleted for 5min at 300g. Tissue pellets were washed in fibroblast growth media followed by a 5min centrifugation at 300g. This step was repeated twice. Finally, the tissue pellet was plated in 3mL of fibroblast growth media on one well of a 0.1% porcine gelatin coated 6-well plate (Corning; plates coated in 0.1% porcine (Sigma) overnight at 37°C). Fibroblast growth media was changed every 3 days, until 2-3 weeks after which fibroblasts were typically sub-confluent and transferred for expansion into a T175 flask (Corning). After 3-4 days cells were transferred into 4 T225 flasks (Corning) for further expansion so that cells could be frozen at 1 million cells per vial in 1mL of freezing media (FBS + 10% Dimethyl sulfoxide), in addition to a cell pellet being obtained for DNA isolation and mutation validation by custom CGH array (Agilent).

Each CDMD skin punch is assigned a unique 4 digit identifier, beginning with CDMD1001, and subsequently increasing. In the cell naming nomenclature 'H' represents the passage of *TERT* immortalization, 'M' represents the passage of LV-MyoD-ER(T) reprogramming, and 'MP' represents the passage of LV-Puro-MyoD-ER(T) reprogramming. Fibroblasts are considered iDRMs once they are transduced with either LV-MyoD-ER(T) or LV-Puro-MyoD-ER(T).

LHCN-M2 cells, a clonal wildtype myoblast immortalized with *TERT* and *CDK4* were a gift from Dr. Woodring Wright and were maintained and plated as a positive control in MyoD staining, and terminal fusion experiments, according to previously described protocols [24]. C2C12 cells were obtained and maintained according to American Type Culture Collection (ATCC) recommendations, and were used as a positive control for myotube fusion.

#### Comparative genomic hybridization (CGH) array design and analysis

A custom 14,022 probe oligonucleotide array was designed with probes tiling the *DMD* gene (Agilent). Genomic DNA was labeled with Cy3, and normal male genomic DNA was labeled with Cy5 using a random priming kit (Agilent) and labeled DNA was co-hybridized to the custom designed array. Arrays were scanned with the DNA Microarray Scanner with SureScan High-Resolution Technology (Agilent) and data were extracted with Feature Extraction Software version 10.5.1.1. The values were extracted from the software and analyzed in R. Base pair positions are reported relative to build HG18 and the log ratio of the Cy3/Cy5 (test/normal) intensity is plotted for all probes.

#### Viral Vectors and Viral Gene Delivery

RRL-SIN-cPPT-hCMV-hTERT and the control, RRL-SIN-cPPT-hCMV-eGFP, were obtained from the UCLA Vector Core. Fibroblasts seeded at 200,000 cells per well in a 6-well plate were transduced overnight at 37°C with 0.1µg/mL of LV-hTERT or LV-GFP virus in 1mL of fibroblast growth media containing 4µL of protamine sulfate (UCLA Pharmacy). The following day fibroblasts were washed twice in 3mL of fibroblast growth media. Transduced fibroblasts were imaged 48-72 hours post-transduction, and then LV-GFP fibroblasts harvested, pelleted, and fixed in 2% paraformaldehyde for analysis by flow-cytometry.

The MyoD-ER(T) construct has been previously described [37]. The puromycin selectable vector was generated by amplifying the MyoD-ER(T) portion of the plasmid using the following

primers: FWD 5'-GTATCGACTAGTCCTCGACAGGACAGGAC-3' and REV 5'-ATAGCCGAATTCTCGCCCGCTTGA-3' (Integrated DNA Technologies). The resulting product was gel purified (Qiagen) and ligated into the pRRLsin.cPPT.CMV.MCS.IRES.Puro vector backbone obtained from the UCLA Vector Core, and validated by Sanger sequencing. Fibroblasts were seeded at 100,000 cells per well in 6-well plates and MyoD-ER(T) lentivirus was transduced at 0.1 $\mu$ g/mL in 1mL of fibroblast growth media with 4 $\mu$ L of protamine sulfate using two days of subsequent 90min 1250rpm centrifugations. Following MyoD-ER(T)-Puro transduction, fibroblasts were passaged  $\pm$  1 $\mu$ g/mL of puromycin (Sigma) in fibroblast growth media (Fig. S4).

#### MyoD Induction, Myotube fusion, and AO Transfection

iDRMs were seeded at 150,000 cells per well in fibroblast growth media in 6-well plates (Corning) pre-coated for 1 hour with 2.5mL of 5 $\mu$ g/mL laminin resuspended in serum free DMEM (BD Biosciences). The following day, 5 $\mu$ M 4OH-tamoxifen (Sigma; resuspended in ethanol) was added in fibroblast growth media for 24 hours. On day 3, cells were washed in 1 x Phosphate Buffered Saline (PBS; Invitrogen), and fusion media containing 1 $\mu$ M 4OH-tamoxifen was added (1:1 Ham's F-10:DMEM (phenol red free, high glucose), 2% Horse Serum, 2% Insulin-Transferrin-Selenium). On Day 7, cells were transfected with 50nM, 100nM or 200nM, 2-O-methyl AO targeting exon 51 (5'-UCAAGGAAGAUGGCAUUUCU-3') (MWG Operon) using the ExGen500 (Fermentas) transfection reagent at a ratio of 5.5 $\mu$ L:1 $\mu$ g of DNA. AO was removed on day 8, cells were washed with 1XPBS, and fresh fusion media containing 1 $\mu$ M 4OH-tamoxifen was added. Forty-eight hours later, cell pellets were harvested and frozen for subsequent RNA isolation and exon skipping analysis [39].

## RNA Isolation, PCR, and qPCR

Total RNA was isolated from cell pellets using the QIAGEN RNeasy Microkit. For exon 51 skipping analysis, 200ng of total RNA was reverse transcribed with an exon 54 gene specific primer [12]. A nested PCR was performed between *DMD* exons 43-52 using previously described primers, and the amplified product run on the Agilent 2100 Bioanalyzer for quantification [12,39]. For MyoD, MyHC, Desmin, MyoG, and GAPDH PCRs, 200ng of total RNA was reverse transcribed with OligodT20 (Invitrogen) using previously described primers and PCR protocols [39].

DNA was isolated using the QIAamp DNA isolation kit (QIAGEN). MyoD-ER(T) was selectively amplified from genomic DNA using primers that span the *MyoD1-Esr1* junction; FWD 5' CCGAACCAGCGGCTACCC-3' and REV 5'-GGCAGGGCTATTCTTCTTAGTGTGCTTAATCAC-3', and the following PCR cycles: 96°C for 2min, 94°C for 20s, 57°C for 30s, 72°C for 20s, repeat steps 2-4 for 33 cycles, and 72°C for 5min. PCR products were run on a 2% agarose gel and visualized with SYBR Safe DNA gel stain.

hTERT was amplified using the primers FWD 5'-AGAGCCAGTCTCACCTTCAAC-3' and REV 5'-GCGGGATCGATTTCAGTCCAGGATGGTCTTG-3', and the following PCR protocol 95°C for 5min, 95°C for 30s, 57°C for 30s, 72°C for 60s, repeat steps 2-4 35 cycles, and 72°C for 10min. PCR products were run on a 2% agarose gel and visualized with SYBR Safe DNA gel stain.

*DMD* and *GAPDH* qPCR was performed on the BioRad iCycler iQ real-time PCR detection system with SensiMix SYBR and Fluorescein kit (Bioline) and with the following primers *DMD* FWD 5'-AAACTCCGAAGACTGCAGAAG-3' and *DMD* REV 5'-GCGGTCATAAATAGTGGTCAAAC-3', and *GAPDH* FWD 5'-GAGCCACATCGCTCAGACAC-3' and *GAPDH* REV 5'-CATGTAGTTGAGGTCAATGAAGG-3' [40]. The amplification protocol was 95°C for 10min, 95°C for 20s, 57°C for 20s, 72°C for 20s, repeat steps 2-4 for 50 cycles.

## Immunofluorescence

Cells were seeded at 25,000 cells per well on laminin coated 12mm sterile glass coverslips in 24 well plates. The next day, 5 $\mu$ M 4OH-tamoxifen was added for 24 hours in fibroblast growth media. For MyoD immunofluorescence iDRMs were then washed with 1XPBS, and fixed with 2% paraformaldehyde (PFA) for 15 minutes. Following PFA treatment, cells were washed in 1XPBS three times, permeabilized with 0.5% Triton-X in PBS for 5min, and blocked in 1%BSA-PBS for 2 hours. Primary MyoD1 (Dako) antibody was added overnight at 4°C at a concentration of 1:100 diluted in 0.1%Triton-X in PBS. The following day primary antibody was removed and secondary antibody directly conjugated to Alexa Fluor 488 goat anti-mouse IgG (H + L) (Invitrogen) was added for 60 min. Coverslips were mounted in ProLong Gold antifade with DAPI (Invitrogen), cured overnight, and then sealed for long-term storage.

For detection of myosin heavy chain protein cells were plated as described above. On day 3, cells were washed with 1XPBS and fusion media containing 1 $\mu$ M tamoxifen was added. iDRMs were fused for 7-10 days before cells were fixed in 2% PFA, washed in 1XPBS, and permeabilized in 0.5% Triton X-100 in TBS for 5 min. After permeabilization, cells were blocked in 20% normal goat serum (Sigma) for 1 hour at room temperature, and then incubated overnight at 4°C. The following day, 1:40 MF20 primary antibody (specific for myosin heavy chain; Developmental Studies Hybridoma Bank) was diluted in 0.05% Tween 20-TBS and incubated overnight at 4°C. Secondary antibody directly conjugated with Alexa Fluor 488 goat anti-mouse IgG (H + L) (Invitrogen) was added at 1:500 for 90 min. Coverslips were mounted in ProLong Gold antifade with DAPI (Invitrogen). Images for both MyoD and MyHC immunostains were acquired on a Zeiss AxioImager Z1 microscope with a 10 $\times$  or 40 $\times$  objective and with the AxioVision Rel. 4.6.3.0 acquisition software.

## Results

### *Primary patient fibroblast cell banking*

We have established a primary fibroblast cell repository, which at the current time contains 35 patient and 14 control cell lines as a resource for investigators and to facilitate research in the muscular dystrophies. We isolated primary dermal human fibroblasts from skin punch biopsies, or procured from the Coriell Institute, and have propagated them in a cell culture system. In total, there are 32 DMD or BMD affected individuals, 4 DMD carrier mothers, and 6 related wildtype individuals. In addition to the DMD families, there are 2 LGMD2A patients, including the parents of one patient, as well as a trio containing a proband with an undiagnosed muscular dystrophy. Table 1 includes information regarding the primary fibroblast identifier, age at biopsy, sex, genetic mutation, familial relationships, and the original source.

### *DMD mutation evaluation by CGH oligonucleotide array*

After isolation and expansion of primary fibroblasts, we evaluated their genomic *DMD* mutational status using a custom 14022 probe CGH oligonucleotide array. On average, oligonucleotide probes are tiled across the *DMD* gene at 158bp intervals, providing approximately 35% overall *DMD* coverage. The CGH array differs from the commonly implemented *DMD* mutation detection method, multiplex-ligation dependent probe amplification (MLPA) assays, in that both exonic and intronic sequences are evaluated allowing more precise identification of chromosomal breakpoints [41-43].

To date, we have evaluated the *DMD* gene in 23 fibroblasts by CGH array to identify, confirm or refine the *DMD* mutation boundaries. We observed a variety of *DMD* mutations including deletions, which affect approximately 65% of all patients (Fig. 2 and Fig. S1) [44]. In addition, genomic duplication events were identified in 7 individuals (Fig. S1). In some instances, large deletions still maintain the mRNA reading frame, resulting in the milder allelic disorder,

Becker muscular dystrophy (BMD) (Fig. S1) [45-47]. It should be noted that DNA point mutations, which affect approximately 15-20% of all DMD patients, are not detected using this method [44]. In patients where a mutation is not observed by CGH array, we perform exome or whole genome sequencing. For example, in CDMD1021 CGH array analysis identified a complex *DMD* rearrangement containing an intron 1 duplication and a deletion of intron 2. In this case the patient was further evaluated by exome sequencing which confirmed an exon 2 duplication event (Table 2). In total, we have performed exome sequencing on seven patients, and have analyzed three patients by whole genome sequencing to further refine the *DMD* genetic diagnosis (Table 2). Validation of the *DMD* mutation is a critical step to screen and characterize available cell lines.

#### *Immortalization of primary fibroblasts with hTERT*

Primary fibroblasts have a finite number of divisions in culture, typically between 20-30 doublings, before becoming senescent [36]. Overexpression of *TERT* delays senescence and extends the replicative capacity of cells in culture by up to 200 doublings [22-24]. In total, 17 fibroblasts have been immortalized by lentiviral overexpression of *hTERT* enabling their long-term use in cell culture systems (Table 2). As a proxy for lentiviral transduction efficiency, fibroblasts are transduced in parallel with a lentiviral vector expressing GFP, which is monitored by fluorescent microscopy and quantified by flow cytometry analysis. After 48-72 hours post-transduction, brightfield and fluorescent microscopy images indicate that fibroblasts are viable and robustly express GFP (Fig. S2). Flow cytometry analysis quantified the percentage of GFP positive cells to be greater than 90% in transduced fibroblasts, suggesting that the majority of the cells were effectively immortalized (Fig. S2). Further, DNA was isolated from LV-hTERT infected fibroblasts and the *TERT* coding sequence PCR amplified indicating successful genomic integration of the vector (Fig. S3).

*MyoD inducibly reprograms fibroblasts into iDRMs capable of fusing into multinucleated myotubes*

To study skeletal muscle disease fibroblasts must be reprogrammed and fused into muscle myotubes. Previous work has shown that overexpression of a single muscle specific transcription factor, MyoD, effectively converts fibroblasts into a muscle cell lineage. Here, we utilized a MyoD-ER(T) fusion protein that has been described for the reprogramming of mouse fibroblasts into myotubes in culture, and was further characterized for its potential in viral mediated dystrophin genetic correction, and subsequent cell replacement therapies in a DMD mouse model [37]. This MyoD-ER(T) fusion protein contains a portion of the mutated, tamoxifen sensitive estrogen receptor that is inserted within the mouse *MyoD1* coding sequence. Using a lentiviral system, we constitutively overexpress MyoD-ER(T) under the cytomegalovirus (CMV) promoter; however, MyoD is only functionally active following tamoxifen exposure, which induces nuclear translocation. Once in the nucleus MyoD-ER(T) coordinates the activation or repression of genes required during muscle lineage commitment and subsequent differentiation [29,37]. This inducible MyoD reprogramming strategy allows for passaging and expansion as fibroblasts, and then muscle lineage specification as is required.

We performed lentiviral MyoD-ER(T) reprogramming and myogenic conversion in 9 *TERT* immortalized human fibroblasts (termed iDRMs). Following LV-MyoD-ER(T) transduction, iDRMs are evaluated for tamoxifen dependent MyoD induction and translocation into the nucleus by immunofluorescence. After 24 hours of 5 $\mu$ M tamoxifen exposure 10-15% of iDRM5017 H10 M15 and iDRM5162 H6 M19 cells expressed MyoD in the nucleus (Fig. 3a-b). The MyoD1 primary antibody does not distinguish between the exogenous MyoD-ER(T) protein and endogenous MyoD1 protein. However, nuclear MyoD was only observed in tamoxifen treated cells suggesting that 1) this is a tamoxifen dependent event and 2) concentration of MyoD protein within the nucleus is a requirement for its detection (Fig. 3a-b). To validate the

genomic integration of the unique MyoD-ER(T) sequence, DNA was isolated from iDRMs and PCR amplification performed spanning the *MyoD1-Esr1* junction. This unique junction is only detected in iDRMs containing the LV-MyoD-ER(T) vector (Fig. 3c). Together, these data indicate the presence of both the unique MyoD-ER(T) sequence and protein in iDRMs, and that tamoxifen exposure regulates its translocation and concentration within the nucleus.

To assess if iDRMs, with about 10-20% of the cells in the population positive for MyoD expression, were capable of myogenesis, iDRM5017 and iDRM5162 cells were evaluated for their ability to fuse into multinucleated myotubes. iDRM5017 and iDRM5162 were seeded on laminin coated plates, exposed to tamoxifen, and then fused in low serum conditions. After ten days cells were harvested and the expression of the muscle differentiation marker, myosin heavy chain, detected by immunofluorescence. As expected, iDRMs that were not exposed to tamoxifen had no nuclear MyoD expression and did not express myosin heavy chain (Fig. 3d). However, after tamoxifen exposure and fusion for ten days in low serum conditions, both iDRM5017 and iDRM5162 formed multinucleated and elongated myotubes that expressed myosin heavy chain (Fig. 3d). The extent of terminal fusion was further quantified by calculating the fusion index, or proportion of myogenic nuclei (nuclei within MyHC<sup>+</sup> cells) relative to the number of nuclei within the entire field of view. iDRM5017 and iDRM5162 contained approximately 15-20% myogenic nuclei (Fig. 3e) [36,48]. During the course of fusion, iDRMs also exhibited a temporal expression of muscle specific genes including, endogenous MyoD, desmin, myosin heavy chain, and dystrophin (Fig. 3f). These data indicate that human fibroblasts can be effectively reprogrammed into a myogenic lineage.

To evaluate the impact of *TERT* overexpression on the subsequent reprogramming and fusion process, CDMD1003 or CDMD1003 H10 were transduced with LV-MyoD-ER(T) and terminal fusion assessed. *TERT* expression did not significantly impact the proportion of MyoD positive cells after a 24 hour exposure to 5 $\mu$ M tamoxifen (Fig. S5a). After ten days of fusion, both

iDRMs expressed myosin heavy chain protein, and displayed comparable fusion indices (Fig. S5b-c). In addition, iDRM1003 M15 and iDRM1003 H10 M16 expressed endogenous MyoD, desmin, myosin heavy chain, and myogenin after ten days of fusion (Fig. S5d).

#### *Improvements in iDRM reprogramming efficiency and terminal fusion and differentiation*

Validation of iDRM reprogramming is a two step process involving the quantification of MyoD positive cells and the evaluation of terminal fusion by determining the fusion index (Fig. 1). After compiling data for all produced iDRMs, the relationship between the percentage of MyoD positive cells and terminal fusion index was significantly correlated (Pearson's correlation;  $P=0.03$ ). Therefore with the goal of creating 1) a stable iDRM with an increased proportion of MyoD positive cells and 2) improving terminal fusion, the MyoD-ER(T) construct was cloned into a puromycin selectable vector. MyoD positivity and terminal fusion were evaluated in the LV-MyoD-ER(T)-Puro selectable vector by comparing to the original LV-MyoD-ER(T) vector and *TERT* immortalized GM05017 fibroblasts. Following lentiviral transduction, iDRMs were first expanded and passaged for two weeks either in the presence or absence of a selective concentration of puromycin (Fig. S4). iDRMs were evaluated for MyoD induction and nuclear localization by immunofluorescence following 24 hours of 5 $\mu$ M tamoxifen treatment. In the absence of tamoxifen cells had no detectable MyoD expression (Fig.4a-b inset); including GM05017 H10, iDRM5017 H10 M23, and iDRM5017 H10MP23. However, compared to non-induced controls, there was a significant induction in the percentage of MyoD positive cells in both tamoxifen treated LV-MyoD-ER(T) or LV-Puro-MyoD-ER(T) iDRMs. The percentage of MyoD positive cells in these treatment groups ranged from 15-45% of the population. After two weeks of puromycin selection, there was a 3 fold enrichment in the proportion of MyoD positive iDRMs as compared to the unselected iDRM controls (Fig. 4b).

Differences in terminal myotube fusion were evaluated in iDRM5017 cells first selected in puromycin for two weeks and then seeded on laminin coated plates and fused in low serum

conditions for seven days. Fused iDRMs were evaluated for the expression of the muscle protein, myosin heavy chain (Fig. 5a). As expected, there was no expression of myosin heavy chain in conditions not treated with tamoxifen (Fig. 5a inset); including, GM05017 H10 fibroblasts, iDRM5017 H10 M23, and iDRM5017 H10 MP23. In contrast, all 3 iDRMs that were exposed to tamoxifen, and exhibited nuclear MyoD expression, also expressed myosin heavy chain, which was quantified by determining the fusion index (Fig. 4b-c, 5a) [36,48]. iDRMs transduced with LV-MyoD-ER(T) and unselected LV-Puro-MyoD-ER(T) exhibited similar fusion levels (Fig. 5a-b). However, LV-Puro-MyoD-ER(T) iDRMs that were selected for two weeks in puromycin prior to fusion demonstrated a statistically significant increase in the proportion of myogenic nuclei (Fig. 5b). During fusion, puromycin selected iDRMs displayed a temporal induction of *DMD* expression relative to H10 fibroblasts, indicating the utility of this model in applications requiring muscle protein and gene expression profiles (Fig. 5c).

#### *iDRMs as a tool to evaluate antisense targeted DMD exon skipping activity*

An application for iDRMs is the evaluation of AO targeted *DMD* exon skipping activity. The basis for AO therapies is due to the nature of the dystrophin protein sequence, which consists of repetitive spectrin repeats in the central domain that are not as critical for dystrophin protein function as the N and C terminal domains. Current clinical exon skipping strategies are aimed at manipulating out of frame *DMD* deletions with AOs so that single adjacent exons are removed, restoring the *DMD* mRNA reading frame. This process produces an internally truncated dystrophin protein, and potentially milder phenotype, as is seen in BMD [45-47,49].

Here we describe the utility of iDRMs in evaluating AO targeted exon 51 skipping in a patient and mutational specific context. Current phase IIb and III clinical trials are primarily focused on skipping *DMD* exon 51, as this single exon skip is relevant for the highest proportion of DMD patients [50]. We utilized a LV-MyoD-ER(T) reprogrammed iDRM5017 with a *DMD* exon 45-50 deletion, for which the mRNA is put back in-frame by the additional exclusion of

*DMD* exon 51. During the fusion process a *DMD* exon 51 specific antisense oligonucleotide (h51AON) is transfected into iDRMs and induces exon skipping in a dose dependent and statistically significant manner (Fig. 6a-b). After ten days of fusion cells remain robust, and in all tamoxifen treated conditions are elongated, multinucleated, and morphologically distinct from non-induced fibroblasts (Fig. 6c). This protocol and methodology is applicable to a broad subset of mutations and antisense oligonucleotides, and could be used to test personalized antisense therapies for DMD in a minimally invasive way.

### *Discussion and Conclusions*

We describe a comprehensive cell based resource for the study of DMD, with applications ranging from defining molecular mechanisms contributing to DMD pathogenesis to the evaluation of potential treatment strategies. To date we have collected and banked 49 primary fibroblasts isolated from patient skin punches or obtained and modified from the Coriell Institute, significantly contributing to the DMD mutational spectrum available for study [20,21]. In addition, we define a process whereby fibroblasts are genetically characterized by CGH array, immortalized for extended use in cell culture, and efficiently reprogrammed and fused into myotubes for the study of muscle diseases. To date, 23 fibroblasts have been analyzed by CGH array to better resolve the breakpoints of deletion or duplication *DMD* mutations, 17 fibroblasts have been immortalized with *TERT*, and 9 iDRMs have been generated via reprogramming with an inducible MyoD-ER(T) lentiviral vector. Expanding upon previous methodologies, we have refined the MyoD-ER(T) vector by cloning in a puromycin resistance gene allowing for the chemical enrichment of LV-MyoD-ER(T) transduced iDRMs. Indeed, puromycin selected iDRMs exhibit a higher proportion of MyoD positive cells after selective tamoxifen induction, which correlates to an improvement in terminal myotube fusion. Further, we detail a fusion protocol including a defined media, timing, and expected morphological changes for the conversion of iDRMs into terminally differentiated muscle myotubes (Fig. 1).

Although the concept of MyoD reprogramming has been previously described, we further refine a methodology that is both consistent and efficient at generating a renewable resource of iDRMs. Previous studies have reprogrammed human fibroblasts into muscle myotubes by constitutive adenoviral MyoD overexpression, followed by immediate cell cycle withdraw, and myogenic differentiation [35]. With this protocol, reprogrammed fibroblasts are a limited resource that must be re-transduced prior to each experiment, introducing inherent variability due to transduction or fusion efficiencies across experiments. Alternative approaches have opted for the use of vectors that implement a *Tet* on inducible system, which selectively activates transcription of MyoD after the addition of the antibiotic tetracycline, or one of its derivatives [36]. We utilize a modified MyoD-ER(T) construct that has been previously described for the reprogramming of mouse fibroblasts into myocytes. Here, we describe its application in converting human patient fibroblasts into iDRMs *in vitro*. In addition, we improve upon previously published protocols by including a puromycin selectable MyoD-ER(T) vector that allows for chemical enrichment of successfully transduced iDRMs. This concept of overexpressing inducible MyoD in fibroblasts has even been suggested as a potential alternative to myoblast and stem cell based therapies for the treatment of DMD [37]. Fibroblasts offer the benefit of being relatively easy to culture, efficiently transduced with lentiviral vectors, and with genetic correction, successfully re-transplanted for study in *in vivo* systems [35,37]. Ultimately, conversion of patient fibroblasts into iDRMs could serve as a pipeline for the investigation of DMD phenotypes and treatments in transplantation settings using *in vivo* models [35-37].

iDRMs have already been showcased as promising and versatile indicators of treatment evaluations in the context of drug discovery research; namely, the study of small molecule enhancers of AO targeted *DMD* exon skipping [39]. A natural complement to such studies is the mechanistic understanding of molecular phenotypes associated with the disease and how these correlate with particular drug treatments. Recently, AO clinical trials have utilized fibroblasts reprogrammed with a constitutive MyoD as a pre-clinical screening tool, to ensure that enrolled

patients do not have aberrant splicing or response to exon 51 specific antisense oligonucleotides [12-15], highlighting the current utility of directly reprogrammed fibroblasts in basic and therapeutic muscular dystrophy research. Widespread investigation of these diverse DMD patient mutations and their responsiveness to clinical therapies may provide a better understanding of genotype-phenotype correlations, how mutations influence disease severity, and how genetic modifiers may impact potential treatments. We have confirmed that iDRMs form multinucleated, elongated myotubes, which can be used as a patient specific means to test the effects of various drug treatments.

Our reprogrammed fibroblasts are convenient to grow in large quantities, and under the appropriate conditions, can be efficiently converted into muscle cells. To that aim, an in depth analysis of the extent to which iDRMs recapitulate primary human myoblasts fused into myotubes is currently being assessed. Nonetheless, the standard operating procedure reported here can be used for the development of iDRMs to be used in a variety of assays requiring expression of muscle genes or muscle proteins for both basic and applied research. This integrative resource allows for investigators to immediately use iDRMs upon request in their own research, or adopt the protocols described here, including banking, immortalization, and re-programming for fibroblasts collected in-house. To our knowledge this is one of the most comprehensive and largest widely available muscular dystrophy specific cell banks, and expands on the number of patients, mutations, and resources that already exist for research purposes [20,21]. We continue to collect and bank primary patient fibroblasts that are obtained both locally and nationally which will be available as a resource for the investigation of muscle diseases.

### *Acknowledgments*

We thank the patients and their families for providing blood or skin punches to support this research. We also thank Natalia Sejbuk for technical support. Viral packaging was performed at the UCLA Vector Core. Tamoxifen inducible MyoD-ER(T) construct was a kind gift from J. Chamberlain. LHCN-M2 was a kind gift from W. Wright. This work was funded from grants from the NIH (1RC1AR058333), the Department of Defense (85280103), and the Foundation to Eradicate Duchenne (special thanks to T. Carson and D. Carson). Support for the research was also provided by the UCLA Muscular Dystrophy Core Center (NIH grant 5P30AR057230) within the Center for Duchenne Muscular Dystrophy at UCLA.

**Figure 1. Strategy for primary patient fibroblast banking, immortalization, and MyoD-ER(T) reprogramming into iDRMs.** Skin punches were collected, processed, and patient fibroblasts isolated after 2-3 weeks in culture. Primary fibroblasts were expanded for 2 weeks, and then preserved for future use or distribution by freezing in 10 cryotube vials containing  $1 \times 10^6$  cells each ( $n=49$ ). Concurrently, in a subset of fibroblasts, DNA was isolated, and the *DMD* mutation identified using a custom CGH tiling array ( $n=23$ ). After further expansion in culture, fibroblasts were immortalized by transducing with a lentiviral vector expressing human *TERT* ( $n=17$ ). These *TERT* immortalized fibroblasts were passaged and frozen at  $1 \times 10^6$  cells per cryotube vial, and following an additional expansion, were transduced with a lentiviral vector expressing an inducible MyoD-ER(T) fusion protein. After LV-MyoD-ER(T) transduction cells were termed iDRMs ( $n=9$ ). For verification of successful reprogramming, iDRMs were plated for validation of MyoD induction following tamoxifen exposure (Day 3) and Myosin Heavy Chain expression after fusion in low serum media (Day 10). Shown below the schematic are representative images of morphological changes during the course of fibroblast collection and reprogramming from (1) isolation of the skin biopsy (inset) and outgrowth of fibroblasts, (2) *TERT* immortalization, and (3)-(4) iDRM fusion into myotubes. Scale bar, 100 $\mu$ m.

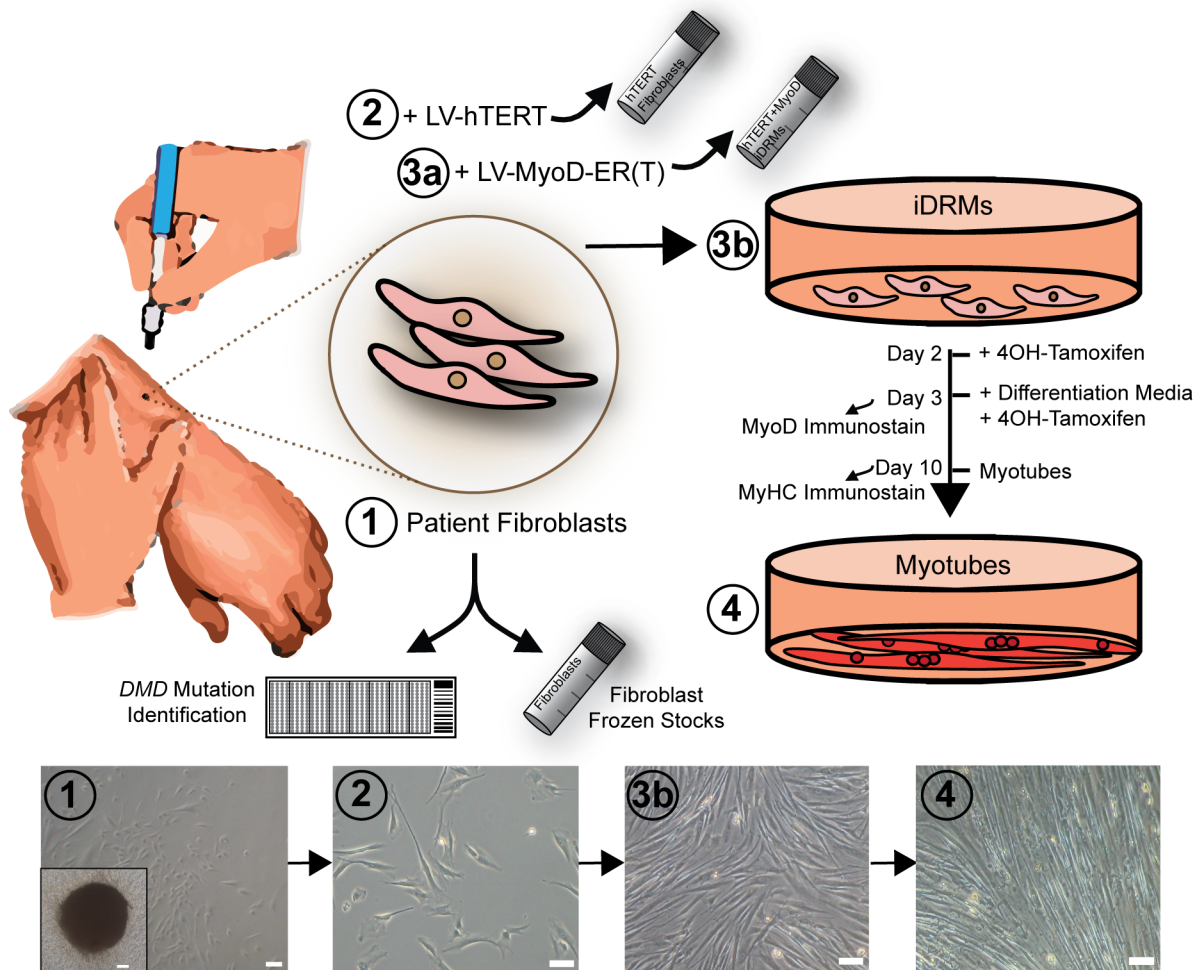


**Figure 2. Copy number variation in a subset of mutations represented in the cDMD cell bank.** A custom CGH array identified or further refined *DMD* gene mutations and breakpoint boundaries. Displayed are copy number data from an individual with a wildtype *DMD* gene, and a DMD patient with a deletion spanning exons 46-47. Probes within the deleted *DMD* region are highlighted in red. Tiled below are the genomic locations of the 79 *DMD* exons, with exon 1 beginning on the right and ending with exon 79 on the left.

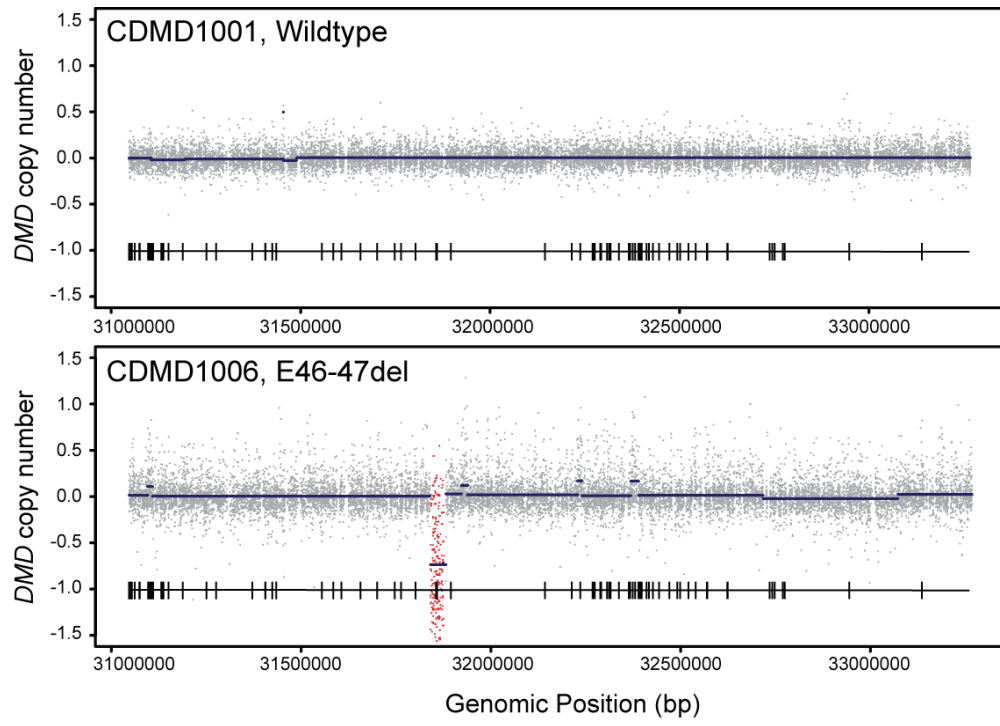


**Figure 3. Inducible MyoD expression and myogenesis in DMD patient iDRMs.**

Immortalized patient fibroblasts were transduced with LV-MyoD-ER(T) and assessed for MyoD induction and myotube fusion capacity. (A) Representative iDRM5017 and iDRM5162 images for MyoD (green) and DNA (blue) immunostain after 24 hours of 5 $\mu$ M tamoxifen exposure. Inset indicates MyoD expression without tamoxifen exposure. Scale bar, 100 $\mu$ m. (B) Quantitation of MyoD positive cells in iDRM5017 and iDRM5162,  $n=3$  images from independent wells. (C) Genomic DNA was isolated from fibroblasts or iDRMs and amplified with primers specific for the *MyoD1-Esr1* junction. Plasmid MyoD-ER(T) DNA was used as a positive control. (D) Representative images showing myosin heavy chain expression (green) and DNA (blue) in iDRM5017 and iDRM5162 fused for ten days in low serum conditions. Inset indicates myosin heavy chain expression without tamoxifen exposure after 10 days of fusion. Scale bar, 100 $\mu$ m. (E) Quantitation of the fusion index in iDRM5017 and iDRM5162 after 10 days of fusion in tamoxifen and low serum conditions,  $n=3$  independent wells per condition. (F) Temporal muscle specific gene expression during the course of fusion in iDRM5162; including, endogenous human MyoD, Desmin, Myosin Heavy Chain (MyHC), Dystrophin, and GAPDH as a loading control.

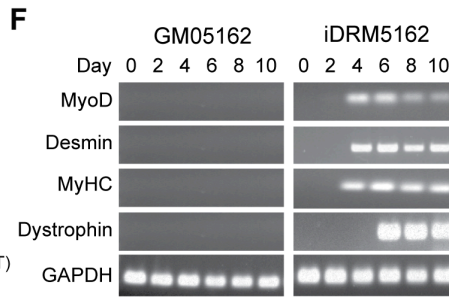
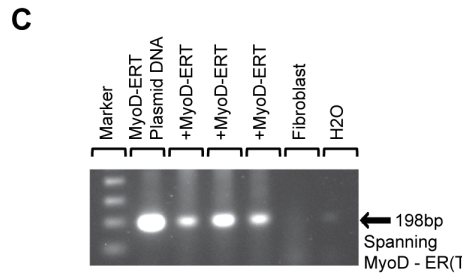
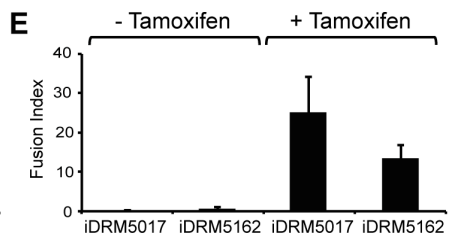
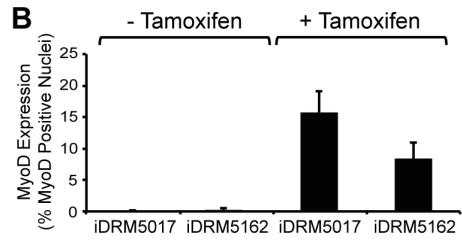
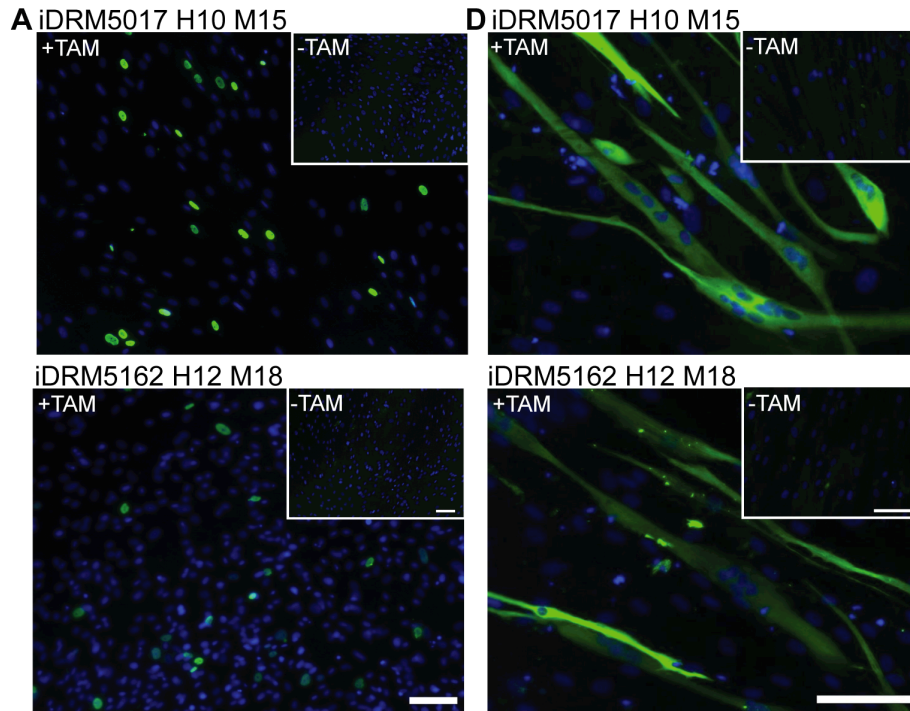


**Figure 4. Tamoxifen exposure induces nuclear MyoD expression in DMD patient iDRMs.** Immortalized patient fibroblasts were transduced with LV-MyoD-ER(T) or LV-Puro-MyoD-ER(T) and then passaged with or without puromycin for two weeks before iDRM reprogramming validation. (A) Representative images for MyoD (green) and DNA (blue) immunostain after a 24 hour time period either with or without 5 $\mu$ M tamoxifen. Inset indicates MyoD expression without tamoxifen exposure. Cell naming nomenclature is as follows; H10, hTERT immortalized fibroblasts; H10 M23, hTERT+LV-MyoD-ER(T); H10 MP23, hTERT+LV-Puro-MyoD-ER(T)  $\pm$  puromycin selection. Scale bar, 100 $\mu$ m. (B) The percentage of MyoD positive cells were quantified in  $n=3$  images per well (without tamoxifen), or  $n=3$  images across independent wells (with tamoxifen). LHCN-M2 wildtype myoblasts were used as a positive control for MyoD expression,  $n=3$  images across independent wells. \* indicates  $P < 0.05$ .  $P$  values were determined using a two tailed student's t-test.

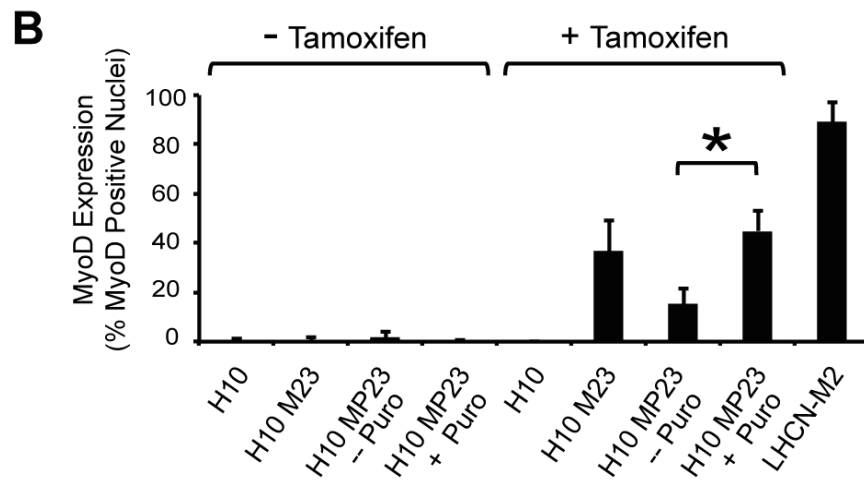
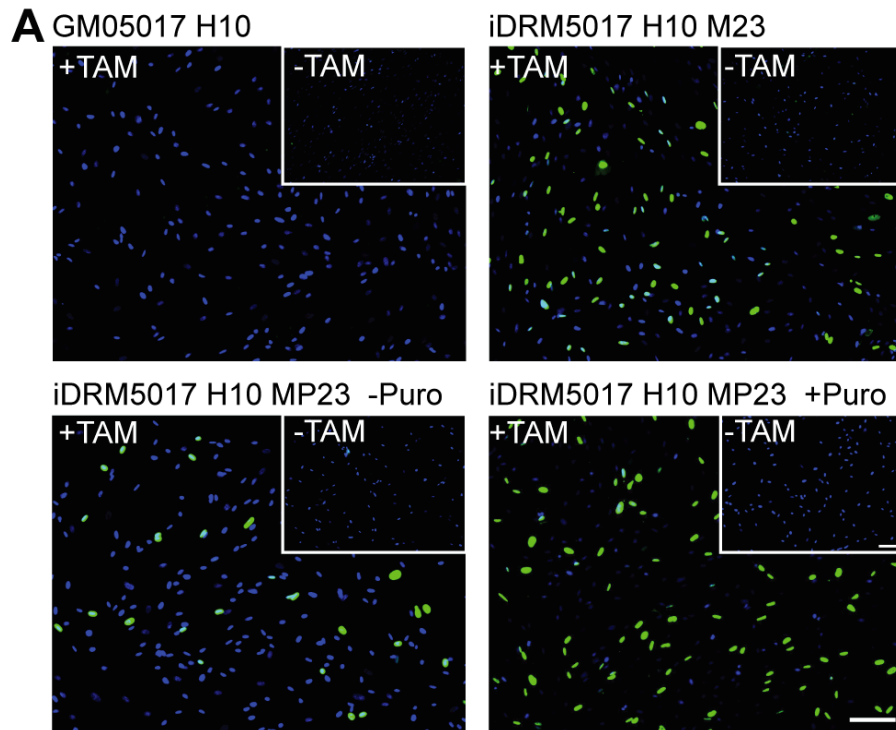


**Figure 5. iDRM patient fibroblasts reprogrammed into myotubes selectively express terminal muscle markers after MyoD induction and fusion.** Cells evaluated for MyoD expression in Figure 5 were fused in low serum conditions for seven days to determine myogenic capacity. (A) Representative images for expression of myosin heavy chain (green), and DNA (blue), in H10, iDRM H10 M23, and iDRM H10 MP23 with and without prior puromycin selection. Inset indicates myosin heavy chain expression without tamoxifen exposure. Scale bar, 50 $\mu$ m. (B) The fusion index was calculated as the percentage of nuclei within a myosin heavy chain positive cell, versus the total nuclei per field of view in both naïve and tamoxifen treated conditions. Error bars indicate  $n=3$  images per well (without tamoxifen) or  $n=4$  images across independent wells (with tamoxifen). C2C12 mouse myotubes were used as a positive control,  $n=3$  images across independent wells. \* indicates  $P < 0.05$ .  $P$  values were determined with a two tailed student's t-test. (C) Quantitative PCR for temporal *DMD* gene expression in H10 fibroblasts, H10 MP23 iDRMs, and LHCN-M2 wildtype myotubes on day 3, 13, and 21 of fusion. Loading was normalized to *GAPDH* expression.

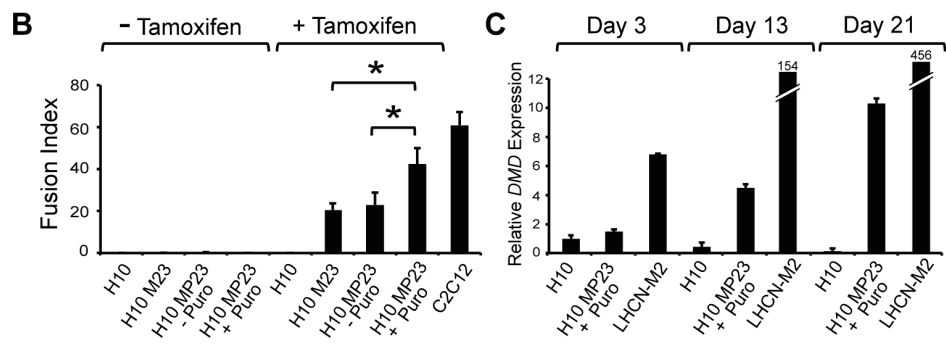
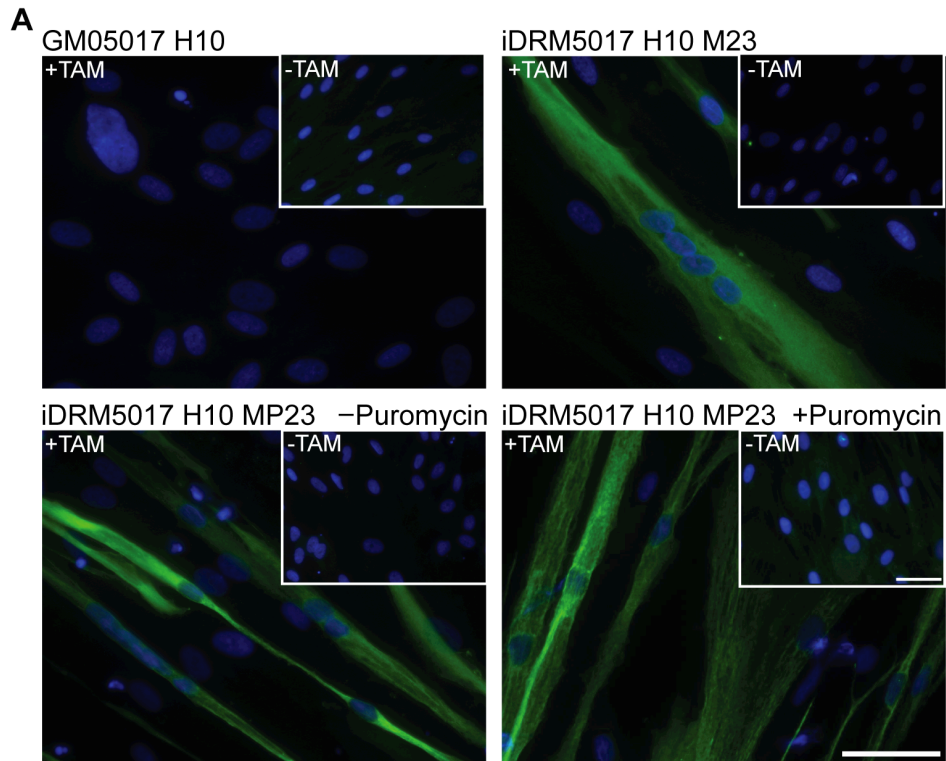
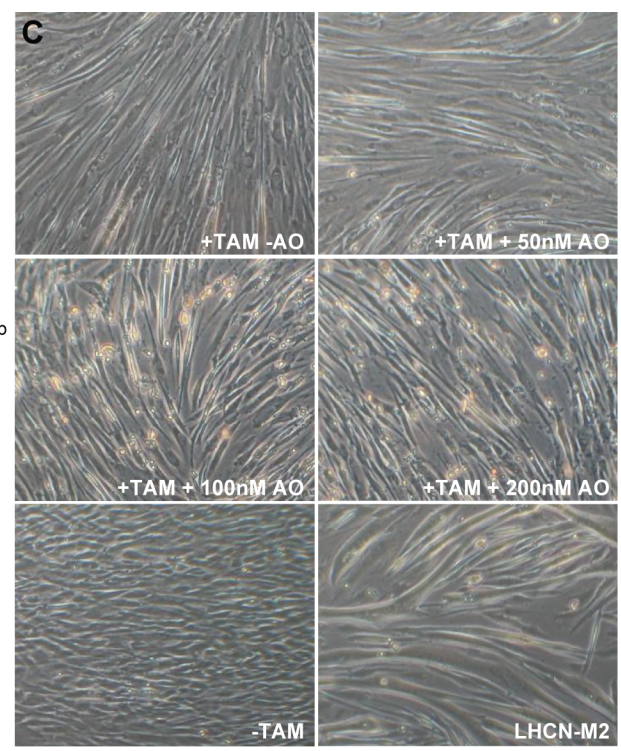
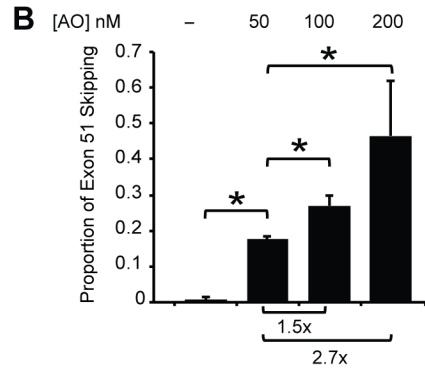
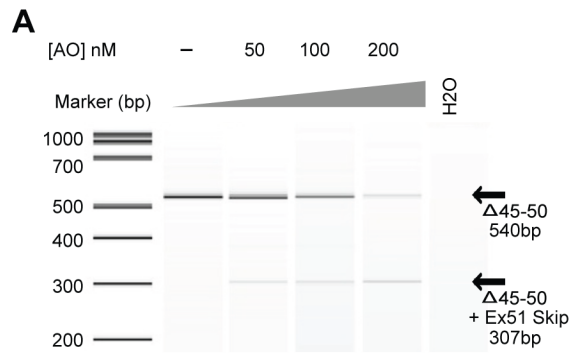


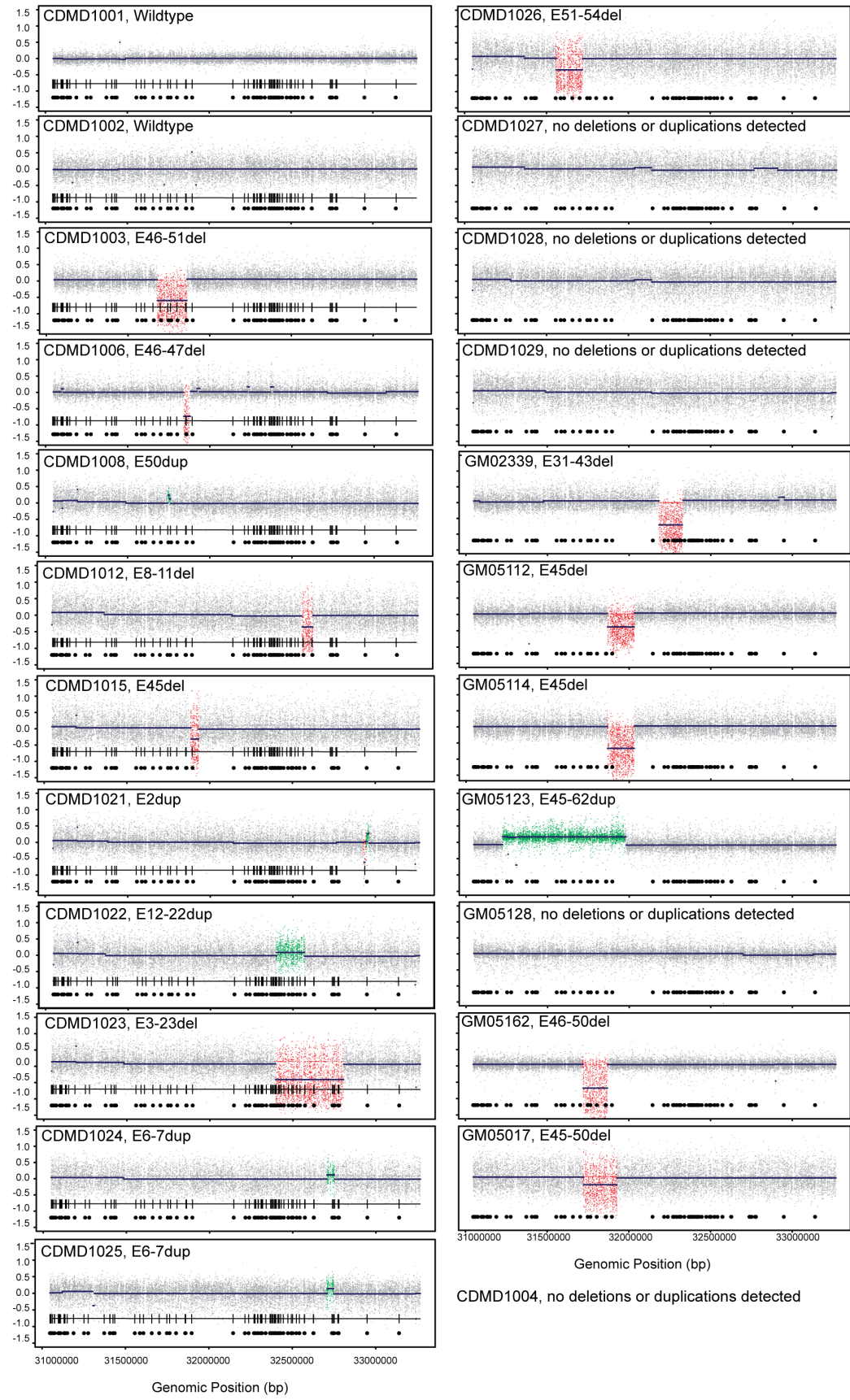
**Figure 6. iDRMs as a clinical model for antisense based exon skipping strategies.**

iDRM5017 H10 M14 with a *DMD* exon 45-50 deletion were treated with tamoxifen, induced for nuclear MyoD expression, and fused for 10 days total. (A) On day 7, iDRMs were transfected with a serial titration of 2'OMe h51AON (5'-UCAAGGAAGAUGGCAUUUCU-3') targeting *DMD* exon 51 for removal from the mRNA. On day 8, h51AON was removed, and cells were harvested for total RNA isolation on day 10. Amplification of the region between *DMD* exons 43-52, and capillary electrophoresis on the Agilent 2100 Bioanalyzer indicates the presence of a full-length mRNA product at 540bp, as well as an exon 51 skipped product at 307bp. (B) Quantification of exon skipping activity depicted as the proportion of exon 51 skipped mRNA product. Error bars indicate  $n=3$  independent wells per condition. \* indicates  $P < 0.05$ .  $P$  values were determined using a two tailed student's t-test. (C) Brightfield images were taken on the final day of fusion (day 10) for the following iDRM5017 conditions; mock transfected, 50nM h51AO, 100nM h51AO, and 200nM h51AO. Bottom left panel- iDRM not exposed to tamoxifen. Bottom right panel- LHCN-M2 wildtype human myotubes fused for 10 days in parallel with iDRMs.

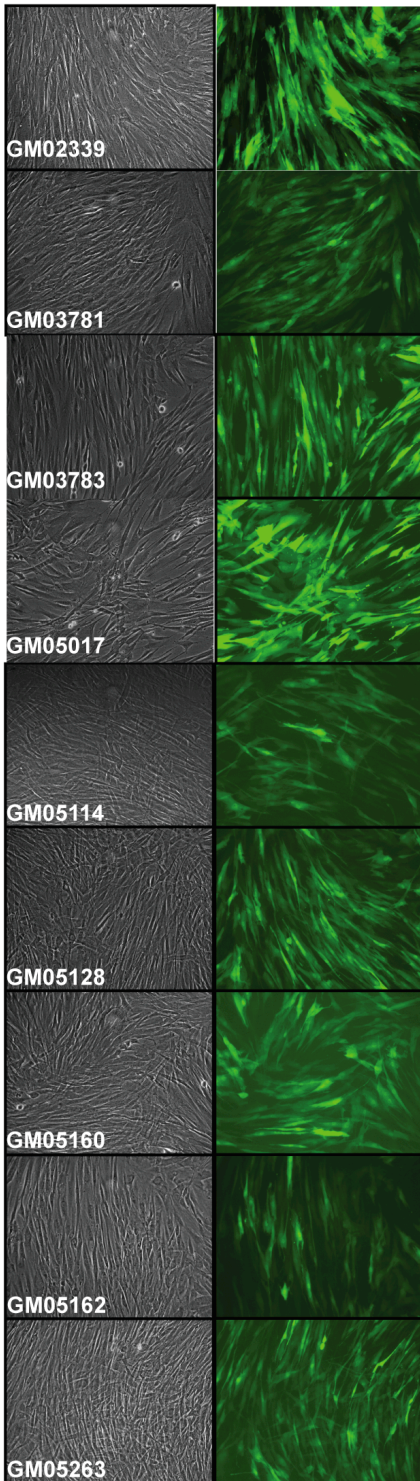
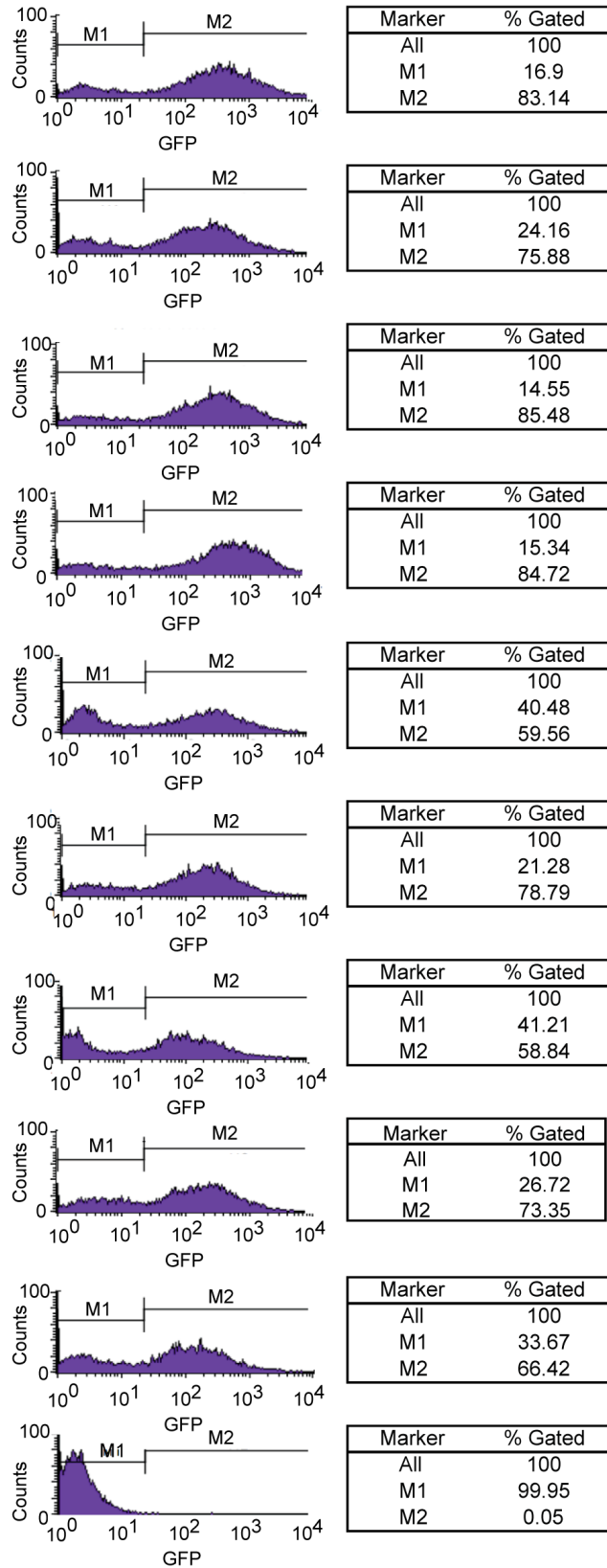


**Supplementary Figure 1. Copy number variation in a subset of CDMD patient fibroblasts.** A custom CGH array was designed to identify and further refine *DMD* gene mutations and breakpoint boundaries. Displayed are copy number data from all assessed primary fibroblasts ( $n=23$ ). Probes within the deleted *DMD* regions are highlighted in red, and probes within amplified genomic regions are highlighted in green. Tiled below are the genomic locations of the 79 *DMD* exons, with exon 1 beginning on the right and ending with exon 79 on the left.

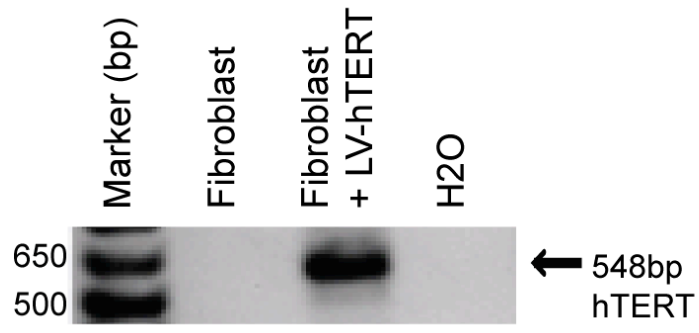
DMD copy number



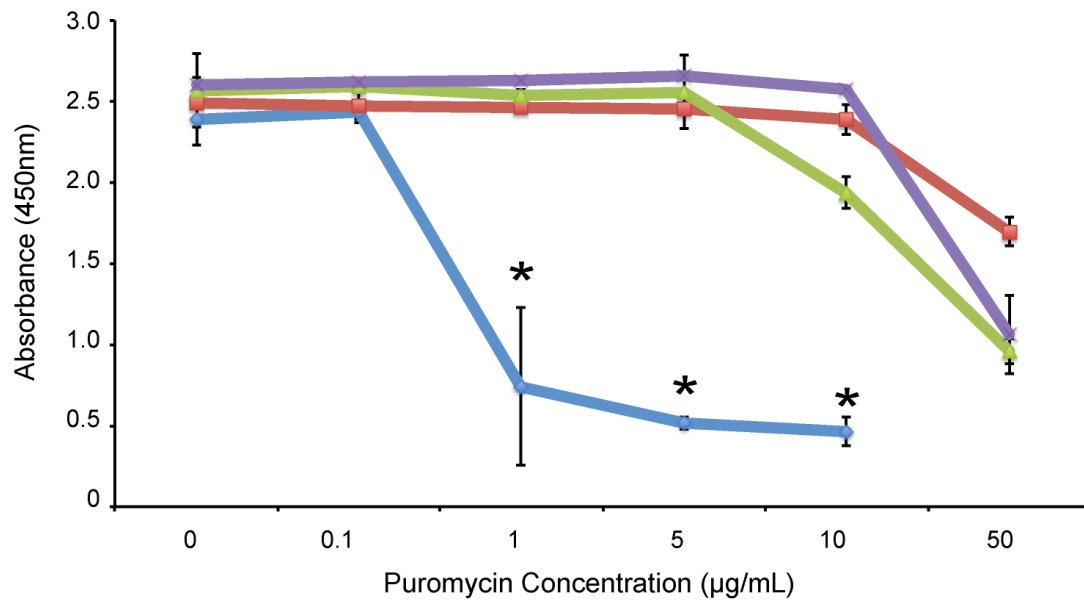
**Supplementary Figure 2. Evaluation of lentiviral hTERT and GFP transduction efficiency in CDMD patient fibroblasts.** (A) Brightfield and GFP fluorescent images from cells 48 hours after transduction with lentivirus. (B) Corresponding quantitation of the GFP positive cell population by flow cytometry. The percentage of GFP positive cells is given in the table for each corresponding CDMD fibroblast.

**A****B**

**Supplementary Figure 3. Genomic insertion of *hTERT* mRNA coding sequence in transduced CDMD fibroblasts.** (A) Human specific hTERT was amplified from genomic DNA isolated from both mock and lentiviral *TERT* transduced fibroblasts.



**Supplementary Figure 4. Determination of puromycin selection concentration in mock and LV-Puro-MyoD-ER(T) transduced fibroblasts.** Immortalized H10 fibroblasts were either mock transduced or transduced with the LV-Puro-MyoD-ER(T) vector. Following transduction, puromycin resistant cells were carried for two weeks in either 1) no puromycin, 2) 0.1µg/mL puromycin or 3) 1µg/mL puromycin. After two weeks, all 4 conditions were plated on a 96 well plate in triplicate in fibroblast growth media. The following day, concentrations of puromycin ranging from 0, 0.1, 1, 10 or 50µg/mL were added for 24 hours. WST-1 (Roche) was then added to cells, incubated at 37°C for 4 hours, and the absorbance at 450nm measured using a fluorescence plate reader. Plotted is the standard deviation across triplicate wells. \* indicates  $P < 0.05$ .  $P$  values were determined with a two tailed student's t-test, and compare H10 immortalized fibroblasts to all other conditions that include a LV-Puro-MyoD-ER(T) vector.



- ◆ Fibroblast + hTERT
- Fibroblast + hTERT + MP23, unselected
- ▲ Fibroblast + hTERT + MP23, selected with 0.1µg/mL puromycin
- ◆ Fibroblast + hTERT + MP23, selected with 1µg/mL puromycin

**Supplementary Figure 5. Impact of *TERT* overexpression on terminal myotube fusion.** CDMD1003 fibroblasts with or without *TERT* immortalization were reprogrammed with LV-MyoD-ER(T) resulting in two iDRMs; iDRM1003 M15 and iDRM1003 H10 M16. iDRMs were plated on laminin coated plates, exposed to 5 $\mu$ M tamoxifen for 24 hours and (A) nuclear expression of MyoD was quantitated,  $n=3$  images across independent wells. (B) Following 10 days of fusion, iDRMs were evaluated by immunostain for expression of myosin heavy chain. Scale bar, 100 $\mu$ m. (C) Myogenic fusion index for iDRM1003 M15 and iDRM1003 H10 M16,  $n=3$  images across independent wells. (D) Muscle specific gene expression after 10 days of fusion; including, endogenous human MyoD, Myosin Heavy Chain (MyHC), Desmin, Myogenin (MyoG), and GAPDH as a loading control. \* indicates  $P < 0.05$ .  $P$  values were determined using a two tailed student's t-test.

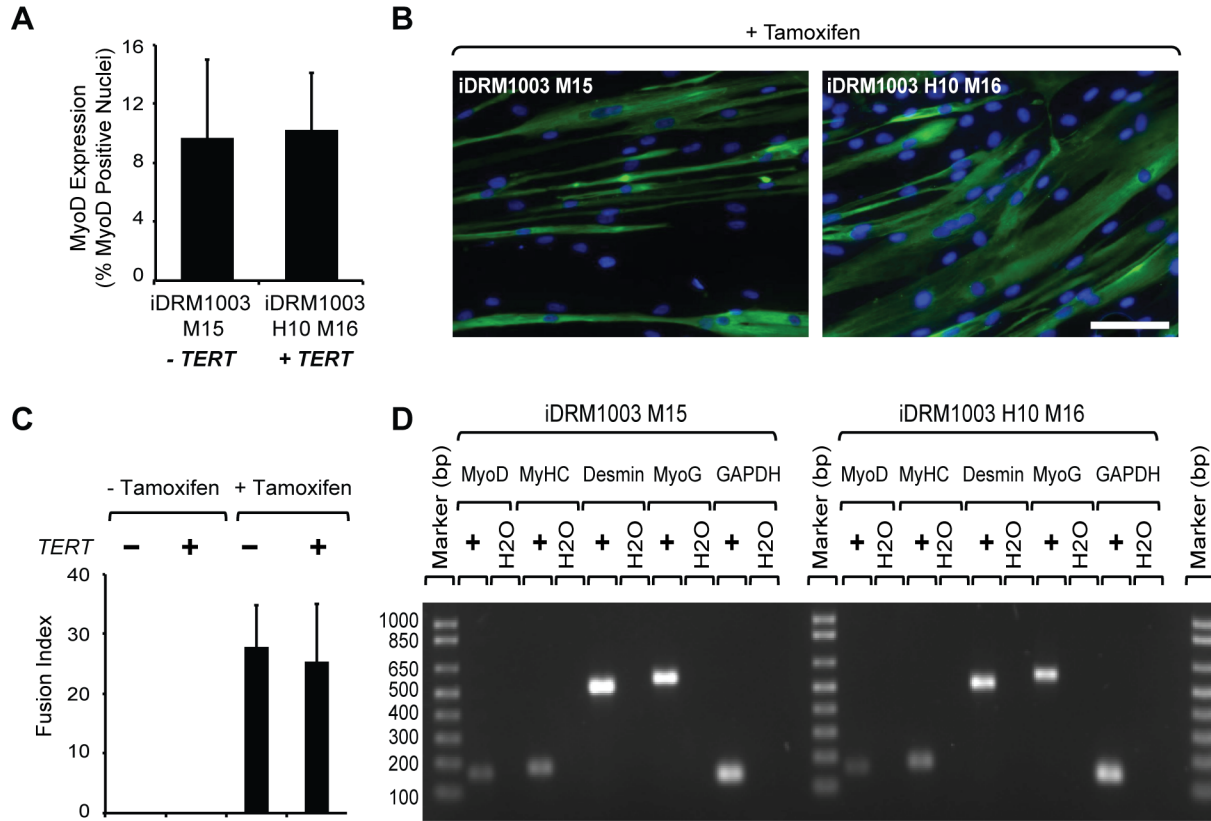


**Table 1.** Available cDMD primary patient fibroblasts.

Sample ID	Sex	Age	DMD Mutation	Genetic Diagnosis and Relationship(s)	Source
CDMD 1001	F	40YR+	WT	Mother of 1003	UCLA
CDMD 1002	M	40YR+	WT	Father of 1003	UCLA
CDMD 1003	M	9YR	E46-51del	DMD affected son of 1001 & 1002	UCLA
CDMD 1004	M	60YR+	WT	-	UCLA
CDMD 1006	M	10YR	E46-47del	DMD affected	CNMC
CDMD 1008	M	13YR	E50dup	DMD affected	UCLA
CDMD 1012	M	12YR	E8-11del	DMD affected	UCLA
CDMD 1013	M	20YR	E51del	DMD affected	Kennedy Krieger Institute
CDMD 1015	M	8YR	E45del	DMD affected	UCLA
CDMD 1021	M	16YR	E2dup	DMD affected	UCLA
CDMD 1022	F	40YR+	[E12-22dup];[=]	Carrier Mother with E12-22 DUP	UCLA
CDMD 1023	M	9YR	E3-23del	DMD affected	UCLA
CDMD 1024	M	10YR	E6-7dup	DMD affected son of CDMD 1025	UCLA
CDMD 1025	F	40YR+	[E6-7dup];[=]	Carrier Mother of CDMD 1024	UCLA
CDMD 1026	M	8YR	E51-54del	DMD affected	UCLA
CDMD 1027	M	20YR	ND	DMD affected	UCLA
CDMD 1028	F	40YR+	c.[4100_deIT];[=]	Carrier Mother of CDMD 1029	UCLA
CDMD 1029	M	10YR	c.4100_deIT	DMD affected son of CDMD 1028	UCLA
CDMD 1037	M	20YR	c.1961_deIT>A, p.LEU654* (E16)	DMD affected	UCLA
CDMD 1039	M	2YR	c.7327_7328del_AC (E51)	DMD affected	UCLA
CDMD 1044	M	5YR	E45-50del	DMD affected	UCLA
CDMD 1045	M	11YR	E45-50del	DMD affected	UC Davis
CDMD 1056	M	13YR	E49-50del	DMD affected	UCLA
CDMD 1062	M	22YR	WT	LGMD2A affected	CCMC
CDMD 1063	M	11YR	E45-50del	DMD affected	UC Davis
CDMD 1064	M	16YR	E45del	DMD affected	UCLA
CDMD 1065	M	7YR	E2-E12dup	DMD affected.	UCLA
CDMD 1066	F	40YR+	[E2-12dup];[=]	Carrier Mother of CDMD 1065	UCLA
CDMD 1067	M	5YR	E2-E12dup	DMD affected.	UCLA
MD1	M	8mos	WT	Undiagnosed muscular dystrophy	UCLA
MD2	F	40YR+	WT	Mother of MD1	UCLA
MD3	M	40YR+	WT	Father of MD1	UCLA
LGMD2A-1	F	29YR	WT	LGMD2A affected	UMN
LGMD2A-2	M	40YR+	WT	Father of LGMD2A-1	UMN
LGMD2A-3	F	40YR+	WT	Mother of LGMD2A-1	UMN

Sample ID	Sex	Age	DMD Mutation	Genetic Diagnosis and Relationship(s)	Source
GM02339	M	20FW	E31-43del	DMD affected	Coriell
GM03604	M	4YR	E19del	DMD affected	Coriell
GM03781	M	11YR	E2or3-17del	DMD affected. Coriell Family ID 533, brother of GM03783	Coriell
GM03783	M	10YR	E2or3-17del	DMD affected. Coriell Family ID 533, brother of GM03781	Coriell
GM05017	M	12YR	E45-50del	DMD affected. Coriell Family ID 174	Coriell
GM05114	M	22YR	E45del	DMD affected. Coriell Family ID 282; brother of GM05112, son of GM05118	Coriell
GM05118	M	44YR	WT	Coriell Family ID 282; father of GM05112, son of GM05114	Coriell
GM05123	M	16YR	E45-62dup	DMD affected. Coriell Family ID 367	Coriell
GM05128	M	15YR	ND	DMD affected. Coriell Family ID 577	Coriell
GM05160	M	57YR	WT	Coriell Family ID 824, father of GM05162	Coriell
GM05162	M	13YR	E46-50del	DMD affected. Coriell Family ID 824, son of GM05160	Coriell
GM05169	M	9YR	E4-43del	DMD affected. Coriell Family ID 619, son of GM05171	Coriell
GM05171	M	49YR	WT	Coriell Family ID 619, father of GM05169	Coriell
GM05263	M	12YR	c.7893delC	DMD affected. Coriell Family ID 767	Coriell

**Table 2.** cDMD genetic confirmation, *TERT* immortalization, and LV-MyoD-ER(T) reprogramming. WT, wildtype. ND, not determined.

Sample ID	DMD Mutation	CGH Array Reported DMD Mutation	Approx CGH L bkpt	Approx CGH R bkpt	Exome Sequencing Reported DMD Mutation	Whole Genome Sequencing Reported DMD Mutation	LV-h <i>TERT</i> Immortalization	LV-MyoD-ER(T) Reprogramming
CDMD1001	WT	WT					+	+
CDMD1002	WT	WT					+	+
CDMD1003	E46-51del	E46-51del	31681035	31860410			+	+
CDMD1004	WT	ND						
CDMD1006	E46-47del	E46-47del	31841327	31881610			+	
CDMD1008	E50dup	E50dup	31745687	31761440	E50dup	+	+	+
CDMD1012	E8-11del	E8-11del	32564413	32629333				
CDMD1013	E51del	pending			E51del	+		
CDMD1015	E45del	E45del	31887521	31932915				
CDMD1021	E2dup	1idup, 2idel	32931466	32959848	E2dup			
CDMD1022	[E12-22dup];[=]	E12-22dup	32399923	32568632				
CDMD1023	E3-23del	E3-23del	32395437	32804986	E3-23del			
CDMD1024	E6-7dup	E6-7dup	32705820	32750232				
CDMD1025	[E6-7dup];[=]	E6-7dup	32709528	32748099				
CDMD1026	E51-54del	E51-54del	31560237	31719007	E51-54del			
CDMD1027	ND	ND						
CDMD1028	c.[4100_delT];[=]	i44dup?				ND		
CDMD1029	c.4100_delT	ND						
CDMD1044	E45-50del	pending					+	+
CDMD1045	E45-50del	pending					+	
CDMD1056	E49-50del	pending					+	
GM02339	E31-43del	E31-43del	32182474	32326643			+	+
GM03781	E2or3-17del	pending					+	
GM03783	E2or3-17del	pending					+	
GM05017	E45-50del	E45-50del	31723152	31927030			+	+
GM05114	E45del	E45del	31867286	32031086			+	+
GM05123	E45-62dup	E45-62dup	31224256	31980749				
GM05128	ND	ND					+	
GM05160	WT	pending					+	
GM05162	E46-50del	E46-50del	31720281	31869209			+	+
GM05263	c.7893delC	pending					+	

## References

1. Monaco AP, Bertelson CJ, Middlesworth W, Colletti CA, Aldridge J, et al. (1985) Detection of deletions spanning the Duchenne muscular dystrophy locus using a tightly linked DNA segment. *Nature* 316: 842-845.
2. Emery AE (2002) The muscular dystrophies. *Lancet* 359: 687-695.
3. Hoffman EP, Brown RH, Jr., Kunkel LM (1987) Dystrophin: the protein product of the Duchenne muscular dystrophy locus. *Cell* 51: 919-928.
4. Bonilla E, Samitt CE, Miranda AF, Hays AP, Salviati G, et al. (1988) Duchenne muscular dystrophy: deficiency of dystrophin at the muscle cell surface. *Cell* 54: 447-452.
5. Petrof BJ, Shrager JB, Stedman HH, Kelly AM, Sweeney HL (1993) Dystrophin protects the sarcolemma from stresses developed during muscle contraction. *Proc Natl Acad Sci U S A* 90: 3710-3714.
6. Bushby K, Finkel R, Birnkrant DJ, Case LE, Clemens PR, et al. (2010) Diagnosis and management of Duchenne muscular dystrophy, part 1: diagnosis, and pharmacological and psychosocial management. *Lancet Neurol* 9: 77-93.
7. Bushby K, Finkel R, Birnkrant DJ, Case LE, Clemens PR, et al. (2010) Diagnosis and management of Duchenne muscular dystrophy, part 2: implementation of multidisciplinary care. *Lancet Neurol* 9: 177-189.
8. McNally EM (2007) New approaches in the therapy of cardiomyopathy in muscular dystrophy. *Annu Rev Med* 58: 75-88.
9. Tinsley J, Deconinck N, Fisher R, Kahn D, Phelps S, et al. (1998) Expression of full-length utrophin prevents muscular dystrophy in mdx mice. *Nat Med* 4: 1441-1444.
10. Perkins KJ, Burton EA, Davies KE (2001) The role of basal and myogenic factors in the transcriptional activation of utrophin promoter A: implications for therapeutic up-regulation in Duchenne muscular dystrophy. *Nucleic Acids Res* 29: 4843-4850.
11. Tinsley JM, Fairclough RJ, Storer R, Wilkes FJ, Potter AC, et al. (2011) Daily treatment with SMTc1100, a novel small molecule utrophin upregulator, dramatically reduces the dystrophic symptoms in the mdx mouse. *PLoS One* 6: e19189.
12. van Deutekom JC, Janson AA, Ginjaar IB, Frankhuizen WS, Aartsma-Rus A, et al. (2007) Local dystrophin restoration with antisense oligonucleotide PRO051. *N Engl J Med* 357: 2677-2686.
13. Kinali M, Arechavala-Gomez V, Feng L, Cirak S, Hunt D, et al. (2009) Local restoration of dystrophin expression with the morpholino oligomer AVI-4658 in Duchenne muscular dystrophy: a single-blind, placebo-controlled, dose-escalation, proof-of-concept study. *Lancet Neurol* 8: 918-928.
14. Goemans NM, Tulinius M, van den Akker JT, Burm BE, Ekhart PF, et al. (2011) Systemic administration of PRO051 in Duchenne's muscular dystrophy. *N Engl J Med* 364: 1513-1522.
15. Cirak S, Arechavala-Gomez V, Guglieri M, Feng L, Torelli S, et al. (2011) Exon skipping and dystrophin restoration in patients with Duchenne muscular dystrophy after systemic

phosphorodiamidate morpholino oligomer treatment: an open-label, phase 2, dose-escalation study. *Lancet* 378: 595-605.

16. Welch EM, Barton ER, Zhuo J, Tomizawa Y, Friesen WJ, et al. (2007) PTC124 targets genetic disorders caused by nonsense mutations. *Nature* 447: 87-91.

17. Mendell JR, Campbell K, Rodino-Klapac L, Sahenk Z, Shilling C, et al. (2010) Dystrophin immunity in Duchenne's muscular dystrophy. *N Engl J Med* 363: 1429-1437.

18. Bowles DE, McPhee SW, Li C, Gray SJ, Samulski JJ, et al. (2012) Phase 1 gene therapy for Duchenne muscular dystrophy using a translational optimized AAV vector. *Mol Ther* 20: 443-455.

19. Price FD, Kuroda K, Rudnicki MA (2007) Stem cell based therapies to treat muscular dystrophy. *Biochim Biophys Acta* 1772: 272-283.

20. Kalman L, Leonard J, Gerry N, Tarleton J, Bridges C, et al. (2011) Quality assurance for Duchenne and Becker muscular dystrophy genetic testing: development of a genomic DNA reference material panel. *J Mol Diagn* 13: 167-174.

21. Mamchaoui K, Trollet C, Bigot A, Negroni E, Chaouch S, et al. (2011) Immortalized pathological human myoblasts: towards a universal tool for the study of neuromuscular disorders. *Skelet Muscle* 1: 34.

22. Bodnar AG, Ouellette M, Frolkis M, Holt SE, Chiu CP, et al. (1998) Extension of life-span by introduction of telomerase into normal human cells. *Science* 279: 349-352.

23. Franco S, MacKenzie KL, Dias S, Alvarez S, Raffi S, et al. (2001) Clonal variation in phenotype and life span of human embryonic fibroblasts (MRC-5) transduced with the catalytic component of telomerase (hTERT). *Exp Cell Res* 268: 14-25.

24. Zhu CH, Mouly V, Cooper RN, Mamchaoui K, Bigot A, et al. (2007) Cellular senescence in human myoblasts is overcome by human telomerase reverse transcriptase and cyclin-dependent kinase 4: consequences in aging muscle and therapeutic strategies for muscular dystrophies. *Aging Cell* 6: 515-523.

25. Hayflick L (1965) The Limited in Vitro Lifetime of Human Diploid Cell Strains. *Exp Cell Res* 37: 614-636.

26. Lassar AB, Paterson BM, Weintraub H (1986) Transfection of a DNA locus that mediates the conversion of 10T1/2 fibroblasts to myoblasts. *Cell* 47: 649-656.

27. Davis RL, Weintraub H, Lassar AB (1987) Expression of a single transfected cDNA converts fibroblasts to myoblasts. *Cell* 51: 987-1000.

28. Weintraub H, Tapscott SJ, Davis RL, Thayer MJ, Adam MA, et al. (1989) Activation of muscle-specific genes in pigment, nerve, fat, liver, and fibroblast cell lines by forced expression of MyoD. *Proc Natl Acad Sci U S A* 86: 5434-5438.

29. Tapscott SJ, Weintraub H (1991) MyoD and the regulation of myogenesis by helix-loop-helix proteins. *J Clin Invest* 87: 1133-1138.

30. Montarras D, Chelly J, Bober E, Arnold H, Ott MO, et al. (1991) Developmental patterns in the expression of Myf5, MyoD, myogenin, and MRF4 during myogenesis. *New Biol* 3: 592-600.

31. Braun T, Buschhausen-Denker G, Bober E, Tannich E, Arnold HH (1989) A novel human muscle factor related to but distinct from MyoD1 induces myogenic conversion in 10T1/2 fibroblasts. *EMBO J* 8: 701-709.
32. Wright WE, Sassoon DA, Lin VK (1989) Myogenin, a factor regulating myogenesis, has a domain homologous to MyoD. *Cell* 56: 607-617.
33. Edmondson DG, Olson EN (1989) A gene with homology to the myc similarity region of MyoD1 is expressed during myogenesis and is sufficient to activate the muscle differentiation program. *Genes Dev* 3: 628-640.
34. Miner JH, Wold B (1990) Herculin, a fourth member of the MyoD family of myogenic regulatory genes. *Proc Natl Acad Sci U S A* 87: 1089-1093.
35. Lattanzi L, Salvatori G, Coletta M, Sonnino C, Cusella De Angelis MG, et al. (1998) High efficiency myogenic conversion of human fibroblasts by adenoviral vector-mediated MyoD gene transfer. An alternative strategy for ex vivo gene therapy of primary myopathies. *J Clin Invest* 101: 2119-2128.
36. Chaouch S, Mouly V, Goyenvalle A, Vulin A, Mamchaoui K, et al. (2009) Immortalized skin fibroblasts expressing conditional MyoD as a renewable and reliable source of converted human muscle cells to assess therapeutic strategies for muscular dystrophies: validation of an exon-skipping approach to restore dystrophin in Duchenne muscular dystrophy cells. *Hum Gene Ther* 20: 784-790.
37. Kimura E, Han JJ, Li S, Fall B, Ra J, et al. (2008) Cell-lineage regulated myogenesis for dystrophin replacement: a novel therapeutic approach for treatment of muscular dystrophy. *Hum Mol Genet* 17: 2507-2517.
38. Karumbayaram S, Lee P, Azghadi SF, Cooper AR, Patterson M, et al. (2012) From skin biopsy to neurons through a pluripotent intermediate under Good Manufacturing Practice protocols. *Stem Cells Transl Med* 1: 36-43.
39. Kendall GC, Mokhonova EI, Moran M, Sejbuk NE, Wang DW, et al. (2012) Dantrolene enhances antisense-mediated exon skipping in human and mouse models of Duchenne muscular dystrophy. *Sci Transl Med* 4: 164ra160.
40. Pombo-Suarez M, Calaza M, Gomez-Reino JJ, Gonzalez A (2008) Reference genes for normalization of gene expression studies in human osteoarthritic articular cartilage. *BMC Mol Biol* 9: 17.
41. Beggs AH, Koenig M, Boyce FM, Kunkel LM (1990) Detection of 98% of DMD/BMD gene deletions by polymerase chain reaction. *Hum Genet* 86: 45-48.
42. Chamberlain JS, Gibbs RA, Ranier JE, Nguyen PN, Caskey CT (1988) Deletion screening of the Duchenne muscular dystrophy locus via multiplex DNA amplification. *Nucleic Acids Res* 16: 11141-11156.
43. Kunkel LM, Snyder JR, Beggs AH, Boyce FM, Feener CA (1991) Searching for dystrophin gene deletions in patients with atypical presentations. *Etiology of Human Diseases at the DNA Level*. New York: Raven Press. pp. 51-60.
44. Muntoni F, Torelli S, Ferlini A (2003) Dystrophin and mutations: one gene, several proteins, multiple phenotypes. *Lancet Neurol* 2: 731-740.

45. Monaco AP, Bertelson CJ, Liechti-Gallati S, Moser H, Kunkel LM (1988) An explanation for the phenotypic differences between patients bearing partial deletions of the DMD locus. *Genomics* 2: 90-95.
46. Baumbach LL, Chamberlain JS, Ward PA, Farwell NJ, Caskey CT (1989) Molecular and clinical correlations of deletions leading to Duchenne and Becker muscular dystrophies. *Neurology* 39: 465-474.
47. Koenig M, Beggs AH, Moyer M, Scherpf S, Heindrich K, et al. (1989) The molecular basis for Duchenne versus Becker muscular dystrophy: correlation of severity with type of deletion. *Am J Hum Genet* 45: 498-506.
48. Charrasse S, Comunale F, Grumbach Y, Poulat F, Blangy A, et al. (2006) RhoA GTPase regulates M-cadherin activity and myoblast fusion. *Mol Biol Cell* 17: 749-759.
49. Aartsma-Rus A, Van Deutekom JC, Fokkema IF, Van Ommen GJ, Den Dunnen JT (2006) Entries in the Leiden Duchenne muscular dystrophy mutation database: an overview of mutation types and paradoxical cases that confirm the reading-frame rule. *Muscle Nerve* 34: 135-144.
50. Aartsma-Rus A, Fokkema I, Verschuuren J, Ginjaar I, van Deutekom J, et al. (2009) Theoretic applicability of antisense-mediated exon skipping for Duchenne muscular dystrophy mutations. *Hum Mutat* 30: 293-299.

## CHAPTER THREE

### Dantrolene Enhances Antisense-Mediated Exon Skipping in Human and Mouse Models of Duchenne Muscular Dystrophy



## Dantrolene Enhances Antisense-Mediated Exon Skipping in Human and Mouse Models of Duchenne Muscular Dystrophy

Genevieve C. Kendall *et al.*  
*Sci Transl Med* 4, 164ra160 (2012);  
DOI: 10.1126/scitranslmed.3005054

Editor's Summary

### Superior Skipping with a Little Help from Dantrolene

Hopes have been raised for patients with Duchenne muscular dystrophy, a genetic disease in which muscles rapidly degenerate in young boys: An antisense oligonucleotide can restore the missing protein dystrophin. Usually, its transcription is truncated because of a mutation in the dystrophin gene, but the antisense drug targets the defect and allows transcription to bypass the mutation—a process called exon skipping. Two clinical trials have shown promising results, with restoration of 2 to 16% of the normal amount of dystrophin. However, these results were too variable and dystrophin levels too low to realize the full potential of exon skipping to improve muscle function. Therefore, to augment the effects of this promising drug, Kendall *et al.* screened a large number of small molecules and found one—dantrolene—that increases antisense-induced exon skipping in a mouse model of muscular dystrophy and in patient cells.

In testing 300 compounds from a drug library on cells also treated with an exon-skipping antisense directed to a human dystrophin reporter gene, the authors found several that scored positive. Of these, they chose dantrolene for further follow-up because it is already used in the clinic (for malignant hyperthermia) and has been tested in Duchenne muscular dystrophy patients, where it showed few side effects. The investigators found that dantrolene promoted exon 23 skipping in cells from *mdx* mice (a mouse model of muscular dystrophy) and exon 51 skipping in patient fibroblasts induced to form myotubes. Dantrolene worked in an animal model of DMD as well. When antisense was injected intravenously into *mdx* mice, dantrolene given systemically augmented exon skipping, resulting in additional dystrophin multiple muscles including the tibialis anterior, gastrocnemius, diaphragm, and quadriceps, but not heart or the triceps. Dantrolene-treated mice were also stronger than those treated with antisense alone and could hang on a wire for 50% longer. Other drugs that, like dantrolene, are antagonists at the ryanodine receptor have the same effect, suggesting that this intracellular calcium channel is the critical target for dantrolene's effect. Exactly how and in what cells this occurs is not yet clear.

This class of ryanodine-targeting drugs may be able to change what has been a promising therapy for patients with muscular dystrophy to a reality, ready for testing.

**A complete electronic version of this article** and other services, including high-resolution figures, can be found at:

<http://stm.sciencemag.org/content/4/164/164ra160.full.html>

**Supplementary Material** can be found in the online version of this article at:

<http://stm.sciencemag.org/content/suppl/2012/12/10/4.164.164ra160.DC1.html>

**Related Resources for this article** can be found online at:

<http://stm.sciencemag.org/content/scitransmed/4/140/140ra89.full.html>

<http://stm.sciencemag.org/content/scitransmed/4/139/139ra85.full.html>

<http://stm.sciencemag.org/content/scitransmed/4/139/139fs19.full.html>

<http://stm.sciencemag.org/content/scitransmed/2/42/42ra54.full.html>

Information about obtaining **reprints** of this article or about obtaining **permission to reproduce this article** in whole or in part can be found at:

<http://www.sciencemag.org/about/permissions.dtl>

*Science Translational Medicine* (print ISSN 1946-6234; online ISSN 1946-6242) is published weekly, except the last week in December, by the American Association for the Advancement of Science, 1200 New York Avenue NW, Washington, DC 20005. Copyright 2012 by the American Association for the Advancement of Science; all rights reserved. The title *Science Translational Medicine* is a registered trademark of AAAS.

## MUSCULAR DYSTROPHY

# Dantrolene Enhances Antisense-Mediated Exon Skipping in Human and Mouse Models of Duchenne Muscular Dystrophy

Genevieve C. Kendall,<sup>1,2,3\*</sup> Ekaterina I. Mokhonova,<sup>3,4\*</sup> Miriana Moran,<sup>3,5</sup> Natalia E. Sejbuk,<sup>3,5</sup> Derek W. Wang,<sup>3,5</sup> Oscar Silva,<sup>5</sup> Richard T. Wang,<sup>1,3</sup> Leonel Martinez,<sup>3,4</sup> Qi L. Lu,<sup>6</sup> Robert Damoiseaux,<sup>7</sup> Melissa J. Spencer,<sup>3,4\*</sup> Stanley F. Nelson,<sup>1,2,3,8\*†</sup> M. Carrie Miceli<sup>2,3,5\*†</sup>

Duchenne muscular dystrophy (DMD) causes profound and progressive muscle weakness and loss, resulting in early death. DMD is usually caused by frameshifting deletions in the gene *DMD*, which leads to absence of dystrophin protein. Dystrophin binds to F-actin and components of the dystrophin-associated glycoprotein complex and protects the sarcolemma from contraction-induced injury. Antisense oligonucleotide-mediated exon skipping is a promising therapeutic approach aimed at restoring the *DMD* reading frame and allowing expression of an intact dystrophin glycoprotein complex. To date, low levels of dystrophin protein have been produced in humans by this method. We performed a small-molecule screen to identify existing drugs that enhance antisense-directed exon skipping. We found that dantrolene, currently used to treat malignant hyperthermia, potentiates antisense oligomer-guided exon skipping to increase exon skipping to restore the mRNA reading frame, the sarcolemmal dystrophin protein, and the dystrophin glycoprotein complex in skeletal muscles of *mdx* mice when delivered intramuscularly or intravenously. Further, dantrolene synergized with multiple weekly injections of antisense to increase muscle strength and reduce serum creatine kinase in *mdx* mice. Dantrolene similarly promoted antisense-mediated exon skipping in reprogrammed myotubes from DMD patients. Ryanodine and Rycal S107, which, like dantrolene, targets the ryanodine receptor, also promoted antisense-driven exon skipping, implicating the ryanodine receptor as the critical molecular target.

## INTRODUCTION

Duchenne muscular dystrophy (DMD) is a lethal X-linked recessive disease characterized by progressive muscle weakness (1). It is the most common childhood form of muscular dystrophy, affecting about 1 of 3500 male births (2). DMD is usually caused by out-of-frame multiexon deletions in the *DMD* gene that disrupt the reading frame of the transcript and impede production of dystrophin protein (3). Dystrophin is an essential component of the dystrophin glycoprotein complex (DGC), which links the actin cytoskeleton to the extracellular matrix (ECM) to provide sarcolemmal stability during muscle contraction and coordinates signal transducers at the sarcolemma. An N-terminal domain in dystrophin binds F-actin, and a C-terminal domain binds  $\beta$ -dystroglycan. The large central rod domain comprises spectrin repeats that are not all critical for protein function. Although the complete absence of dystrophin leads to rapid muscle degeneration, deletions in the rod domain that retain the reading frame result in a milder allelic disorder, Becker muscular dystrophy. These in-frame deletions can produce a

partially functional, albeit internally truncated, dystrophin protein capable of retaining the DGC at the sarcolemmal membrane and protecting the sarcolemma from contraction-induced damage (4–6).

An emerging therapy, exon skipping, targets individual exons for exclusion from mRNA by using an antisense oligonucleotide (AO) tailored to the patient's DNA mutation to change out-of-frame *DMD* mutations to in-frame deletions. AOs have successfully promoted *DMD* exon skipping and restored dystrophin protein expression in mice, dogs, and humans in clinical trials (5, 7–12). High-dose, chronic administration of an exon 23-directed AO in the *mdx* mouse substantially reduces pathology and increases muscle function, highlighting the promise of this therapy for human DMD (7, 13). About half of all DMD patients could be treated by AOs targeting one of six different exons (exons 51, 45, 53, 44, 52, 50), all of which are currently under development (14). Initial clinical trials are targeting *DMD* exon 51 skipping, which could potentially treat ~13% of *DMD* patients.

Two independent trials targeting human *DMD* exon 51, using 2'-O-methyl (2'OMe) phosphorothioate or phosphorodiamidate morpholino (PMO) backbone AO chemistries, have demonstrated early success (8–10). A recent phase 1 to 2a clinical trial with 2'OMe AO (6 mg/kg; Pro051/GSK2402968) given subcutaneously weekly increased dystrophin protein to 1.8 to 15.6% of normal levels after 12 weeks of treatment in DMD patients (8). In addition, PMO (20 mg/kg) directed against exon 51 (AVI4658/Eteplirsen) given intravenously weekly increased dystrophin protein to an average of 4.1% of normal levels after 12 weeks of therapy in patients with DMD (15). In both studies, exon-skipping efficacy and dystrophin expression varied greatly among patients, muscle groups, and individual fibers within a muscle (8, 15, 16). It is therefore unlikely that the amount of dystrophin produced by these AOs will be sufficient to optimally restore long-term function of diseased muscles. Rather,

<sup>1</sup>Department of Human Genetics, David Geffen School of Medicine, University of California, Los Angeles, Los Angeles, CA 90095, USA. <sup>2</sup>Molecular Biology Institute, University of California, Los Angeles, Los Angeles, CA 90095, USA. <sup>3</sup>Center for Duchenne Muscular Dystrophy, University of California, Los Angeles, Los Angeles, CA 90095, USA. <sup>4</sup>Department of Neurology, David Geffen School of Medicine, University of California, Los Angeles, Los Angeles, CA 90095, USA. <sup>5</sup>Department of Microbiology, Immunology, and Molecular Genetics, David Geffen School of Medicine and College of Letters and Sciences, University of California, Los Angeles, Los Angeles, CA 90095, USA. <sup>6</sup>Department of Neurology, McColl-Lockwood Laboratory of Muscular Dystrophy Research, Carolinas Medical Center, Charlotte, NC 28231, USA. <sup>7</sup>California Nanosciences Institute, University of California, Los Angeles, Los Angeles, CA 90095, USA. <sup>8</sup>Department of Pathology and Laboratory Medicine, University of California, Los Angeles, Los Angeles, CA 90095, USA. \*These authors contributed equally to this work.

†To whom correspondence should be addressed. E-mail: cmiceli@ucla.edu (M.C.M.); snelson@ucla.edu (S.F.N.)

improvements in exon-skipping efficiency and a more uniform restoration of dystrophin protein in all muscle groups with low AO dose could render chronic administration of expensive AOs practical or reduce toxicity. Here, we describe the implementation of a strategy to identify compounds that synergize with AOs to promote exon skipping and identify dantrolene, an already Food and Drug Administration (FDA)-approved drug with the capacity to potentiate *DMD* exon skipping.

## RESULTS

### High-throughput screening identifies compounds that enhance AO-mediated *DMD* exon skipping

We screened the BioMol library of small-molecule drugs using a mouse myoblast cell line (C2C12) that expressed a human *DMD* exon 50 green fluorescent protein (Ex50GFP)-based reporter (17), adapted to minimize experimental variation when used in an automated, quantitative fluorescent scanning system. In the reporter cells, skipping of *DMD* exon 50 resulted in fluorescent GFP expression, which was quantified with a high-resolution and high-throughput cell imaging system to observe fluorescence per cell. The molecules in the library were screened at an effective concentration of 1 or 10  $\mu\text{M}$  in the presence or absence of a suboptimal concentration of 2'OMe AO (h50AON) that targeted the splice acceptor site of human *DMD* exon 50. AO was added before incubation of the cells with the small-molecule drugs to identify molecules that facilitate AO-mediated exon skipping rather than AO delivery and to avoid complications of enhanced drug delivery by the AO transfection reagent. Compounds were rank-ordered on the basis of the average fluorescence intensity, and the top 5% of the compounds from the with-AO screens (+AO) ( $n = 15$ ) were chosen as lead hits (Fig. 1 and table S1). Within the group of drugs identified in the +AO screen, there was an overrepresentation of compounds modulating intracellular calcium, including dantrolene and ryanodine, both known to target the ryanodine receptor (18).

Eight of the most readily available compounds were selected for secondary screening in serial titrations, and three caused a 10% increase in fluorescence when given with the Ex50GFP +AO treatment when compared to the reporter line without AO, as well as exhibited dose dependence: cyclopiazonic acid, dantrolene, and H-7 (fig. S1). We followed up hits that only had activity in the context of sensitizing +AO screen to minimize the likelihood of identifying compounds with promiscuous skipping activity. Dantrolene was of high interest because it is used clinically as a chronic treatment for malignant hyperthermia and muscle spasticity (19, 20). Additionally, oral dantrolene is a potential therapy for DMD patients because it reduces calcium leak through the ryanodine receptor (21, 22). In DMD patients treated with dantrolene daily for 2 years, serum creatine kinase (CK) levels (an index of muscle membrane damage) were slightly reduced, and there was a modest improvement on the manual muscle test, without substantial harmful side effects (21). Similarly, dantrolene treatment of *mdx* mice lowers serum CK (22). Therefore, dantrolene was an attractive candidate to evaluate first as a modulator of exon skipping in vivo in *mdx* mice and in vitro in human cells carrying *DMD* mutations.

### Dantrolene increases exon skipping in cultured *mdx* mouse and DMD patient cells

Dantrolene enhancement of AO-directed *DMD* exon skipping was assessed in primary mouse and human muscle cells with *DMD* muta-

tions. The *mdx* mouse is a popular DMD model in which skipping of the exon 23 nonsense mutation results in rescue of an internally deleted *DMD* transcript, dystrophin protein expression, and improved muscle function. In C57BL/6 and *mdx* mouse myoblasts that had been fused to form myotubes in culture, dantrolene potentiated the effects of 2'OMe AO M23D (overlapping splice donor site from +02 to -18) to facilitate *Dmd* exon 23 skipping (Fig. 2, A to C). Increasing concentrations of M23D shifted the *Dmd* mRNA from the full-length, unskipped form to exon 23-skipped or dual exon 22- and exon 23-skipped forms (Fig. 2A). A suboptimal dose of 100 nM M23D generated about 10% of the maximal skipping observed with 600 nM M23D in myotubes and was selected for further measurements of exon 23-skipping potentiation. After incubating myotubes with suboptimal M23D, the AO was removed, and dantrolene was added for 48 hours, which is a sufficient time to allow for the 16 hours required to complete transcription and splicing of new *Dmd* mRNA (23). mRNA containing exons 20 to 26 was assessed for exon 23 skipping by reverse transcription polymerase chain reaction (RT-PCR) (5). Dantrolene increased the amount of exon 23-skipped mRNA at both 25 and 50  $\mu\text{M}$  (Fig. 2, A to C). *Dmd* exon 23 skipping was quantified in these same RNA samples with a TaqMan-based assay with primer-probe sets spanning the *Dmd* splice junctions of exons 22 to 24 (exon skip-specific junction) and exons 22 to 23 (full-length specific junction) (Fig. 2B). Dantrolene increased M23D-mediated *Dmd* exon 23 skipping twofold relative to myotubes treated only with M23D (Fig. 2B). In the absence of M23D, dantrolene failed to induce exon 23 skipping, indicating that it acts synergistically with AO to promote skipping.

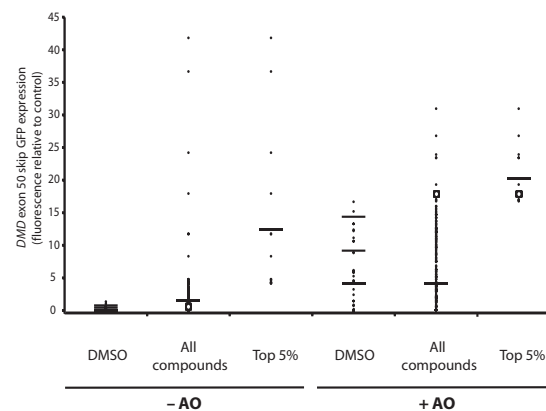


**Fig. 1.** High-throughput screening identifies dantrolene as a modulator of AO-mediated human *DMD* exon 50 skipping. Results of the high-throughput screen for enhancers of AO-mediated *DMD* exon 50 skipping. The orphan ligand, ion channel, enzyme inhibitor, and endocannabinoid libraries from the BioMol chemical library ( $n = 300$ ) were screened at 1 or 10  $\mu\text{M}$  in the presence or absence of 2'OMe 27-mer h50AON (-19 to +8) targeting human *DMD* exon 50. Successful skipping of *DMD* exon 50 created in-frame GFP expression and fluorescence. Each plotted data point represents the average normalized fluorescence of six replicates in the -AO screen and three replicates in the +AO screen for the DMSO carrier controls, all compounds, and the top 5% (15 compounds). Open circles, fluorescence for dantrolene; bold horizontal lines, mean fluorescence; other horizontal lines, 1 and 2 SDs away from the mean.

Dantrolene also increased human *DMD* exon 51 skipping in DMD patient fibroblast-derived inducible directly reprogrammable myotubes (iDRMs), demonstrating efficacy in a disease-relevant mutational context. iDRMs are DMD patient dermal fibroblasts transduced with HTERT and inducible MyoD vectors (24) that can transdifferentiate into multinuclear myotubes in culture upon 4OH-tamoxifen induction of MyoD and exposure to differentiation media. The *DMD* genomic mutation in iDRM5017 was confirmed as an exon 45 to 50 deletion, predicted to be rendered in frame by skipping *DMD* exon 51 (fig. S2).

Within 6 days of 4OH-tamoxifen induction of MyoD activity and cell fusion, the iDRM DMD cells became multinucleated and expressed multiple muscle differentiation markers, including myosin heavy chain, myogenin, ryanodine receptor type 1 (RyR1), and (mutant) dystrophin mRNA or protein (fig. S3). We assessed exon 51 skipping activity with an exon 51 2'OMe AO (h51AON) that had a sequence equivalent to Pro051 directed at an exonic splicing enhancer (ESE) sequence (10). AO was added after fusion for 1 day and was removed from the supernatant before dantrolene addition for 2 days. A nested RT-PCR was

performed between *DMD* exons 43 and 52 to determine the amount of exon 51 skipping. Dantrolene enhanced exon 51 skipping in the presence of the suboptimal dose of AO by up to 10-fold relative to the vehicle control (Fig. 2D). Therefore, dantrolene exhibited synergy with two different AOs that target distinct regions of the *DMD* mRNA transcript in both human and mouse DMD myotubes. Because up to 13% of DMD mutations can be rendered in frame by *DMD* exon 51 skipping and clinical trials aimed at AO-directed exon 51 skipping are under way, these findings demonstrate the potential efficacy of dantrolene in synergizing with skipping AOs in therapeutically relevant systems.

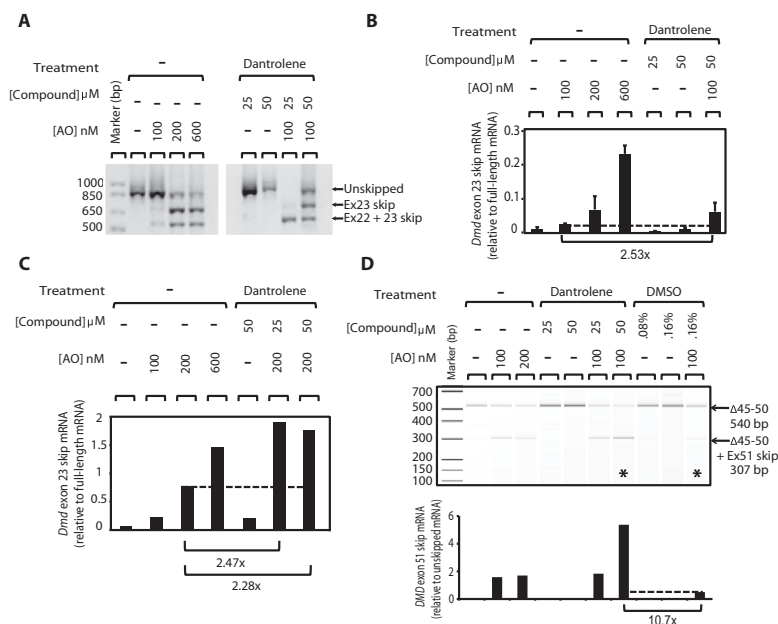


**Fig. 2.** Dantrolene synergizes with AO to promote *DMD* exon skipping in mouse and human DMD myotubes in culture. **(A)** Effect of dantrolene on AO M23D-induced exon 23 skipping in primary mouse myoblasts fused to myotubes in culture, assessed with nested RT-PCR. Exon 23 skipping was evaluated in cultured myotubes transfected with 2'OMe M23D (+02 to -18) or mock-transfected. Four hours after transfection, AO was removed, and myotubes were treated with dantrolene for 48 hours. Nested RT-PCR was performed between exons 20 and 26 (5). The full-length mRNA product [901 base pairs (bp)] and the exon 23-skipped and exon 22 to 23 double-skipped mRNA products (688 and 542 bp, respectively) are shown. **(B)** Effect of dantrolene on AO M23D-induced exon 23 skipping in cultured myotubes, assessed with a TaqMan-based assay. Quantified *Dmd* exon 23-skipped transcript levels were obtained with primer-probe sets spanning the specific splice junctions of exons 22 to 24 (exon 23 skip product) and exons 22 to 23 (full-length product) (39). *C<sub>t</sub>* values were normalized to the ribosomal gene *Rplp0* and are displayed as the relative exon 23 skip/full-length mRNA levels. Error bars indicate means  $\pm$  SD of qPCR triplicates. **(C)** Effect of dantrolene on AO M23D-induced exon 23 skipping in *mdx* cultured myotubes, assessed with nested RT-PCR between *Dmd* exons 20 and 26 and quantitated with densitometry. **(D)** Effect of dantrolene on h51AON-induced exon 51 skipping in human iDRM cells, assessed with a nested RT-PCR. Immortalized patient fibroblasts with a *DMD* exon 45 to 50 deletion were transduced with a lentiviral vector expressing inducible MyoD to create iDRMs (24). iDRM5017s induced for MyoD activity were cultured in the presence of h51AON for 24 hours, after which dantrolene or vehicle was added in fresh media. Total RNA was isolated 2 days later, and a nested RT-PCR was performed spanning exons 43 to 52. *DMD* exon 51 skipping was quantitated with the Agilent Bioanalyzer and is represented as the mRNA ratio of the exon 51 skip (307-bp product) relative to the unskipped (540-bp product). All experiments were repeated independently at least twice.

### Dantrolene synergizes with intramuscular PMOE23 to enhance *Dmd* exon 23 skipping in *mdx* mice

To assess the ability of dantrolene to potentiate AO-mediated exon skipping *in vivo* in a mouse model of DMD, we systemically administered dantrolene in combination with a single local intramuscular injection of morpholino AO into the tibialis anterior (TA) of *mdx* mice. PMOE23 hybridizes to the mutated exon 23 splice donor site +07 to -18, thus forcing exclusion of exon 23, which, when removed from the mRNA, creates an in-frame *Dmd* message. PMOE23 (10 μg) was used as a positive control, and 2 μg was selected as a suboptimal dose (7). To evaluate whether dantrolene could synergize with PMOE23 to skip *Dmd* exon 23 and result in dystrophin protein expression, we administered dantrolene at doses of 10 or 20 mg/kg per day by intraperitoneal injection for 9 days after suboptimal PMOE23 injection (table S2). The TA was harvested on the 10th day and divided for analysis into six to nine sequential intervals to ensure that the entire length of the muscle was analyzed for *Dmd* exon-skipping activity.

Tissue from four central intervals was pooled for Western blot analysis. Treatment with dantrolene at either dose in combination with 2  $\mu$ g of PMOE23 increased expression of dystrophin protein to levels equivalent to those induced by the higher 10- $\mu$ g dose of PMOE23 (Fig. 3, A and B).

We also stained TA cross-sections and found that dystrophin protein was properly localized to the sarcolemma (Fig. 3D). Further, when we quantitated total fluorescence from the TA by scanning the four maximal consecutive intervals per mouse for each experimental group (Fig. 3C), we found that dystrophin quantification by immunofluorescence and Western blot was highly concordant, showing an approximate equivalence between the 10- $\mu$ g dose of PMOE23 alone and the 2- $\mu$ g dose of PMOE23 in combination with dantrolene (Fig. 3, B and

C). Central intervals from an independent experiment were analyzed for increased exon 23 skipping by RT-PCR and a TaqMan-based assay, providing corroboration that dantrolene synergizes with intramuscular injection of PMOE23 to facilitate mRNA exon skipping (Fig. 4, A and B, and fig. S4). Corresponding dystrophin protein levels are shown in fig. S4. Dantrolene rescued dystrophin expression only in the presence of PMOE23, reflecting synergistic activity of dantrolene with PMOE23 in vivo to promote exon skipping.

#### Dantrolene synergizes with PMOE23 to promote dystrophin expression in multiple *mdx* muscles

Systemic administration of dantrolene and PMOE23 enhanced *Dmd* exon 23 skipping and induced appropriately localized dystrophin protein

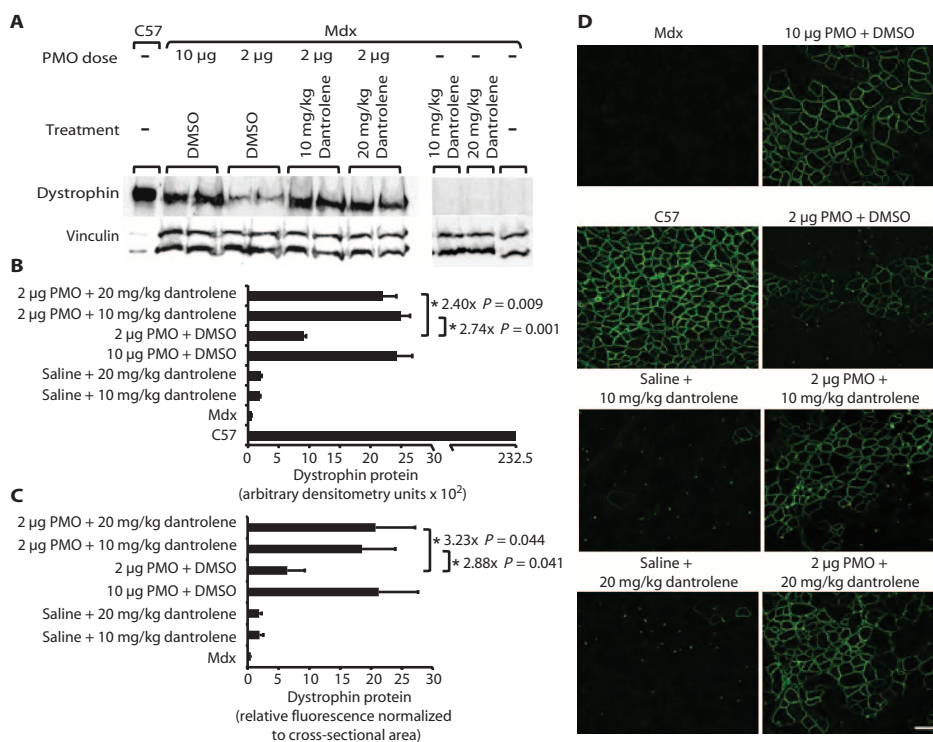


**Fig. 3.** Dantrolene synergizes with intramuscularly injected PMOE23 to restore sarcolemmal dystrophin protein expression in *mdx* mice. One dose of 10 or 2  $\mu$ g of morpholino PMOE23 (+07 to -18) was injected into the TA of *mdx* mice on day 1, and dantrolene was administered by intraperitoneal injection at 10 or 20 mg/kg per day for 9 days. The TA was harvested on day 11, sectioned, and ordered into six to nine 850- $\mu$ m serial intervals spanning the entire muscle. (A) Effect of dantrolene on PMOE23-induced skipped dystrophin protein expression shown by representative dystrophin immunoblots. Control C57Bl/6 protein was loaded at 5  $\mu$ g per lane, and *mdx* samples were loaded at 50  $\mu$ g per lane. (B) Effect of dantrolene on PMOE23-induced skipped dystrophin protein in the TA muscle as measured by densitometry of MANDYS8 immunoblots. Data were averaged for all mice from each treat-

ment group. (C) Effect of dantrolene on PMOE23-induced skipped dystrophin protein in the TA as detected by quantitative immunofluorescence. Total fluorescence from TA cross-sections was quantitated with an automated scanner and normalized to surface area scanned. Total fluorescence from four maximal consecutive intervals for every mouse in each treatment group was averaged and plotted as percentage of C57Bl/6 control. For *mdx* and C57Bl/6 control values, three intervals from one to two mice were used. (D) Effect of dantrolene on PMOE23 sarcolemmal dystrophin expression as illustrated by representative images from (C) exhibiting sarcolemmal dystrophin expression after treatment with PMOE23 + dantrolene. Scale bar, 100  $\mu$ m. Error bars in (B) and (C) represent the means  $\pm$  SD of three mice per experimental group. *P* values were determined with a Student's *t* test.

in multiple skeletal muscles. A single intravenous dose of PMOE23 (10 mg/kg) was used as a suboptimal dose, alone or in combination with twice-daily dosing of dantrolene (10 mg/kg per day) intraperitoneally for 6 days (7, 25) (table S3). A single intravenous dose of PMOE23 (100 mg/kg) was used as a positive control. We harvested skeletal muscles for analysis on day 7, including the quadriceps, gastrocnemius, TA, diaphragm, triceps, and heart. Muscles were assessed for (i) increased amounts of skipped *Dmd* exon 23 mRNA species, (ii) dystrophin protein rescue by Western blot and quantitative immunostaining, (iii) appropriate dystrophin subcellular localization, and (iv) restoration of other DGC components to the sarcolemmal membrane. Dantrolene significantly increased *Dmd* exon 23 mRNA skipping in an aggregate analysis of pooled skeletal muscle groups (Fig. 5A). Analysis of individual muscle groups demonstrated that dantrolene enhanced skipping in the gastrocnemius, TA, diaphragm, and quadriceps (fig. S5A). The effect was not apparent in the triceps, which have been previously described as difficult to target with systemic AOs (7). No skipping was observed in heart muscle under any condition. Western blot analysis for dystrophin protein was concordant with mRNA skipping in all muscle groups analyzed (Fig. 5, C and D, and figs. S5C and S6). Densitometry-based Western blot quantification of dystrophin in the quadriceps, gastrocnemius, TA, and diaphragm muscle from three treated mice per group

showed a mean threefold increase in protein abundance when PMOE23 (10 mg/kg) was administered with dantrolene compared to PMOE23 with vehicle (Fig. 5C). Quantitative dystrophin immunofluorescence corroborated the Western blot results (Figs. 5B and 6 and fig. S5B). Immunostaining revealed the presence of both the N and C termini of dystrophin and the correct sarcolemmal localization (Fig. 5E). Serial sections of the quadriceps indicated that fibers with dystrophin expression also exhibited other components of the DGC at the sarcolemma ( $\alpha$ -sarcoglycan and  $\beta$ -dystroglycan) (Fig. 5E). Dantrolene treatment together with PMOE23 (10 mg/kg) rescued the expression of  $\alpha$ -sarcoglycan and  $\beta$ -dystroglycan. The ability of rescued dystrophin to recruit other members of the DGC demonstrates its capacity to perform this critical function in vivo. Together, these data demonstrate that dantrolene synergizes with suboptimal doses of systemic PMOE23 to facilitate exon skipping and rescue dystrophin protein and sarcolemmal DGC expression in multiple muscles.

#### Dantrolene synergizes with repeated, systemic PMOE23 to improve muscle function in *mdx* mice

To determine whether dantrolene synergizes with AO administered over a longer period with multiple AO injections, we assessed *mdx* mice injected intravenously with PMOE23 (10 mg/kg) once weekly for 3 weeks alone or in combination with twice-daily dantrolene (10 mg/kg per day). Muscles were harvested on day 22, and RNA was analyzed from the TA for amounts of skipped and full-length *Dmd* mRNA. Again, we found that mice treated with the PMOE23 plus dantrolene combination showed enhanced *Dmd* mRNA exon 23 skipping relative to animals treated with either PMOE23 or dantrolene alone, demonstrating that synergy also occurred in the context of sustained treatment (Fig. 7A). PMOE23 treatment over a 2- to 3-week period leads to functional improvement in the *mdx* model as shown by reduced serum CK or increased skeletal muscle maximum tetanic force (7, 26). Therefore, our treatment protocol enabled us to assess whether enhanced exon 23 skipping was translated into functional gain over the course of sustained treatment. CK concentrations in the serum are elevated in *mdx* mice due to impaired muscle membrane integrity, and thus, reduction of serum CK often accompanies increased muscle function (27–29). We measured CK concentrations on day 16, 1 day after the third systemic PMOE23 injection, and found that mice treated with the PMOE23 and dantrolene combination showed significantly reduced CK concentrations relative to animals treated with PMOE23 alone (Fig. 7B). Similarly, mice were assessed for overall muscle strength by measuring the length of time they could hang on a wire. *mdx* mice treated with PMOE23 and dantrolene in combination were stronger than those treated with either PMOE23 or dantrolene alone (Fig. 7C). These findings demonstrate that dantrolene can enhance exon 23 skipping and rescue muscle function in the context of sustained treatment in *mdx* mice, a situation closer to that expected for patients in the clinic.

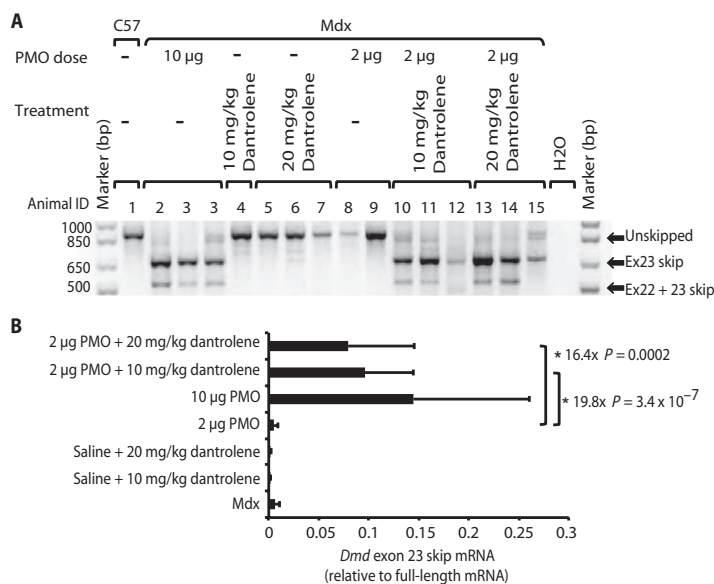


**Fig. 4.** Dantrolene synergizes with intramuscular PMOE23 to promote *DMD* exon 23 skipping in *mdx* mice. **(A)** Effect of dantrolene on PMOE23 induction of skipped *Dmd* mRNA in the TA muscle. Exon 23 skipping was detected by nested RT-PCR between *Dmd* exons 20 and 26. Full-length or exon 23-skipped RT-PCR banding patterns from representative mice are shown. **(B)** Effect of dantrolene on PMOE23 induction of skipped *Dmd* mRNA in TA muscle as assessed by quantitative TaqMan assay. Two central intervals from a single TA muscle/mouse were assessed, and the average ratio of exon 23-skipped to unskipped mRNA species is plotted for each treatment group (means  $\pm$  SD) [mice per group;  $n = 2$  saline + dantrolene (10 mg/kg) and 2  $\mu$ g PMOE23 groups,  $n = 3$  in all other experimental groups].  $P$  values were determined with a Student's  $t$  test. Assessment of dystrophin protein expression from this same experiment is shown in fig. S4.

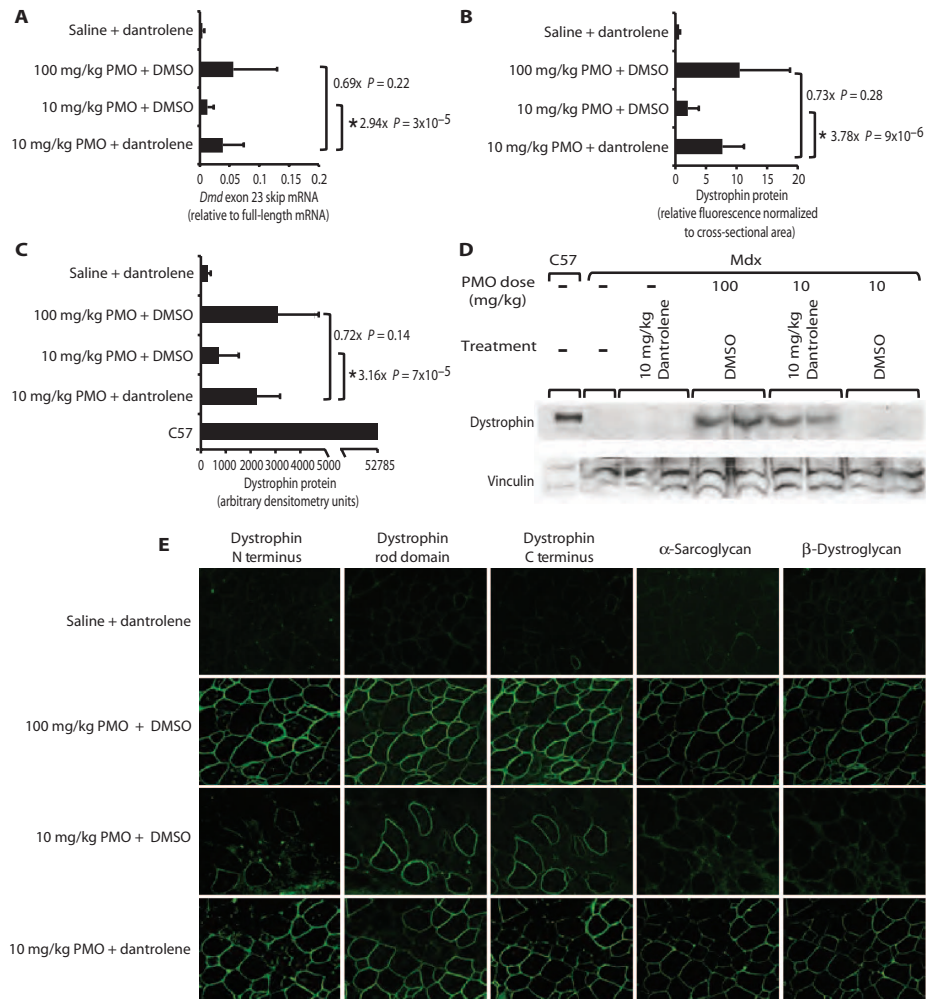


**Fig. 5.** Dantrolene synergizes with intravenously delivered PMOE23 to promote exon 23 skipping and rescue sarcolemmal dystrophin and DGC in *mdx* mice. A single systemic dose of 100 mg/kg or suboptimal 10 mg/kg of morpholino PMOE23 was administered intravenously by tail vein injection on day 1, followed by intraperitoneal injections of dantrolene (10 mg/kg per day) until harvesting on day 7. **(A)** Effect of dantrolene on PMOE23 induction of *Dmd* exon 23 skipping assessed by qPCR for the quadriceps, gastrocnemius, TA, and diaphragm. mRNA from each muscle in each treatment group was quantified independently, and data from all four muscle groups were averaged and plotted as the mean of exon 23-skipped/full-length mRNA ratio. **(B)** Effect of dantrolene on PMOE23-induced skipped dystrophin protein as measured by quantitative immunofluorescence of skeletal muscles. One cross-section per muscle per animal was evaluated for dystrophin expression, and data are presented as relative fluorescence normalized to cross-sectional area for each treatment group. **(C)** Effect of dantrolene on PMOE23-induced skipped dystrophin protein as measured by Western blot of skeletal muscles. Western blots from each

muscle were quantitated by densitometry and averaged across the four muscles for each treatment group. **(D)** Representative Western blots for dystrophin protein expression from gastrocnemius muscles are shown. C57Bl/6 protein was loaded at  $1/10$  of the protein concentration of experimental samples. **(E)** Effect of dantrolene on PMOE23-induced rescue of DGC components as illustrated by representative immunofluorescence images of serial cross-sections from treated *mdx* quadriceps. Dystrophin was detected with antibodies specific to the N terminus (Manex1a), rod domain (MANDYS8), and C terminus (Ab15277). Additional DGC components,  $\alpha$ -sarcoglycan and  $\beta$ -dystroglycan, were detected with NCL- $\alpha$ -SARC and NCL- $\beta$ -DG antibodies, respectively. Scale bar, 50  $\mu$ m. Error bars in (A) to (C) represent means  $\pm$  SD of readout for four muscles of all mice in each treatment group [ $n = 3$  animals or  $n = 12$  observations in saline + dantrolene and PMOE23 (100 mg/kg) + DMSO;  $n = 4$  animals or  $n = 16$  observations in PMOE23 (10 mg/kg) with dantrolene or DMSO]. *P* values were determined with a Student's *t* test. Muscle assays presented here in aggregate (A to C) are shown individually in fig. S5.

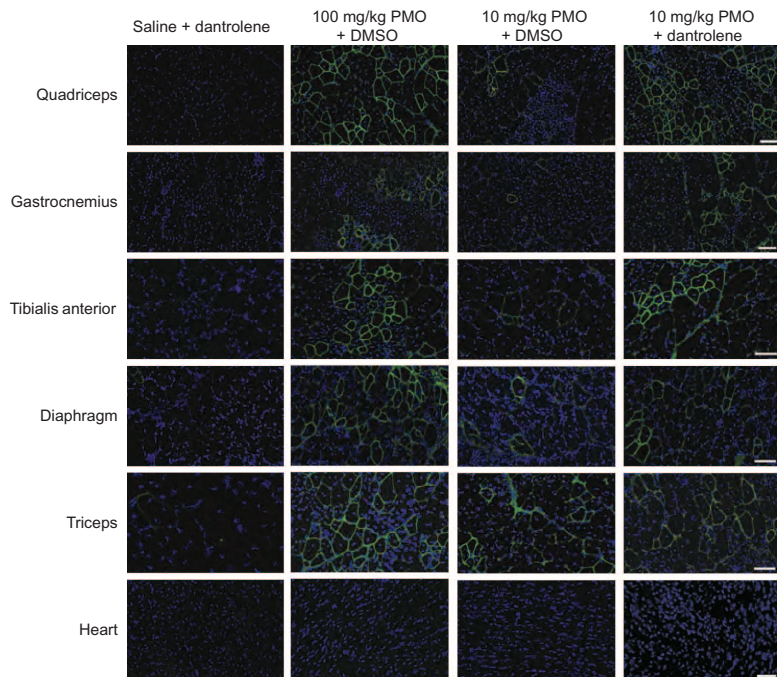


**Fig. 6.** Dantrolene and PMOE23 treatment rescue sarcolemmal dystrophin protein in multiple skeletal muscles. Representative micrographs of dystrophin immunostaining images of muscle cross-sections from the quadriceps, gastrocnemius, TA, and diaphragm of representative mice analyzed in Fig. 5B. Representative dystrophin immunostaining images for triceps and heart are also shown. Nuclei were labeled with DAPI (blue), and dystrophin expression was detected using MANDYS8 (green). Scale bars, 100  $\mu$ m.

#### Dantrolene and other RyR antagonists enhance exon skipping in DMD patient iDRM cells

Dantrolene targets the RyR and modulates its activity (30, 31). As a first step in determining whether RyR antagonism is responsible for dantrolene exon-skipping activity, we asked whether other RyR antagonists could similarly enhance AO-mediated exon skipping. To this end, we assessed the abilities of ryanodine, Rycal S107, and dantrolene to facilitate AO-mediated exon 51 skipping in myotubes differentiated from DMD patient iDRM5017. We found that all three compounds enhanced AO-mediated *DMD* exon 51 skipping at concentrations known to modulate RyR activity (32–38) (Fig. 8). These findings suggest that RyR may be the molecular target responsible for dantrolene exon-skipping activity and highlight RyR modulators as a class worthy of additional investigation as enhancers of exon skipping.

#### DISCUSSION

A high-throughput screen identified compounds that synergize with AO to promote *DMD* exon skipping, including dantrolene, which we dem-

onstrated can synergistically enhance AO-directed exon skipping in in vitro and in vivo mouse and in vitro human models of DMD. Dantrolene alters *DMD* mRNA splicing when administered together with suboptimal doses of AO both in vitro in mouse and human cell systems, as well as in multiple skeletal muscles with intramuscular and intravenous delivery of PMOE23 in the *mdx* mouse. We used several independent assays to demonstrate that dantrolene enhanced *DMD* exon skipping and dystrophin and DGC rescue in *mdx* mice in vivo, including quantitation of skipped mRNA by quantitative PCR (qPCR), dystrophin protein by immunoblot and quantitative immunofluorescence, and rescue of sarcolemmal DGC proteins by immunofluorescence.

Our results suggest that dantrolene synergizes with *DMD*-directed AOs to enhance targeted *DMD* exon skipping. Given that the original screen and the in vitro assessments test the effect of dantrolene after AO has been taken up by the cells, it is unlikely that dantrolene is exerting its effect by enhancing AO intracellular delivery. Rather, we hypothesize that it enhances exon skipping through interaction with specific molecular targets that indirectly modulate splicing activity. When used in combination with AO directed at a splice acceptor (h50AON), splice donor (M23D AO and PMOE23), or ESE (h51AON) (all of which effectively decrease the recognition of the exon by the spliceosome), dantrolene promotes the relative exclusion of *DMD* exons. Our

screen relied on robust quantification of an exon-skipping reporter in a muscle lineage cell in the presence or absence of suboptimal AO (17, 39). This is in contrast to previous screens that were performed in nonmuscle lineage cells (25) or that used coarse quantitative approaches (25) without the inclusion of sensitizing AO.

Small molecules have been used previously to increase exon-skipping efficiency in patient cells with a rare point mutation in *DMD* exon 31 that disrupts an ESE binding site for the SRp30c splicing factor. In that study, an inhibitor for Clks, which phosphorylates sarcoplasmic reticulum proteins, increased mutant but not normal exon 31 skipping in cultured cells (40). However, this compound is not suitable for use in vivo, nor is it generalizable to a significant fraction of DMD-affected individuals. In contrast, dantrolene enhances AO-mediated exon 51 skipping, overcoming common out-of-frame *DMD* mutations and has already been demonstrated safe in DMD patients. Dantrolene enhanced skipping activity for AOs targeting human exon 50, human exon 51, and mouse exon 23 with both 2'OMe and morpholino chemistries, demonstrating that we have identified a drug that appears effective regardless of the sequence specificity of the AO or of the AO backbone chemistry. This

versatility could be useful given the spectrum of mutations that require various AO sequences and chemistries, broadening dantrolene's potential clinical applicability (14, 41, 42). Further, dantrolene is already FDA-approved and was safely administered for 2 years as an oral (8 mg/kg per day) treatment in DMD patients (21). Finally, we note that dantrolene or other identified compounds may influence skipping of additional exons or exons in other cell types and thus may be relevant to a broad spectrum of therapeutic applications (41, 42).

It is not yet clear whether dantrolene/AO combination therapy is targeting muscle precursors or fully differentiated myofibers in vivo. Our initial screen demonstrated that the effect was observed within the C2C12 myoblast reporter cell line, suggesting that myoblast muscle stem cell precursors may be a target cell. Nevertheless, dantrolene was effective at enhancing AO-mediated skipping in *in vitro* differentiated and fused mouse myotube cultures, suggesting that fully differentiated myotubes may be an alternate or additional *in vivo* target. Improved *in vitro* and *in vivo* muscle cell models of DMD with relevant human mutations in induced pluripotent stem cells and iDRMs will help address these issues (24, 43, 44).

Although we do not know the precise mechanism by which dantrolene facilitates exon skipping, it may act through its known target, the RyR. RyR regulates calcium release from the sarcoplasmic reticulum during excitation-contraction coupling in skeletal muscle. Further, RyR on the nucleoplasmic reticulum regulates calcium signaling in the nucleus (45), and because calcium regulates splicing in other settings (46), dantrolene modulation of RyR-mediated calcium flux in muscle is a plausible mechanism of its activity. Three structurally diverse compounds—dantrolene, ryanodine, and S107—each known to antagonize RyR activity through a distinct molecular mechanism [including the stabilization of RyR domain interactions, regulation of ion translocation from the RyR pore, and allosteric modulation of accessory proteins (35, 36, 38, 47–49)] all enhance AO-mediated exon 51 skipping, strengthening this suggestion.

Hypernitrosylation of RyR in DMD causes calcium leakage and downstream DMD pathology as a result of calcium-regulated protein degradation (36). Thus, dantrolene and Ryicals, which reduce this leak, have been proposed as potential therapeutics for DMD, independent of the exon-skipping effect described here. It is unlikely that the synergistic action of dantrolene on exon skipping is secondary to inhibition of calcium-dependent protein degradation, because exon 23 skipping occurs in cultured myotubes from both dystrophic (*mdx*) and nondystrophic mice (Fig. 2, A to D). We found no functional benefit of treatment of *mdx* mice with dantrolene alone for 3 weeks, consistent with the observed therapeutic effects resulting from synergy of dantrolene with AO to potentiate exon skipping. Nonetheless, potential activity of dantrolene from non-splicing-related effects of calcium modulation may provide additional benefit to protect DMD muscle from pathogenic consequences when used for longer treatment periods (18, 21).

AVI4658/Eteplirsen and Pro051/GSK2402968 were demonstrated safe as single agents in phase 1 to 2 clinical trials and induced skipped dystrophin protein at 0 to 18% of normal dystrophin protein levels. Ongoing phase 2b to 3 trials are under way in an attempt to demonstrate functional benefit to gain FDA approval. Early results from phase 2b extension studies are promising, trending toward functional benefit for both AO treatments (50, 51). However, mouse and human studies predict that at least 20 to 30% of normal dystrophin levels will be needed for optimal efficacy (16, 52). Therefore, therapeutics such as dantrolene that enable enhanced skipping activity and increase dystrophin protein production may be necessary to gain FDA approval of this class of agents or alternatively may improve function beyond that required for approval (52). Skipping enhancers could also improve the practicality of long-term treatment with antisense therapeutics by reducing the dose of AO needed, lowering cost, or limiting toxicity. In addition, enhancing the efficacy of AOs may increase dystrophin expression in suboptimally targeted muscles, thereby increasing the therapeutic value of these agents.

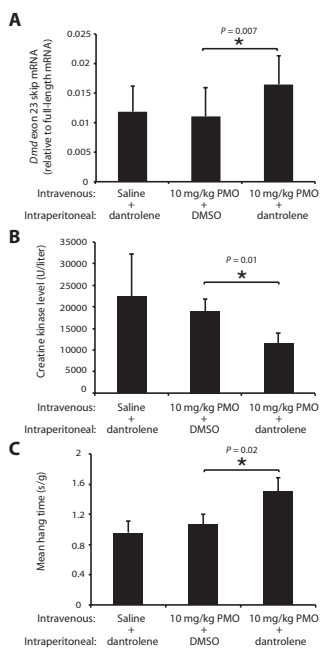


**Fig. 7.** Dantrolene synergizes with intravascularly delivered PMOE23 to promote *Dmd* exon 23 skipping and improve muscle strength in *mdx* mice. Weekly systemic doses of saline or morpholino PMOE23 (10 mg/kg) were administered to *mdx* mice on days 1, 8, and 15. Dantrolene or vehicle was administered intraperitoneally twice daily at a final dose of 10 mg/kg per day until harvesting on day 22. (A) Effect of dantrolene on PMOE23-induced exon 23 skipping in the TA muscle after 3 weeks of treatment assessed by quantitative TaqMan assay of *Dmd* exon 23 skipping. Data are plotted as ratio of skipped to full-length *Dmd* mRNA. (B) Effect of dantrolene on muscle membrane damage assessed by serum CK levels in mice treated for 16 days. (C) Effect of dantrolene on muscle function assessed using the taut wire test and measuring the latency to fall. The average hang time across five trials was calculated for each mouse and then normalized to weight (s/g). Error bars in (A) represent means  $\pm$  SD [mice per condition;  $n = 4$  saline + dantrolene,  $n = 5$  PMOE23 + DMSO (10 mg/kg) or dantrolene]. Error bars in (B) and (C) represent means  $\pm$  SEM among mice in each group [mice per condition;  $n = 4$  saline + dantrolene,  $n = 8$  to 9 PMOE23 (10 mg/kg) + DMSO or dantrolene].  $P$  values were calculated in (A) and (B) with Student's  $t$  test, and  $P$  values in (C) with a two-way repeat analysis of variance (ANOVA) model.

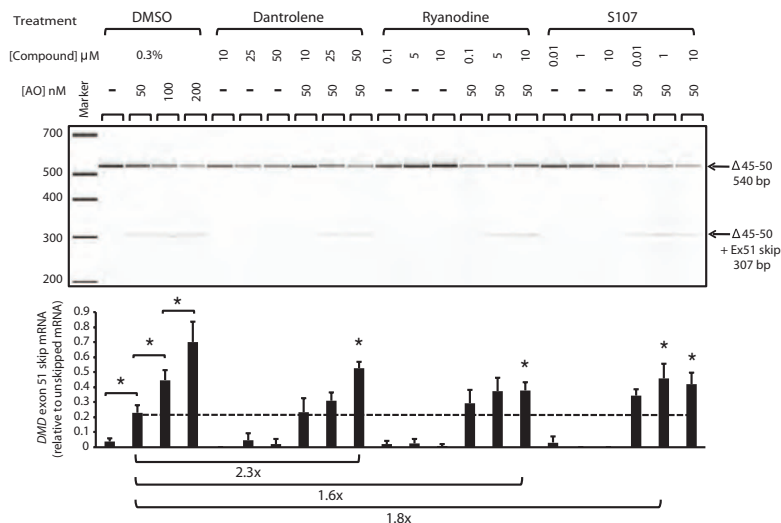


**Fig. 8.** Ryanodine receptor antagonists enhance AO-directed *DMD* exon 51 skipping in a patient cell line. iDRM5017 was treated with h51AON for 24 hours followed by the addition of vehicle or known RyR antagonists: dantrolene, ryanodine, or Rycal S107 in dose titrations. Two days later, RNA was harvested and *DMD* mRNA exon 51 skipping was detected by nested RT-PCR spanning exons 43 to 52, quantified using the Agilent Bioanalyzer, and plotted as the ratio of *DMD* exon 51–skipped isoform relative to unskipped mRNA. A representative subset of wells is shown in the electropherogram. Error bars represent means  $\pm$  SD of three replicates. \* $P < 0.05$ .  $P$  values were determined with a Student's  $t$  test, and the experiment was repeated twice.

## MATERIALS AND METHODS

### High-throughput and secondary screening

A stable clone was generated from C2C12 cells transfected with a human exon 50 *DMD* GFP reporter (Ex50GFP) (17). Ex50GFP myoblasts were seeded at a density of 4000 cells per well into uncoated 384-well plates in myoblast growth media [phenol red–free Dulbecco's modified Eagle's medium (DMEM), 15% fetal bovine serum (FBS), 1 $\times$  L-glutamine, and 1 $\times$  penicillin/streptomycin]. Cells were incubated for 4 hours either with ( $n = 3$  replicates) or without ( $n = 6$  replicates) 300 nM 2'-Ome phosphorothioate h50AON (–19 to +8) (5'-AACUCCUCU-UUAAACAGAAAAGCAUAC-3') targeting exon 50 skipping by masking the intron-exon boundary at the 3' intron 49 splice acceptor site. h50AON was transfected with FuGENE (Roche) at a ratio of 3  $\mu$ l of FuGENE/1  $\mu$ g of DNA. After h50AON incubation, the BioMol library ( $n = 300$  compounds; endocannabinoid library, enzyme inhibitor, ion channel, orphan ligand) was screened at 1 or 10  $\mu$ M concentration, with a final concentration of 1% dimethyl sulfoxide (DMSO) carrier. The final well volume was 50  $\mu$ l. Forty-eight hours later, DNA was stained with Hoechst (100  $\mu$ g/ml; Sigma) and incubated for 30 min at 37°C. Immediately after Hoechst incubation, fluorescence was measured with MicroXpress, with GFP fluorescence having an exposure setting of 350 ms and Hoechst at 21 ms. Analysis was performed with MetaXpress. Raw fluorescence values were normalized to carrier controls by subtracting the average DMSO fluorescence ( $n = 24$  wells per plate). After normalization, each compound's readout was

averaged across replicates, and the SD across screens was determined. Negative fluorescence values were set to 0 in Fig. 1. The “with-AO” and “without-AO” screens were rank-ordered on the basis of the average fluorescence, and the top 5% ( $n = 15$  from the with-AO screen and  $n = 15$  from the without-AO screen) were prioritized for secondary screening (table S1).

Secondary screening was performed in the Ex50GFP reporter myoblasts and in C2C12 cells either with or without a 100 nM suboptimal dose of h50AON. All four conditions were seeded at 4000 cells per well in uncoated 384-well plates. h50AON was incubated with cells for 2.5 to 4 hours before the addition of compound. Compound dilutions were added initially at 100 or 80  $\mu$ M (dissolved in DMSO), and 1:1 dilutions were performed over a 12- or 16-point range. Cells were incubated with compounds for 24 to 48 hours before imaging with MicroXpress. Before imaging, cells were incubated for 30 min with Hoechst (100  $\mu$ g/ml). Acquisition was performed with MicroXpress and analyzed by determining the percentage of cells that were fluorescent. Compounds were considered positive if the Ex50GFP reporter with h50AON had greater

than 10% fluorescence than the other three conditions and exhibited evidence of a dose response.

### Cell culture and AO transfection

Primary mouse myoblasts were isolated from the quadriceps of a C57Bl/6 or *mdx* mouse and were carried in culture with 20% FBS in DMEM + fibroblast growth factor (2 ng/ $\mu$ l). For *Dmd* exon 23–skipping assays, cells were seeded onto ECM (Sigma)–coated plates in growth media. On day 2, growth media were removed and fusion media (2% horse serum in phenol red–free DMEM) were added. On day 3, a 2'-Ome phosphorothioate AO M23D (+02 to –18) (5'-GGCCAAACCUCGGCUUACCU-3') was transfected into cells with FuGENE at a ratio of 3  $\mu$ l:1  $\mu$ g of DNA. M23D concentrations ranged from 100 to 600 nM, with 100 or 200 nM M23D representing the suboptimal dose. Four hours after AO M23D or mock transfection, cells were washed with 1 $\times$  phosphate-buffered saline (PBS) and dantrolene (Sigma; dissolved in DMSO), or carrier control was added in fresh fusion media. After a 48-hour incubation with dantrolene, cells were harvested for analysis.

Primary human dermal fibroblasts (GM05017) from a DMD patient were obtained from Coriell and were maintained in growth media (DMEM with 15% FBS, 1% nonessential amino acids, 1% penicillin/streptomycin). The genomic *DMD* deletion between exons 45 and 50 was confirmed with a custom comparative genomic hybridization (CGH) array with 14,022 probes tiling the *DMD* gene (Agilent; fig. S2). Fibroblasts were immortalized with lentiviral hTERT and subsequently transduced with previously described tamoxifen-inducible lentiviral MyoD (24) to create iDRM5017. For exon 51 skipping experiments, DMD patient–derived

iDRM5017 was seeded onto laminin (BD Biosciences)-coated plates in growth media. On day 2, 5  $\mu$ M 4OH-tamoxifen (Sigma) was added in growth media. The following day, fusion media [2% horse serum, 2% insulin-transferrin-selenium (Sigma), 1:1 serum-free DMEM to Ham's F-10] with 1  $\mu$ M 4OH-tamoxifen were added to the cells. A *DMD* exon 51 2' OMe phosphorothioate AO (5'-UCAAGGAAGAUGGCAUUUCU-3') (MWG Operon) at position +68 to +87 was transfected into cells on day 7 with ExGen 500 (Fermentas) at a ratio of 5.5  $\mu$ l:1  $\mu$ g of DNA. AO concentrations ranged from 50 to 200 nM, with 50 or 100 nM AO being the suboptimal dose. The following day, the AO complex was removed, cells were washed with 1 $\times$  PBS, and titrations of drug or carrier (DMSO) were added for 48 hours, after which the cells were harvested. Quantitation was performed by capillary electrophoresis on the Agilent 2100 Bioanalyzer.

### RNA isolation, RT-PCR, and qPCR

RNA was isolated with TRIzol (Invitrogen; mouse cells) and the Qiagen RNeasy Micro Kit (human cells and intervals from the TA muscle). RNA was isolated from frozen skeletal muscle with the Qiagen RNeasy Fibrous Tissue Kit. Total RNA from mice was reverse-transcribed with oligo(dT)<sub>20</sub> (Invitrogen). A nested RT-PCR was performed between *Dmd* exons 20 and 26 (5). Products were run on a 2% agarose gel and visualized with ethidium bromide. Densitometry quantitation of gels was performed in ImageJ. The quantitative TaqMan assay to assess specific full-length or skipped *Dmd* exon 23 mRNAs used primer-probe sets that have been previously described (39). Briefly, primer-probe sets specific to the internal loading control, *Rplp0*, are complexed with primer-probe sets that amplify either the *Dmd* full-length or exon 23 skip product. The skip-to-full-length mRNA ratio was calculated as:

$$2^{[(CT_{RS} - CT_S) - (CT_{RFL} - CT_{FL})]}$$

in which CT<sub>RS</sub> and CT<sub>RFL</sub> are the C<sub>t</sub> values for the ribosomal gene in either the skip (S) or the full-length (FL) reaction. CT<sub>S</sub> and CT<sub>FL</sub> are the C<sub>t</sub> values corresponding to detection of *Dmd* exon 23-skipped or full-length mRNA product. In human cells, dystrophin complementary DNA (cDNA) was reverse-transcribed with 200 ng of RNA with a *DMD* exon 54-specific primer. A nested RT-PCR between *DMD* exons 43 to 52 was then performed with previously described primers (10). For detection of muscle markers, 100 to 400 ng of RNA were reverse-transcribed into cDNA with oligo(dT)<sub>20</sub> and RT-PCRs were performed for endogenous MyoD, desmin, myogenin, utrophin, myosin heavy chain, and glyceraldehyde-3-phosphate dehydrogenase (GAPDH) as input control.

### Sequences of primers used for RT-PCR

The following primers were used for RT-PCR of various muscle markers.

For identifying muscle markers in reprogrammed fusing myotubes, 100 to 400 ng of RNA were reverse-transcribed with oligo(dT)<sub>20</sub>.

MyoD: forward, 5'-GCAGGTGTAACCGTAACC-3'; reverse, 5'-ACGTACAAATTCCTGTAGC-3' (53)

Myosin heavy chain: forward, 5'-CTGGCTCTCTCTTTGTTGG-3'; reverse, 5'-AGTTTCATTTGGGGATGATGC-3'

Desmin: forward, 5'-CCTACTCTGCCCTCAACTTC-3'; reverse, 5'-AGTATCCCAACACCCTGCTC-3' (53)

Myogenin: forward, 5'-GCCACAGATGCCACTACTTC-3'; reverse, 5'-CAACTTCAGCACAGGAGACC-3' (53)

GAPDH: forward, 5'-GAGCCACATCGCTCAGACAC-3'; reverse, 5'-CATGTAGTTGAGGTCAATGAAGG-3' (54)

RyR1 PCR1: forward, 5'-CATCAACTATGTCACCAGCATCCG-3'; reverse, 5'-GGCTGAACCTTAGAAGAGTC-3'

RyR1 PCR2: forward, 5'-GAGACCTTCTATGATGCAGC-3'; reverse, 5'-AGAGCTCGTGGATGTTCTC-3'

Utrophin: forward, 5'-TGTCGGTTCACCGCCAGAGT-3'; reverse, 5'-GTGGCCTGCTGGGAACATTT-3' (55).

The thermocycler conditions for MyoD, myosin heavy chain, desmin, myogenin, and GAPDH were 94°C for 2 min, followed by 33 cycles of 94°C for 30 s, 62°C for 30 s, and 72°C for 30 s, with a final extension of 72°C for 10 min.

Amplification of the RyR1 required a nested PCR. Conditions for the first ryanodine receptor PCR were 95°C for 5 min, 20 cycles of 95°C for 30 s, 56°C for 2 min, 72°C for 90 s, and a final extension of 72°C for 10 min. The nested PCR conditions were 95°C for 5 min, 35 cycles of 95°C for 30 s, 59°C for 2 min, 72°C for 90 s, and a final extension of 72°C for 10 min.

Thermocycler conditions for the amplification of utrophin required a single PCR. Conditions were 94°C for 5 min, 94°C for 1 min, 60°C for 1 min, 72°C for 1 min, repeat steps 2 to 4 for 35 cycles, and a final extension of 72°C for 10 min.

### Western blot

Total protein was isolated from flash-frozen skeletal muscle from both the membrane and the cytoplasmic fractions. Briefly, muscle tissue was homogenized for 1 min in 1 ml of ice-cold Mito buffer [0.2 mM EDTA, 0.25 mM sucrose, 10 mM tris-HCl (pH 7.4)] with protease/phosphatase inhibitor cocktail (Pierce) and deoxyribonuclease/ribonuclease and subjected to low-speed (1500g) centrifugation for 10 min at 4°C. The supernatant was centrifuged at 100,000g (high-speed centrifugation) for 1 hour for isolation of membrane fraction. Isolated membranes and pellet after low-speed centrifugation were combined and resuspended in 300  $\mu$ l of extraction buffer [50 mM tris-HCl (pH 7.4), 7 M urea, 2 M thiourea, 4% CHAPS, 2% SDS, 50 mM  $\beta$ -mercaptoethanol]. Protein concentration in solubilized pellet and supernatant after high-speed centrifugation (cytoplasmic fraction) was determined by 2-D Quant Kit (GE Healthcare Life Sciences). Fifty micrograms of total protein from dystrophic mice, or 5  $\mu$ g from wild type (for Fig. 3), or 40  $\mu$ g from dystrophic mice and 4  $\mu$ g from wild type (for figs. S4 and S6) were run on a 6% polyacrylamide gel and transferred onto a nitrocellulose membrane for 2 hours at 4°C. The membrane was blocked for 1 hour in 5% milk and then incubated with MANDYS8 (Sigma) against dystrophin or anti-vinculin hVin-1 (Sigma), a skeletal muscle membrane protein not associated with the DGC that was used as a loading control. Dystrophin and vinculin were detected in the low- and high-speed pellets (myofibrillar/membrane fraction), but not in the cytoplasmic fraction. For analysis, dystrophin protein levels were normalized to the vinculin loading control and then pooled across treatment groups or muscles to determine the average dystrophin rescue. Densitometry analysis was performed with AlphaImager HP gel documentation system (Alpha Innotech Corporation) and FluorChem FC2 System Software (version 3.1.1).

### Immunofluorescence

Unfixed 10- $\mu$ m tissue sections were air-dried and washed 2  $\times$  2 min in tris-buffered saline (TBS). Sections were then incubated in MOM immunoglobulin G (IgG) blocking reagent (Vector Labs) for 1 hour and washed 2  $\times$  2 min in TBS with 0.1% Tween 20. After washes, sections

were incubated with primary antibodies MANDYS8 (dystrophin rod domain), Ab15277 (dystrophin C terminus; Abcam), and Manx1A (dystrophin N terminus; Developmental Studies Hybridoma Bank).  $\alpha$ -Sarcoglycan was detected with NCL- $\alpha$ -SARC (Novocastra),  $\beta$ -dystroglycan with NCL- $\beta$ -DG (Novocastra), and DNA with 4',6-diamidino-2-phenylindole (DAPI). Secondary labeling was performed with fluorescein isothiocyanate (FITC) anti-mouse or FITC anti-rabbit (Vector Labs). Sections were mounted in Vectashield Mounting Medium (Vector Labs). Whole-muscle cross-sections were scanned with a 5 $\times$  objective and were analyzed with Ariol SL-50 (Applied Imaging Corp.).

For immunofluorescence in cell culture, myotubes were grown on laminin-coated coverslips and were fixed in 2% paraformaldehyde for 10 min at 37°C maintaining a 1:1 ratio between culture media and fixative. Washes were performed in TBS and then further permeabilized in 0.5% Triton X-100 in TBS for 5 min. Cells were blocked in 20% normal goat serum for 1 hour at room temperature followed by overnight at 4°C. The following day, MF20 (antibody specific for myosin heavy chain; Developmental Studies Hybridoma Bank) was diluted in TBS with 0.05% Tween 20 and incubated overnight at 4°C. Secondary antibody directly conjugated with Alexa Fluor 488 goat anti-mouse IgG (H + L) (Invitrogen) was added for 90 min at room temperature. Coverslips were mounted in ProLong Gold antifade with DAPI (Invitrogen). Images were acquired on a Zeiss AxioImager Z1 microscope with a 10 $\times$  objective and with the AxioVision Rel. 4.6.3.0 acquisition software.

#### Mice and tissue preparation

Procedures involving all *mdx* mice were approved by the Institutional Animal Care and Use Committee (IACUC) of the University of California, Los Angeles (UCLA). For experiments with intramuscular injections of PMO, the TA muscle was harvested and frozen in Tissue-Tek CRYO-OCT Compound (optimal cutting temperature; Andwin Scientific). Ten-micrometer sections were taken across the entire TA muscle and ordered into 850- $\mu$ m intervals; within each interval, 5 sections (10  $\mu$ m each) were designated for immunostaining, 40 sections (400- $\mu$ m length of tissue) for RT-PCR, and 40 sections (400- $\mu$ m length of tissue) for Western blot analysis. Analysis of each interval provided a sampling along the entire TA muscle. Typically, there were six to nine intervals per mouse. For Western blot analysis, four consecutive intervals were pooled to prepare sufficient protein (total of 1600- $\mu$ m length). Central sections representing four to seven intervals were analyzed by immunofluorescence staining. Central intervals were also used for RT-PCR analysis. No difference in exon-skipping activity or dystrophin restoration was observed on the basis of gender. For experiments with systemic injections of PMO, the quadriceps, gastrocnemius, TA, and triceps were harvested, and the right muscle was frozen in OCT for sectioning and analysis by immunohistochemistry, whereas the left muscle was snap-frozen and cut in half for analysis by Western blot and RT-PCR. For the diaphragm and heart, one-half of the muscle was designated for immunohistochemistry and one-fourth for Western blot and RT-PCR.

#### Functional analysis of skeletal muscles

Muscle membrane integrity was evaluated by measuring serum CK levels. Blood was collected by retro-orbital bleeding of the mice, serum was isolated, and CK analysis was performed with the Genzyme Creatine Kinase kit (BioPacific Diagnostic Inc.).

Improvement in overall muscle strength and condition was assessed with the recorder blinded to mouse treatment group by using a taut

wire test modified from Gomez *et al.* (56). Latency to fall (in seconds) was recorded for five consecutive trials, with a 1-min break occurring in between each trial. The average hang time across five trials was calculated for each mouse and then normalized to individual weights.

#### PMO and dantrolene in vivo administration

PMOE23 morpholino (5'-GGCCAAACCTCGGCTTACCTGAAAT-3'; Gene Tools) was injected intramuscularly into the TA muscle in 25  $\mu$ l of saline. Intravenous administration was performed through the tail vein in 200  $\mu$ l of saline or retro-orbitally in 50  $\mu$ l. Dantrolene (Sigma) was resuspended in DMSO, heated to 50°C, and diluted in saline (final 20% DMSO) before twice-daily intraperitoneal injections.

#### SUPPLEMENTARY MATERIALS

www.sciencetranslationalmedicine.org/cgi/content/full/4/164/164ra160/DC1  
 Fig. S1. Confirmation of enhancement of exon skipping is demonstrated in 12- or 16-point titrations on the *DMD* exon 50 reporter cell line.  
 Fig. S2. Custom CGH array confirms deletion breakpoints in GM05017 used to create iDRM 5017.  
 Fig. S3. DMD patient-derived iDRM5017 temporally express muscle markers at the RNA and protein level during the fusion process.  
 Fig. S4. Dantrolene rescues dystrophin protein in the TA muscle after intramuscular injection of PMOE23.  
 Fig. S5. Dantrolene synergizes with PMOE23 to promote systemic exon 23 skipping and dystrophin protein rescue in the *mdx* mouse.  
 Fig. S6. Representative Western blots demonstrate sarcolemmal dystrophin expression in the quadriceps, TA, and diaphragm after systemic PMOE23/dantrolene injection.  
 Table S1. Top 5% of compounds from the BioMol  $\pm$  h50AON high-throughput screens.  
 Table S2. Treatment groups for the local administration of PMOE23 in combination with systemic dantrolene shown in Fig. 3.  
 Table S3. Treatment groups for the systemic administration of PMOE23 in combination with systemic dantrolene shown in Figs. 5 and 6 and figs. S5 and S6.

#### REFERENCES AND NOTES

1. A. E. Emery, The muscular dystrophies. *Lancet* **359**, 687–695 (2002).
2. A. E. Emery, Population frequencies of inherited neuromuscular diseases—A world survey. *Neuromuscul. Disord.* **1**, 19–29 (1991).
3. A. P. Monaco, C. J. Bertelson, W. Middlesworth, C. A. Colletti, J. Aldridge, K. H. Fischbeck, R. Bartlett, M. A. Pericak-Vance, A. D. Roses, L. M. Kunkel, Detection of deletions spanning the Duchenne muscular dystrophy locus using a tightly linked DNA segment. *Nature* **316**, 842–845 (1985).
4. A. Nakamura, K. Yoshida, K. Fukushima, H. Ueda, N. Urasawa, J. Koyama, Y. Yazaki, M. Yazaki, T. Sakai, S. Haruta, S. Takeda, S. Ikeda, Follow-up of three patients with a large in-frame deletion of exons 45–55 in the Duchenne muscular dystrophy (*DMD*) gene. *J. Clin. Neurosci.* **15**, 757–763 (2008).
5. C. J. Mann, K. Honeyman, A. J. Cheng, T. Ly, F. Lloyd, S. Fletcher, J. E. Morgan, T. A. Partridge, S. D. Wilton, Antisense-induced exon skipping and synthesis of dystrophin in the *mdx* mouse. *Proc. Natl. Acad. Sci. U.S.A.* **98**, 42–47 (2001).
6. G. Dickson, M. L. Roberts, D. J. Wells, S. A. Fabb, Recombinant micro-genes and dystrophin viral vectors. *Neuromuscul. Disord.* **12** (Suppl. 1), S40–S44 (2002).
7. J. Alter, F. Lou, A. Rabinowitz, H. Yin, J. Rosenfeld, S. D. Wilton, T. A. Partridge, Q. L. Lu, Systemic delivery of morpholino oligonucleotide restores dystrophin expression bodywide and improves dystrophic pathology. *Nat. Med.* **12**, 175–177 (2006).
8. N. M. Goemans, M. Tulinius, J. T. van den Akker, B. E. Burn, P. F. Ekhardt, N. Heuvelmans, T. Holling, A. A. Janson, G. J. Platenburg, J. A. Siplens, J. M. Sitsen, A. Aartsma-Rus, G. J. van Ommen, G. Buyse, N. Darin, J. J. Verschuuren, G. V. Campion, S. J. de Kimpe, J. C. van Deutekom, Systemic administration of PRO051 in Duchenne's muscular dystrophy. *N. Engl. J. Med.* **364**, 1513–1522 (2011).
9. M. Kinali, V. Arechavala-Gomez, L. Feng, S. Cirak, D. Hunt, C. Adkin, M. Guglieri, E. Ashton, S. Abbs, P. Nihoyannopoulos, M. E. Garralda, M. Rutherford, C. McCulley, L. Popplewell, I. R. Graham, G. Dickson, M. J. Wood, D. J. Wells, S. D. Wilton, R. Kole, V. Straub, K. Bushby, C. Sewry, J. E. Morgan, F. Muntoni, Local restoration of dystrophin expression with the morpholino oligomer AVI-4658 in Duchenne muscular dystrophy: A single-blind, placebo-controlled, dose-escalation, proof-of-concept study. *Lancet Neurol.* **8**, 918–928 (2009).

10. J. C. van Deutekom, A. A. Janson, I. B. Ginjaar, W. S. Frankhuizen, A. Aartsma-Rus, M. Bremmer-Bout, J. T. den Dunnen, K. Koop, A. J. van der Kooij, N. M. Goemans, S. J. de Kimpe, P. F. Ekhar, E. H. Venneker, G. J. Platenburg, J. J. Verschuur, G. J. van Ommen, Local dystrophin restoration with antisense oligonucleotide PRO051. *N. Engl. J. Med.* **357**, 2677–2686 (2007).
11. T. Yokota, Q. L. Lu, T. Partridge, M. Kobayashi, A. Nakamura, S. Takeda, E. Hoffman, Efficacy of systemic morpholino exon-skipping in Duchenne dystrophy dogs. *Ann. Neurol.* **65**, 667–676 (2009).
12. Q. L. Lu, C. J. Mann, F. Lou, G. Bou-Gharios, G. E. Morris, S. A. Xue, S. Fletcher, T. A. Partridge, S. D. Wilton, Functional amounts of dystrophin produced by skipping the mutated exon in the *mdx* dystrophic mouse. *Nat. Med.* **9**, 1009–1014 (2003).
13. A. Crisp, H. Yin, A. Goyenville, C. Betts, H. M. Moulton, Y. Seow, A. Babbs, T. Merritt, A. F. Saleh, M. J. Gait, D. J. Stuckey, K. Clarke, K. E. Davies, M. J. Wood, Diaphragm rescue alone prevents heart dysfunction in dystrophic mice. *Hum. Mol. Genet.* **20**, 413–421 (2011).
14. A. Aartsma-Rus, I. Fokkema, J. Verschuur, I. Ginjaar, J. van Deutekom, G. J. van Ommen, In the human. *Neuromuscul. Disord.* **17**, 913–918 (2007).
15. S. Cirak, V. Arechavala-Gomez, M. Guglieri, L. Feng, S. Torelli, K. Anthony, S. Abbs, M. E. Garralda, J. Bourke, D. J. Wells, G. Dickson, M. J. Wood, S. D. Wilton, V. Straub, R. Kole, S. B. Shrewsbury, C. Sewry, J. E. Morgan, K. Bushby, F. Muntoni, Exon skipping and dystrophin restoration in patients with Duchenne muscular dystrophy after systemic phosphorodiamidate morpholino oligomer treatment: An open-label, phase 2, dose-escalation study. *Lancet* **378**, 595–605 (2011).
16. M. Neri, S. Torelli, S. Brown, I. Ugo, P. Sabatelli, L. Merlini, P. Spitali, P. Rimessi, F. Gualandi, C. Sewry, A. Ferlini, F. Muntoni, Dystrophin levels as low as 30% are sufficient to avoid muscular dystrophy in the human. *Neuromuscul. Disord.* **17**, 913–918 (2007).
17. Y. Hu, B. Wu, A. Zillmer, P. Lu, E. Benrashid, M. Wang, T. Doran, M. Shaban, X. Wu, Q. L. Lu, Guanidine analogues enhance antisense oligonucleotide-induced exon skipping in dystrophin gene in vitro and in vivo. *Mol. Ther.* **18**, 812–818 (2010).
18. X. H. Wehrens, A. R. Marks, *Ryanodine Receptors: Structure, Function, and Dysfunction in Clinical Disease. Developments in Cardiovascular Medicine* (Springer, New York, 2005), p. 330.
19. K. P. Glahn, F. R. Ellis, P. J. Halsall, C. R. Müller, M. M. Snoeck, A. Urwyler, F. Wappler; European Malignant Hyperthermia Group, Recognizing and managing a malignant hyperthermia crisis: Guidelines from the European Malignant Hyperthermia Group. *Br. J. Anaesth.* **105**, 417–420 (2010).
20. A. Verrotti, R. Greco, A. Spalice, F. Chiarelli, P. Iannetti, Pharmacotherapy of spasticity in children with cerebral palsy. *Pediatr. Neurol.* **34**, 1–6 (2006).
21. T. E. Bertorini, G. M. Palmieri, J. Griffin, M. Igarashi, A. Hinton, J. G. Karas, Effect of dantrolene in Duchenne muscular dystrophy. *Muscle Nerve* **14**, 503–507 (1991).
22. J. G. Quinlan, S. R. Johnson, F. J. Samaha, Dantrolene normalizes serum creatine kinase in MDX mice. *Muscle Nerve* **13**, 268–269 (1990).
23. C. N. Tennyson, H. J. Klamut, R. G. Worton, The human dystrophin gene requires 16 hours to be transcribed and is cotranscriptionally spliced. *Nat. Genet.* **9**, 184–190 (1995).
24. E. Kimura, J. J. Han, S. Li, B. Fall, J. Ra, M. Haraguchi, S. J. Tapscott, J. S. Chamberlain, Cell-lineage regulated myogenesis for dystrophin replacement: A novel therapeutic approach for treatment of muscular dystrophy. *Hum. Mol. Genet.* **17**, 2507–2517 (2008).
25. A. Malerba, F. C. Thorogood, G. Dickson, I. R. Graham, Dosing regimen has a significant impact on the efficiency of morpholino oligomer-induced exon skipping in *mdx* mice. *Hum. Gene Ther.* **20**, 955–965 (2009).
26. B. Wu, P. Lu, E. Benrashid, S. Malik, J. Ashar, T. J. Doran, Q. L. Lu, Dose-dependent restoration of dystrophin expression in cardiac muscle of dystrophic mice by systemically delivered morpholino. *Gene Ther.* **17**, 132–140 (2010).
27. L. P. Rowland, Biochemistry of muscle membranes in Duchenne muscular dystrophy. *Muscle Nerve* **3**, 3–20 (1980).
28. A. McArdle, R. H. Edwards, M. J. Jackson, Time course of changes in plasma membrane permeability in the dystrophin-deficient *mdx* mouse. *Muscle Nerve* **17**, 1378–1384 (1994).
29. B. Wu, B. Xiao, C. Cloer, M. Shaban, A. Sali, P. Lu, J. Li, K. Nagaraju, X. Xiao, Q. L. Lu, One-year treatment of morpholino antisense oligomer improves skeletal and cardiac muscle functions in dystrophic *mdx* mice. *Mol. Ther.* **19**, 576–583 (2011).
30. F. Zhao, P. Li, S. R. Chen, C. F. Louis, B. R. Fruen, Dantrolene inhibition of ryanodine receptor  $Ca^{2+}$  release channels. Molecular mechanism and isoform selectivity. *J. Biol. Chem.* **276**, 13810–13816 (2001).
31. N. L. Thomas, A. J. Williams, Pharmacology of ryanodine receptors and  $Ca^{2+}$ -induced  $Ca^{2+}$  release. *WIREs Membr. Transp. Signal.* **1**, 383–397 (2012).
32. T. Ohta, M. Endo, Inhibition of calcium-induced calcium release by dantrolene at mammalian body temperature. *Proc. Jpn. Acad.* **62**, 329–332 (1986).
33. T. Ohta, M. Endo, T. Nakano, Y. Morohoshi, K. Wanikawa, A. Ohga, Ca-induced Ca release in malignant hyperthermia-susceptible pig skeletal muscle. *Am. J. Physiol.* **256**, C358–C367 (1989).
34. E. Buck, I. Zimanyi, J. J. Abramson, I. N. Pessah, Ryanodine stabilizes multiple conformational states of the skeletal muscle calcium release channel. *J. Biol. Chem.* **267**, 23560–23567 (1992).
35. M. Fill, J. A. Copello, Ryanodine receptor calcium release channels. *Physiol. Rev.* **82**, 893–922 (2002).
36. A. M. Bellinger, S. Reiken, C. Carlson, M. Mongillo, X. Liu, L. Rothman, S. Matecki, A. Lacampagne, A. R. Marks, Hypernitrosylated ryanodine receptor calcium release channels are leaky in dystrophic muscle. *Nat. Med.* **15**, 325–330 (2009).
37. D. C. Andersson, M. J. Betzenhauser, S. Reiken, A. C. Meli, A. Umanskaya, W. Xie, T. Shiomi, R. Zalk, A. Lacampagne, A. R. Marks, Ryanodine receptor oxidation causes intracellular calcium leak and muscle weakness in aging. *Cell Metab.* **14**, 196–207 (2011).
38. D. C. Andersson, A. R. Marks, Fixing ryanodine receptor  $Ca^{2+}$  leak—A novel therapeutic strategy for contractile failure in heart and skeletal muscle. *Drug Discov. Today Dis. Mech.* **7**, e151–e157 (2010).
39. D. A. O’Leary, O. Sharif, P. Anderson, B. Tu, G. Welch, Y. Zhou, J. S. Caldwell, I. H. Engels, A. Brinker, Identification of small molecule and genetic modulators of AON-induced dystrophin exon skipping by high-throughput screening. *PLoS One* **4**, e8348 (2009).
40. A. Nishida, N. Kataoka, Y. Takeshima, M. Yagi, H. Awano, M. Ota, K. Itoh, M. Hagiwara, M. Matsuo, Chemical treatment enhances skipping of a mutated exon in the dystrophin gene. *Nat. Commun.* **2**, 308 (2011).
41. P. Sazani, R. Kole, Therapeutic potential of antisense oligonucleotides as modulators of alternative splicing. *J. Clin. Invest.* **112**, 481–486 (2003).
42. S. M. Hammond, M. J. Wood, Genetic therapies for RNA mis-splicing diseases. *Trends Genet.* **27**, 196–205 (2011).
43. W. E. Lowry, R. Richter, R. Yachechko, A. D. Pyle, J. Tchieu, R. Sridharan, A. T. Clark, K. Plath, Generation of human induced pluripotent stem cells from dermal fibroblasts. *Proc. Natl. Acad. Sci. U.S.A.* **105**, 2883–2888 (2008).
44. C. H. Zhu, V. Mouly, R. N. Cooper, K. Mamchaoui, A. Bigot, J. W. Shay, J. P. Di Santo, G. S. Butler-Browne, W. E. Wright, Cellular senescence in human myoblasts is overcome by human telomerase reverse transcriptase and cyclin-dependent kinase 4: Consequences in aging muscle and therapeutic strategies for muscular dystrophies. *Aging Cell* **6**, 515–523 (2007).
45. P. Marius, M. T. Guerra, M. H. Nathanson, B. E. Ehrlich, M. F. Leite, Calcium release from ryanodine receptors in the nucleoplasmic reticulum. *Cell Calcium* **39**, 65–73 (2006).
46. J. Krebs, The influence of calcium signaling on the regulation of alternative splicing. *Biochim. Biophys. Acta* **1793**, 979–984 (2009).
47. S. Kobayashi, M. L. Bannister, J. P. Gangopadhyay, T. Hamada, J. Parnes, N. Ikemoto, Dantrolene stabilizes domain interactions within the ryanodine receptor. *J. Biol. Chem.* **280**, 6580–6587 (2005).
48. H. J. Besch, C. H. Shao, K. R. Bidasee, in *Ryanodine Receptors: Structure, Function and Dysfunction*, X. H. Wehrens, A. R. Marks, Eds. (Springer, New York, 2005), pp. 179–189.
49. E. Rousseau, J. S. Smith, G. Meissner, Ryanodine modifies conductance and gating behavior of single  $Ca^{2+}$  release channel. *Am. J. Physiol.* **253**, C364–C368 (1987).
50. N. M. Goemans, M. Tulinius, M. van den Hauwe, A. Kroksmark, G. Buyse, R. J. Wilson, J. van Deutekom, S. J. de Kimpe, G. V. Campion, P4.27 forty eight-week follow-up data from a phase I/IIa extension study of systemic PRO051/GSK2402968 in Duchenne muscular dystrophy: Comparison with contemporaneous controls for 6-min walking distance test. *Neuromuscul. Disord.* **21**, 712 (2011).
51. A. Opar, Exon-skipping drug pulls ahead in muscular dystrophy field. *Nat. Med.* **18**, 1314 (2012).
52. S. F. Phelps, M. A. Hauser, N. M. Cole, J. A. Rafael, R. T. Hinkle, J. A. Faulkner, J. S. Chamberlain, Expression of full-length and truncated dystrophin mini-genes in transgenic *mdx* mice. *Hum. Mol. Genet.* **4**, 1251–1258 (1995).
53. C. H. Cui, T. Uyama, K. Miyado, M. Terai, S. Kyo, T. Kiyono, A. Umezawa, Menstrual blood-derived cells confer human dystrophin expression in the murine model of Duchenne muscular dystrophy via cell fusion and myogenic transdifferentiation. *Mol. Biol. Cell* **18**, 1586–1594 (2007).
54. M. Pombo-Suarez, M. Calaza, J. J. Gomez-Reino, A. Gonzalez, Reference genes for normalization of gene expression studies in human osteoarthritic articular cartilage. *BMC Mol. Biol.* **9**, 17 (2008).
55. A. O. Gramolini, G. Karpati, B. J. Jasmin, Discordant expression of utrophin and its transcript in human and mouse skeletal muscles. *J. Neuropathol. Exp. Neurol.* **58**, 235–244 (1999).
56. C. M. Gomez, R. Maselli, J. E. Gundeck, M. Chao, J. W. Day, S. Tamamizu, J. A. Lasalde, M. McNamee, R. L. Wollmann, Slow-channel transgenic mice: A model of postsynaptic organellar degeneration at the neuromuscular junction. *J. Neurosci.* **17**, 4170–4179 (1997).

**Acknowledgments:** We thank J. Wen, P. Maurizio, and J. Overman for technical support and C. Magyar for assistance with muscle section scanning. Small-molecule screen was performed within the UCLA Molecular Screening Shared Resource. Viral packaging was performed at the UCLA Vector Core. Scanning and quantitative analysis of muscle cross-sections were performed at the UCLA Translational Pathology Core Laboratory. Tamoxifen-inducible lentiviral MyoD was a gift from J. Chamberlain. **Funding:** This work was funded from grants from the NIH (1RC1AR058333), the Department of Defense (85280103), and the Foundation to Eradicate Duchenne (special thanks to T. Carson and D. Carson and their bull roasting friends). Support for the research was also provided by the UCLA Muscular Dystrophy Core Center (NIH grant 5P30AR057230) within the Center for Duchenne

## RESEARCH ARTICLE

---

Muscular Dystrophy at UCLA. **Author contributions:** G.C.K. led the implementation of in vitro and mouse experiments and informatic analysis of screen data and performed the RNA skipping quantification experiments. E.I.M. performed muscle sectioning and quantitative immunohistochemistry and Western blotting for dystrophin. G.C.K. and E.I.M. contributed equally as first authors. M.M. helped design and perform the high-throughput screen and primary data analysis with input from R.D. D.W.W., N.E.S., O.S., L.M., and R.T.W. provided technical support. Q.L.L. provided Ex50GFP C2C12 reporter cell line further developed for these studies. G.C.K., M.C.M., and S.F.N. wrote the manuscript with input from the other authors. M.C.M. and S.F.N. conceived the project, designed the experiments, supervised the entire study, and contributed equally. M.J.S. helped design, supervise, and implement the mouse studies together with M.C.M. and S.F.N. and advised all of the studies. M.C.M., M.J.S., and S.F.N. contributed equally as senior authors, and M.C.M. and S.F.N. will serve as corresponding authors. **Competing interests:** S.F.N., M.C.M., and M.M. are inventors on a pending patent on identification of small molecules that enhance exon skipping filed by

UCLA. **Data and materials availability:** The C2C12 cell line expressing enhanced GFP containing one human dystrophin exon was provided by Q.L.L. for screening and further selection and was made available through a material transfer agreement.

Submitted 28 September 2012

Accepted 19 November 2012

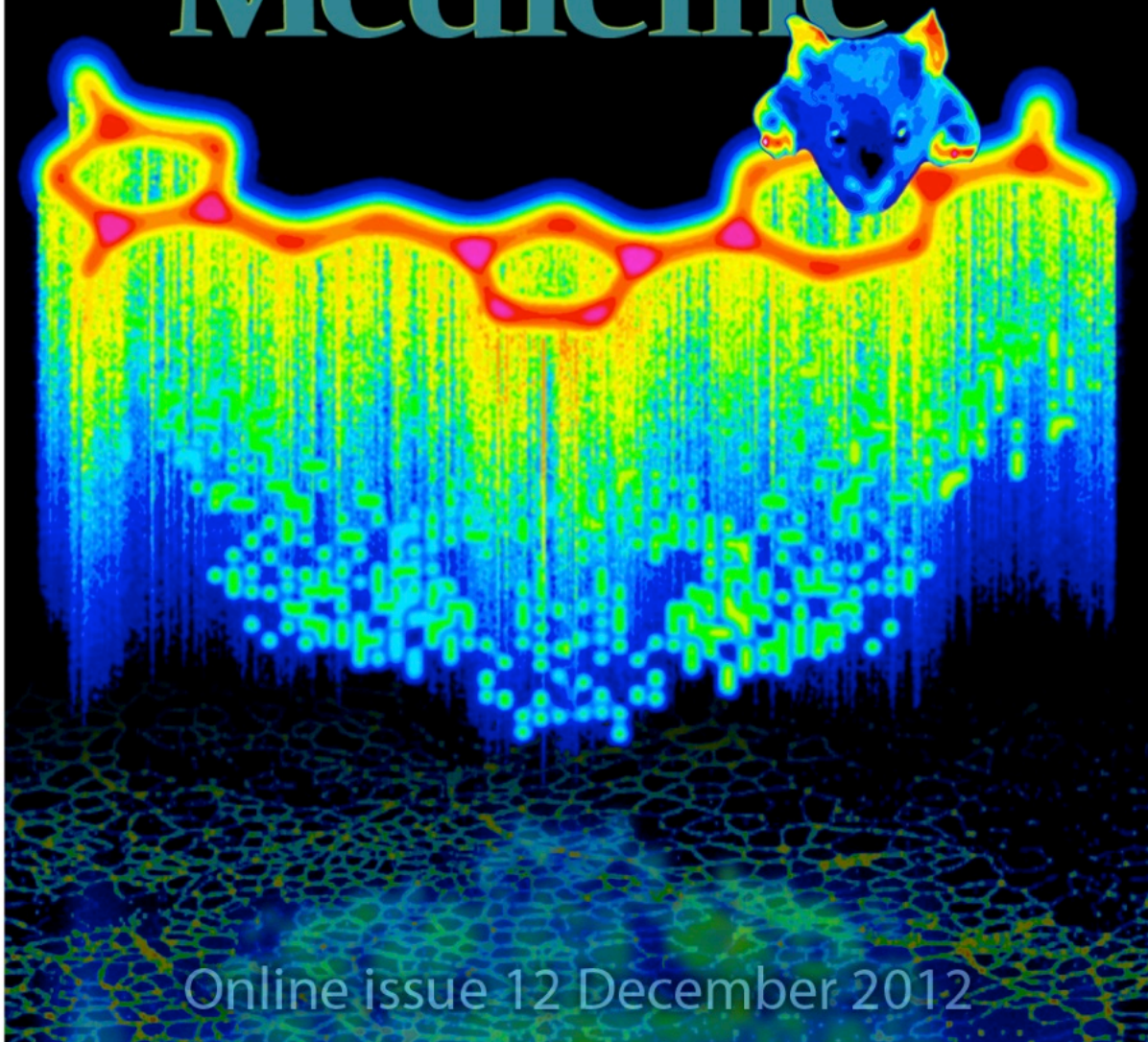
Published 12 December 2012

10.1126/scitranslmed.3005054

**Citation:** G. C. Kendall, E. I. Mokhonova, M. Moran, N. E. Sejbuk, D. W. Wang, O. Silva, R. T. Wang, L. Martinez, Q. L. Lu, R. Damoiseaux, M. J. Spencer, S. F. Nelson, M. C. Miceli, Dantrolene enhances antisense-mediated exon skipping in human and mouse models of Duchenne muscular dystrophy. *Sci. Transl. Med.* **4**, 164ra160 (2012).

**ONLINE COVER** Mouse on the Wire. A mouse hanging on a wire during a test of muscle strength. Mice with a mutant dystrophin gene, which have a muscular dystrophy–like disease, can only hang for about 20 seconds before they lose their grip and fall to the ground. An antisense oligonucleotide being developed to treat the disease in people only helps a little bit. But if the mice also receive the drug dantrolene (shown as the wire), they are stronger and can hang for 30 seconds or so. *Kendall et al.* found this powerful potentiator in a small molecule screen. It also works in human cells and may help patients with Duchenne's muscular dystrophy. [CREDIT: G. KENDALL/UCLA; IMAGES: M.C. MICELI, S. NELSON, E. MOKHONOVA, M. SPENCER]

# Science Translational Medicine



Online issue 12 December 2012

Supplementary Materials

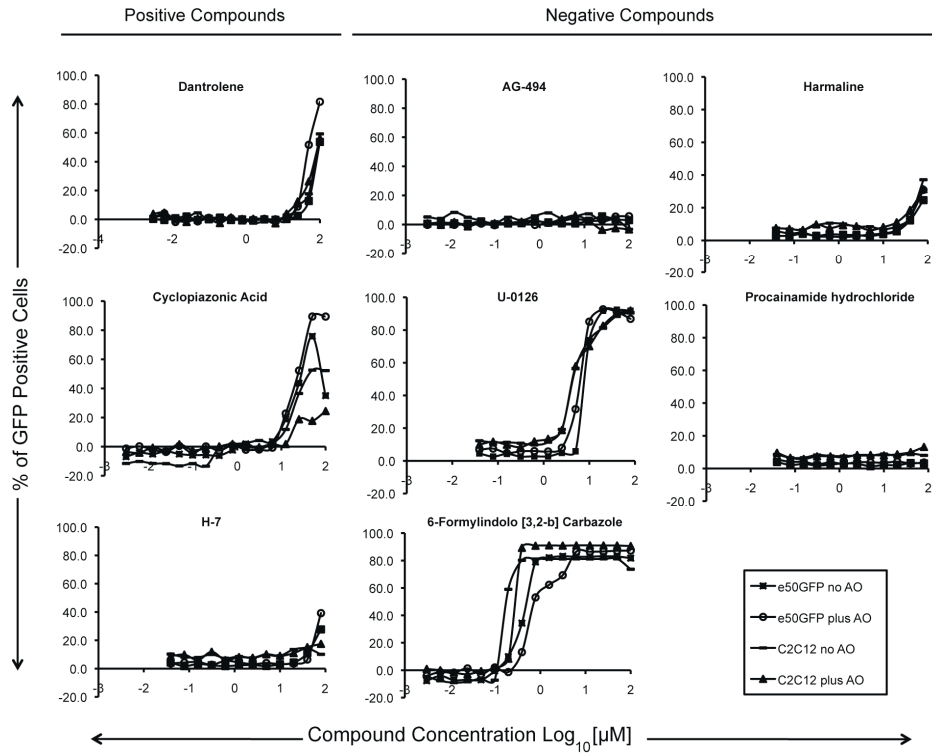


**Fig. S1. Confirmation of enhancement of exon skipping is demonstrated in 12- or 16-point titrations on the *DMD* exon 50 reporter cell line.** Secondary screening was performed on 8 of 15 compounds identified in the +h50AON high-throughput screen to evaluate synergy with h50AON to enhance human exon 50 reporter skipping. 12 or 16 point titrations of compounds were added to C2C12 myoblasts and the Ex50-GFP reporter cells in the absence or presence of h50AON. To be considered positive, compounds must have exhibited a dose response and greater than 10% increased fluorescence in the Ex50-GFP reporter line with h50AON as compared to the without h50AON condition.

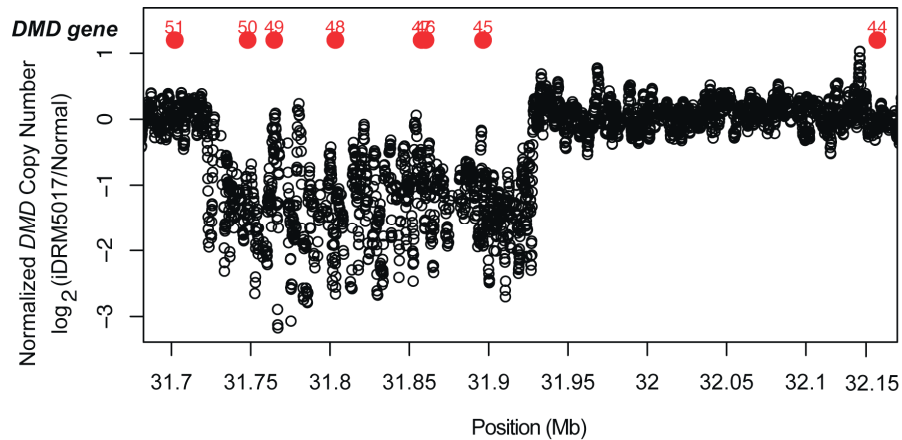


**Fig. S2. Custom CGH array confirms deletion breakpoints in GM05017 used to create iDRM 5017.** A custom oligonucleotide array was designed with 14,022 probes tiling the *DMD* gene with a resolution of approximately 1 probe every 160bp (Agilent). Probe number one maps to genomic position chrX:31047266 and probe 14,022 maps to genomic position chrX:33267570. Genomic DNA from iDRM5017 was labeled with Cy3, and non-mutated human genomic DNA was labeled with Cy5 using a random priming kit (Agilent) and labeled DNA was co-hybridized to the custom designed array. Arrays were scanned with the DNA Microarray Scanner with Surescan High-Resolution Technology (Agilent) and data were extracted with Feature Extraction Software version 10.5.1.1. The values were extracted from the software and analyzed in R. Probes 4409 to 5615 demonstrated lower Cy3 signal and are consistent with a deletion from chrX: 31928123 in intron 44 to chrX: 31725186 in intron 50, which includes exons 45-50 of *DMD*. Base pair positions are reported relative to build HG18 and the log ratio of the Cy3/Cy5 (iDRM5017/normal) intensity is plotted for all probes.

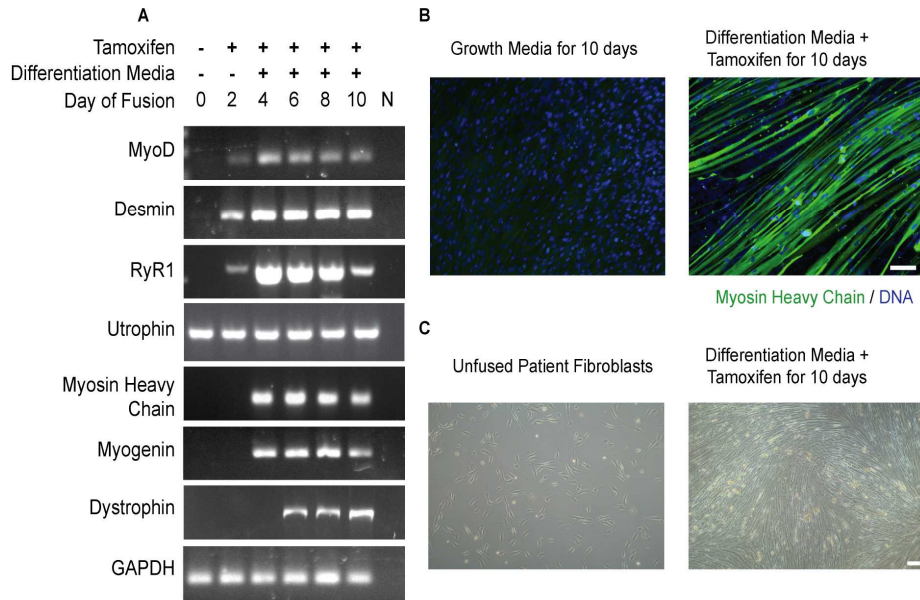


**Fig. S3. DMD patient-derived iDRM 5017 temporally express muscle markers at the RNA and protein level during the fusion process.** GM05017 DMD patient derived iDRM expressing H-TERT and inducible ER-myod were seeded onto laminin coated dishes in growth media (DMEM with 15% FBS, 1% nonessential amino acids, 1% pen/strep). The following day MyoD activity was induced with 5 $\mu$ M 4OH-tamoxifen in growth media for 24 hours. On day 3 the growth media was removed and replaced with fusion media (2% horse serum, 2% insulin-transferrin-selenium (Sigma), 1:1 phenol red-free DMEM to Ham's F-10) containing 1 $\mu$ M 4OH-tamoxifen. The iDRM5017 cells were incubated in fusion media with 1 $\mu$ M 4OH-tamoxifen until harvesting at day 10. **(A)** During the fusion process iDRM 5017 cells temporally expressed indicated genes as detected by RT-PCR. **(B)** Myosin heavy chain was expressed in multinucleated elongated cells consistent with differentiation into myotubes. Nuclei were stained with DAPI (blue). iDRM 5017 cells remaining in growth media without 4OH-tamoxifen failed to express myosin heavy chain (upper left panel). Scale bar, 100 $\mu$ m. **(C)**

Phase contrast micrographs of transformed fibroblasts in growth medium (left panel) or fusion medium with 4OH-tamoxifen (right panel) for 10 days. Scale bar, 200 $\mu$ m.

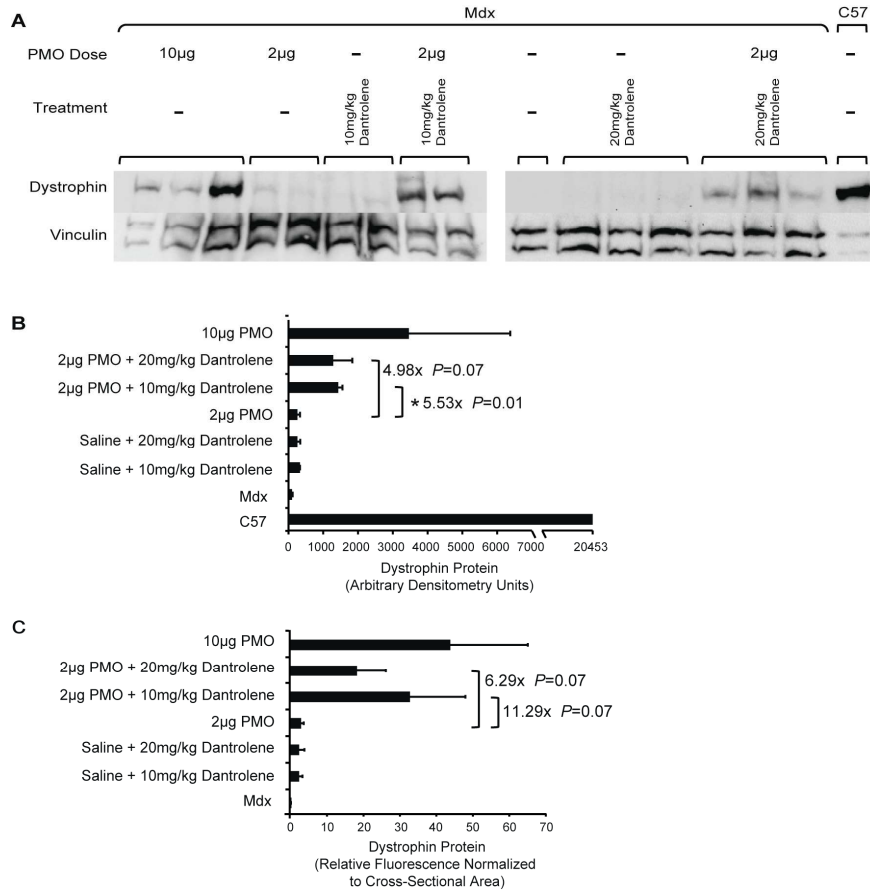


**Fig. S4. Dantrolene rescues dystrophin protein in the TA muscle after intramuscular injection of PMOE23. (A)** Representative Western blot showing dystrophin expression detected using MANDYS8 in the TA muscle from mice in each treatment group. Four of the outermost TA intervals were used for immunoblotting. Vinculin immunoblotting served as a loading control. Protein isolates from C57BL/6 mice were loaded at one-tenth the isolates from *mdx* mice treatment groups. **(B)** Quantitation of dystrophin protein rescue. Dystrophin levels quantitated by densitometry units were normalized to vinculin loading control levels and then averaged across mice in a given treatment group ( $n=3$  mice for all groups other than saline + 10mg/kg dantrolene and 2 $\mu$ g PMOE23, where  $n=2$ ). **(C)** Quantitative fluorescence of dystrophin expression from muscle cross-sections

as described in Figure 3c. Quantitation of dystrophin immunostain of whole muscle cross sections from 3-4 central continuous intervals, of the TA muscle for every mouse. Data were averaged across 3-4 central TA intervals for each independent mouse, and then these values averaged across mice in each treatment group. Dystrophin protein rescue is plotted as the percentage of C57BL/6 (set at 100). Data are from the same experiment as in Fig. 4.

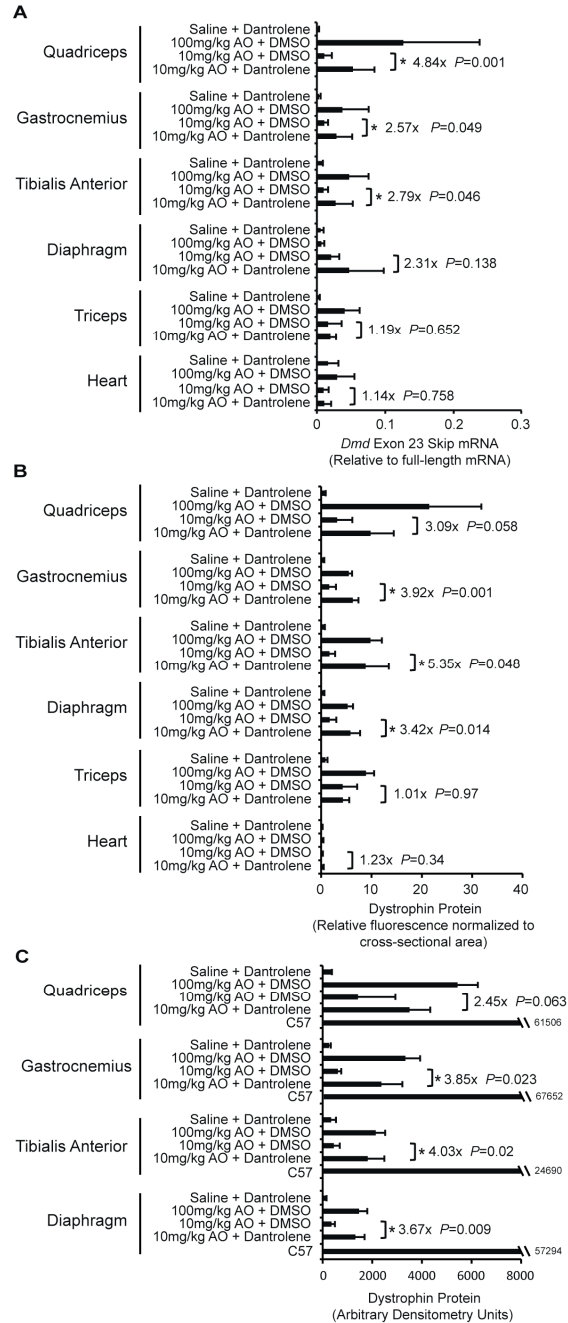


**Fig. S5. Dantrolene synergizes with PMOE23 to promote systemic exon 23 skipping and dystrophin protein rescue in the *mdx* mouse. (A)** Effect of Dantrolene treatment from the individual muscle groups represented in Figs. 5 and 6, is assessed by qPCR and is expressed as the relative ratio of *Dmd* exon 23 skip/full-length mRNA. The increase in the proportion of exon 23 skipped mRNA species in the 10mg/kg PMOE23 + dantrolene as compared to the carrier control is given followed by the p value for each skeletal muscle. **(B)** Quantitation of dystrophin immunofluorescence for individual muscle groups from the experiment represented in Figs. 5 and 6. The right quadriceps, gastrocnemius, tibialis anterior, and triceps muscles, and ½ of the diaphragm and heart muscles were harvested for sectioning and immunofluorescence staining. Quantitative fluorescence was calculated for each individual muscle by scanning one central muscle cross section per mouse, normalizing for cross-sectional area, and then averaging across  $n=3$  or  $n=4$  mice per treatment group. Data is plotted as the percent of C57BL/6 (set at 100). **(C)** Densitometry analysis of dystrophin protein detected by immunoblotting for the individual muscle groups from the experiment represented in Figs. 5 and 6. Dystrophin signal was normalized to the vinculin loading control before comparisons across treatment groups. Error bars represent the s.d. of  $n=3$  mice for saline + dantrolene and 100mg/kg PMOE23+DMSO, and  $n=4$  mice for 10mg/kg PMOE23+ either DMSO or dantrolene. P value is calculate using the student's t test. Data in this figure are represented in aggregate in Fig. 5.

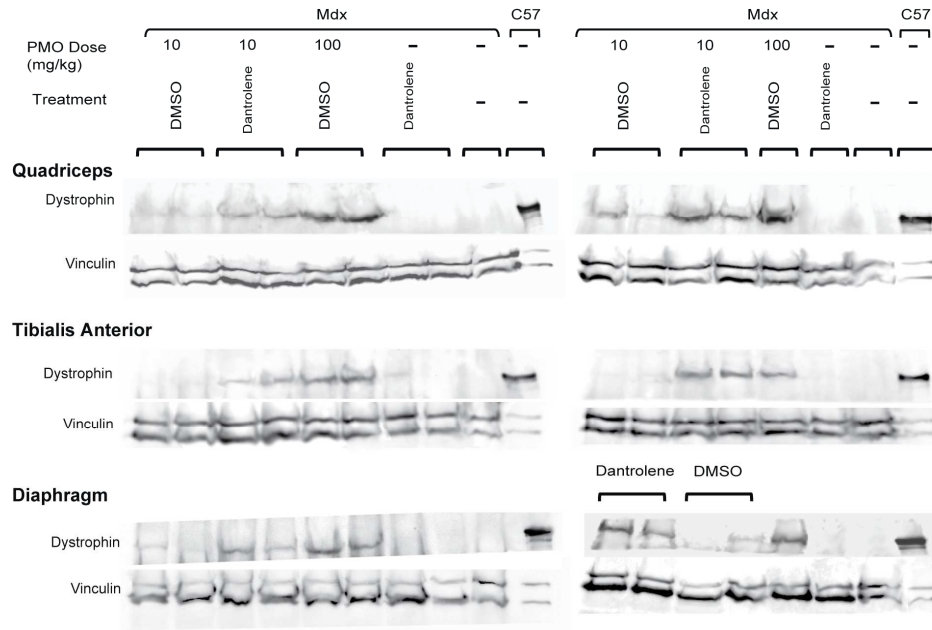


**Fig. S6. Representative Western blots demonstrate sarcolemmal dystrophin expression in the quadriceps, TA, and diaphragm after systemic PMOE23/dantrolene injection.** Dystrophin expression using MANDYS8 antibody is shown for the quadriceps, tibialis anterior, and diaphragm muscles of treated mice. 40 $\mu$ g of protein was loaded for each muscle for the *mdx* mice, and 4 $\mu$ g of protein was loaded for the C57BL/6 control. Data in this figure are represented in aggregate in Figure 5. Each lane represents an independent mouse.

Compound	Fluorescence (Plate 1)	Fluorescence (Plate 2)	Fluorescence (Plate 3)	Fluorescence (Plate 4)	Fluorescence (Plate 5)	Fluorescence (Plate 6)	Average Fluorescence (n=6)	Standard Deviation	Library	Target
GF 109203X	22.19	15.01	13.67	66.78	64.46	68.48	41.76	27.36	Enzyme Inhibitor	Protein kinase C inhibitor.
Ro 31-8220	17.56	50.61	46.79	38.49	31.21	34.94	36.60	11.81	Enzyme Inhibitor	Protein kinase C inhibitor.
Harmaline HCl	31.97	27.56	27.06	22.50	16.09	19.75	24.15	5.80	Orphan Ligand	Possible endogenous beta-carboline derivative.
Indirubin	4.64	-0.42	6.43	89.35	3.42	3.88	17.88	35.08	Enzyme Inhibitor	GSK-3beta and CDK5 inhibitor.
5-Iodotubercidin	-0.41	6.65	9.13	18.27	30.70	6.10	11.74	11.08	Enzyme Inhibitor	Inhibits ERK2, adenosine kinase, CK1, CK2, and insulin receptor kinase.
Dichlorobenzamil	22.19	15.01	13.67	4.78	7.44	6.66	11.63	6.58	Ion Channel	Calcium Channels
Indirubin	24.66	2.02	6.44	8.35	6.60	1.51	8.26	8.48	Orphan Ligand	Endogenous
Wortmannin	4.99	3.07	4.23	5.92	6.44	3.78	4.74	1.29	Enzyme Inhibitor	Phosphatidylinositol 3-kinase inhibitor.
Docosetetra-7Z,10Z,13Z,16Z-enoyl dopamine	-1.65	5.21	7.47	2.30	9.50	5.44	4.71	3.94	Endocannabinoid	-
Tetrandrine	3.15	2.41	5.39	4.64	5.03	6.64	4.54	1.54	Ion Channel	Calcium Channels
AG-879	1.23	3.24	3.46	6.94	8.93	2.08	4.31	2.99	Enzyme Inhibitor	Tyrosine kinase inhibitor.
Cantharidin	11.40	-1.04	0.63	5.55	4.34	4.45	4.22	4.33	Enzyme Inhibitor	PP1 and PP2A inhibitor.
AG-494	5.92	1.23	1.65	7.58	3.54	5.26	4.20	2.50	Enzyme Inhibitor	Tyrosine kinase inhibitor.
Niguldipine	5.07	1.34	3.34	8.06	6.06	0.84	4.12	2.80	Ion Channel	Calcium Channels
Oleoyl dopamine	2.78	1.51	12.34	3.21	3.30	1.32	4.08	4.14	Endocannabinoid	-

#### BioMol Screen Results: Top 5% of Compounds in the Without h50AON Screen

Compound	Fluorescence (Plate 1)	Fluorescence (Plate 2)	Fluorescence (Plate 3)	Average Fluorescence (n=3)	Standard Deviation	Library	Target
6-Formylindolo [3,2-b] Carbazole	30.05	30.08	32.59	30.90	1.46	Orphan Ligand	Endogenous
Cyclopiazonic Acid	29.57	33.40	17.24	26.74	8.44	Ion Channel	Intracellular Calcium
H-7	29.03	30.45	12.11	23.87	10.20	Enzyme Inhibitor	Inhibits PKA, PKG, MLCK, and PKC.
U-0126	17.87	35.65	16.65	23.39	10.63	Enzyme Inhibitor	MEK inhibitor.
AG-494	19.38	25.36	25.25	23.33	3.42	Enzyme Inhibitor	Tyrosine kinase inhibitor.
Harmaline HCl	15.00	42.55	0.22	19.26	21.48	Orphan Ligand	Possible endogenous beta-carboline derivative.
Dantrolene	16.32	11.76	26.51	18.20	7.55	Ion Channel	Intracellular Calcium
Pinacidil	15.64	27.20	11.56	18.13	8.11	Ion Channel	Potassium Channels
Procainamide	13.80	19.66	20.81	18.09	3.76	Ion Channel	Sodium Channels
1,1'-Ethylidene-bis-L-Tryptophan	20.72	11.15	22.18	18.02	5.99	Orphan Ligand	Bioactive tryptophan derivative
Tyrphostin 46	8.61	30.70	14.09	17.80	11.50	Enzyme Inhibitor	EGF receptor kinase, p56, and PDGF receptor kinase inhibitor.
AG-825	17.24	23.38	11.53	17.38	5.93	Enzyme Inhibitor	HER1-2 tyrosine kinase inhibitor.
AG-490	7.17	30.27	13.54	16.99	11.93	Enzyme Inhibitor	JAK-2 tyrosine kinase inhibitor.
H-9	18.09	19.17	13.25	16.84	3.16	Enzyme Inhibitor	Protein Kinase Inhibitor
Ryanodine	7.93	28.86	13.31	16.70	10.87	Ion Channel	Intracellular Calcium

#### BioMol Screen Results: Top 5% of Compounds in the With h50AON Screen

**Table S1. Top 5% of compounds from the BioMol ± h50AON high-throughput screens.** Compounds were rank ordered based on the average normalized fluorescence and the top 5% ( $n=15$ ) are given for the “with AO” or “without AO” high-throughput screens. Within the hits identified in the with AO screen, there was a significant over-representation of compounds modulating intracellular calcium ( $P=0.003$ ; Fisher’s Exact Test).

Group Number	Intramuscular Dose of PMOE23 ( $\mu$ g) in saline	Intraperitoneal Dose of Dantrolene (mg/kg) in 20% DMSO in saline	Intraperitoneal Dose of 20% DMSO in saline	Number of Mice per Group	Sex	Age
1	Saline	10	-	3	F	17 weeks
2	Saline	20	-	3	F	16 weeks
3	10 $\mu$ g	-	+	3	M	15 weeks
4	2 $\mu$ g	-	+	3	F	15 weeks
5	2 $\mu$ g	10	-	3	M	15 weeks
6	2 $\mu$ g	20	-	3	F	15 weeks

**Table S2. Treatment groups for the local administration of PMOE23 in combination with systemic dantrolene shown in Fig. 3.**

Group Number	Intravenous Dose of PMOE23 (mg/kg) in saline	Intraperitoneal Dose of Dantrolene (mg/kg) in 20% DMSO in saline	Intraperitoneal Dose of 20% DMSO in saline	Number of Mice per Group	Sex	Age
1	Saline	10	-	3	M	6 weeks
2	100mg/kg (2mg)	-	-	3	2F + 1M	6 weeks
3	10mg/kg (.2mg)	-	+	4	F	6 weeks
4	10mg/kg (.2mg)	10	+	4	F	6 weeks

**Table S3. Treatment groups for the systemic administration of PMOE23 in combination with systemic dantrolene shown in Figs. 5 and 6 and figs. S5 and S6.**

## CHAPTER FOUR

High-throughput Chemical Genetics Identifies Structurally Similar Small Molecules  
that Enhance Antisense-Targeted *DMD* Exon Skipping

## *Abstract*

Duchenne muscular dystrophy is a progressive muscle wasting disease typically caused by large multi-exon deletions in the *DMD* gene. One of the most promising therapies is antisense oligonucleotide (AO) targeted *DMD* exon skipping, yet exon skipping in ongoing clinical trials remains inefficient. Here, we perform a high-throughput screen designed to identify small molecules that specifically increase antisense-targeted *DMD* exon skipping activity. We find a subset of active small molecules with shared 2-D structures that also enhance AO targeted *DMD* exon 51 skipping in a clinically relevant reprogrammed patient iDRM. One group of the most active structurally similar compounds share a known molecular target of calmodulin inhibition, suggesting the importance of  $\text{Ca}^{2+}$  regulation and its impact on  $\text{Ca}^{2+}$  binding proteins in regulating exon skipping activity.

## *Introduction*

Duchenne muscular dystrophy (DMD) is the most common childhood muscular dystrophy affecting 1/4,000 males worldwide [1]. DMD is caused by mutations in the X-linked *DMD* gene, which encodes dystrophin, a protein that when absent compromises sarcolemma stability [2-5]. Resulting consequences include a cyclical degeneration and regeneration process in which muscle satellite cells are continuously replacing damaged myofibers [6,7]. Skeletal muscle is further insulted by immune cells that scavenge necrotic tissue, adipose cells replacing dystrophic muscle and fibrosis [8-11]. This culminates in an environment in which skeletal and cardiac muscle is progressively rendered non-functional, leading to respiratory or cardiac complications, and patient death by the third decade of life [12,13]. To date, no FDA approved therapies directly address the underlying genetic defect. Corticosteroids can prolong ambulation for up to 3 years and improve patient quality of life, but are not curative [14,15].

Several potential DMD therapies are in pre-clinical development or ongoing clinical trials [16-19]. The most progressed therapy is antisense oligonucleotide (AO) targeted *DMD* exon skipping. Two AO chemical backbones, 2-O-methyl (2'OMe) and morpholino (PMO), are in Phase IIb and Phase III clinical trials and target an exonic splice enhancer (ESE) element to skip *DMD* exon 51, addressing 13% of all DMD mutations [20-24]. After weekly systemic administration in DMD patients AOs rescued dystrophin expression ranging from 0-15% or 47% of normal levels [21,25]. Based on data from transgenic *mdx* mice and allelic diseases, X-linked dilated cardiomyopathy and Becker muscular dystrophy, it is predicted that 20-30% of normal dystrophin levels may be required for a therapeutic benefit [26-28]. In addition, antisense based therapies have variable exon skipping efficiencies within the same muscle, across muscle types, and between patients and types of deletions indicating potential for improvements [21,23,29].

There are many strategies to address limitations of AO distribution and exon skipping efficacy *in vivo* [30-33]. We have focused on finding independent molecular targets that potentiate antisense based exon skipping. Our previous work identified dantrolene, a FDA approved drug that increased AO targeted exon skipping activity in a high-throughput screen (HTS), in human and mouse cell models, and in *mdx* mice treated with AO provided a functional benefit [33]. Dantrolene and other small molecule inhibitors of the Ryanodine Receptor (RyR1) also increased exon 51 skipping in a patient iDRM, suggesting this as the relevant molecular target. This highlights the advantage of a HTS workflow, which identifies compounds with significant biological activity and effectively re-purposes their use. We focused on identifying FDA approved drugs that modulated exon skipping activity given that these drugs typically have known molecular targets and toxicity profiles.

Here, we perform an independent HTS to identify additional molecular targets and to better understand relevant pathways and interactions for small molecule potentiation of AO exon skipping in skeletal muscle. Further, we combine HTS data with a structure based

clustering analysis in which 2-D descriptors and hierarchical clustering segregate biologically active from inactive compounds [34,35]. We found that compounds with similar 2-D structures possessed comparable exon skipping activity in the screen [36]. Therefore, we hypothesized that a structure-activity relationship could guide our understanding of molecular targets and responsible signaling pathways for this observed exon skipping effect [37]. This approach identified several active small molecules, two of which had the greatest exon skipping activity and are structurally similar, Fluphenazine and Trifluoperazine. These two drugs share several known molecular targets, including inhibition of calmodulin (CaM), an intracellular Ca<sup>2+</sup>-binding protein, highlighting the importance of calcium regulation in potentiating antisense based therapies [38,39].

### *Materials and Methods*

#### *High-throughput screen in the Ex50GFP reporter cell line*

A stable clone was generated from C2C12 cells transfected with a human exon-50 *DMD* GFP reporter (ex50GFP) [32]. Ex50GFP myoblasts were seeded at a density of 4,000 cells per well into uncoated 384 well plates in myoblast growth media (Phenol red free DMEM, 15% FBS, 1X L-glutamine and 1X Pen/Strep). Cells were incubated for 4 hours either with or without ( $n=2$  replicates) 300nM of 2'-O-methyl phosphorothioate h50AON (-19+8) 5'-AACUCCUCUUUAACAGAAAAGCAUAC-3' targeting exon 50 skipping by masking the intron-exon boundary at the 3' intron 49 splice acceptor site. h50AON was transfected using FUGENE (Roche) at a ratio of 3 $\mu$ L FUGENE:1 $\mu$ g DNA. Following h50AON incubation, the Prestwick library ( $n=1120$ , across 4 plates) was screened in duplicate at a 10 $\mu$ M concentration with a final concentration of 1% DMSO carrier. The final well volume was 50 $\mu$ L. Forty-eight hours later DNA was stained with Hoescht (Sigma) by adding 100 $\mu$ g/mL final concentration and incubating for 30min at 37 °C. Following Hoescht incubation, fluorescence was measured using MicroXpress with GFP fluorescence having an exposure setting of 350ms and Hoescht at 21ms.

### *High-throughput screen normalization and analysis*

Analysis of high-throughput screening data was performed using a custom script in MatLab (R2011a). Each screen was normalized in a step-wise fashion first on an intra-plate basis, and then across plates ( $n=4$  plates). Rows ( $n=22$  elements per row) were normalized by dividing the fluorescence for each well ( $\Psi_{\text{well}}$ ) by the mean of the entire row ( $\mu\Psi_{\text{row}}$ ), and then multiplying by the mean plate fluorescence ( $\mu\Psi_{\text{plate}}$ ) (shown in equation 1). Columns ( $n=14$  elements) were then normalized using the same strategy (shown in equation 2).

$$(1) \varphi_{\text{norm}} = \frac{\varphi_{\text{well}}}{\mu\varphi_{\text{row}}} \times \mu\varphi_{\text{plate}}$$

$$(2) \varphi_{\text{norm}} = \frac{\varphi_{\text{well}}}{\mu\varphi_{\text{column}}} \times \mu\varphi_{\text{plate}}$$

Interplate normalization was performed as follows. Row fluorescence ( $\Psi_{\text{row}}$ ) was divided by the row means of all four plates ( $\mu\Psi_{\text{rows}}$ ), and multiplied by the mean fluorescence from all plates ( $\mu\Psi_{\text{plates}}$ ) (shown in equation 3). Columns were then normalized using the same strategy (shown in equation 4). Duplicate plates from independent screening days were then averaged and normalized.

$$(3) \varphi_{\text{norm}} = \frac{\varphi_{\text{row}}}{\mu\varphi_{\text{rows}}} \times \mu\varphi_{\text{plates}}$$

$$(4) \varphi_{\text{norm}} = \frac{\varphi_{\text{column}}}{\mu\varphi_{\text{columns}}} \times \mu\varphi_{\text{plates}}$$

To determine compound performance in the screens the Z score was calculated by comparing the normalized fluorescence of each compound to that of the DMSO controls on all plates ( $n=128$ ). The Z score was calculated for the ‘Compound only’ and ‘Compound+AO’ screen using equation 5.

$$(5) Z = (\varphi_{compound} - \mu\varphi_{dms0})/\sigma_{dms0}$$

For the ratio analysis additional steps were taken so that the ‘Compound+AO’ screen and ‘Compound only’ screen could be directly compared. To find the overall effect of adding AO on fluorescence readouts, the mean fluorescence values from the DMSO controls for the ‘Compound+AO’ screen were divided by the DMSO controls in the ‘Compound only’ screen. This number was 2.52. Therefore, all ‘Compound+AO’ normalized fluorescence values were divided by 2.52, followed by the division of the corresponding ‘Compound only’ fluorescence values. The ratio Z score was then calculated using equation 5. Hierarchical clustering analysis on screen performance was performed in Matlab.

### *2-D Structural Clustering*

A 2-D structure-based clustering algorithm was applied to the Prestwick libraries to determine if common structural motifs were responsible for exon skipping activity using the ChemmineR package in R (Version 3.0.1) [40]. Compound library SDF files were clustered into discrete similarity groups with the binning clustering function that determines compound similarity utilizing multiple user-defined cutoffs. SDF files were also obtained for 4009 ligands with crystal structures bound to their respective protein targets from the Research Collaboratory for Structural Bioinformatics Protein Data Bank (PDB). In both cases, after a heuristic search in which the libraries were clustered with a range of cut-offs the optimal threshold for similarity cutoff was determined to be 0.65, which is near suggested values that have been previously published [40,41].

### *Compounds*

The following compounds were obtained from Sigma-Aldrich: Quinacrine dihydrochloride (CAS# 6151-30-0), Yohimbinic acid monohydrate (CAS# 27801-27-2), Menadione (CAS# 58-27-5), Fluphenazine dihydrochloride (CAS# 146-56-5), Trifluoperazine dihydrochloride (440-17-5).

Piperacetazine (CAS# 3819-00-9) was obtained directly from the Prestwick Small Molecule library resource. Rauwolfscine hydrochloride (CAS# 6211-32-1) was obtained from Santa Cruz Biotechnology, Inc.

#### *MyoD Induction, Myotube fusion, and AO Transfection*

iDRMs (inducible directly reprogrammable myotubes) were seeded at 150,000 cells per well in fibroblast growth media (DMEM (+phenol red, high glucose) + 15% Fetal Bovine Serum (FBS) + 1% Nonessential amino acids + 1% pen/strep) in 6-well plates (Corning) pre-coated for 1 hour with 2.5mL of 5µg/mL laminin in serum free DMEM (BD Biosciences). The following day, 5µM 4OH-tamoxifen (Sigma; resuspended in ethanol) was added in fibroblast growth media for 24 hours. On day 3, cells were washed in 1 x Phosphate Buffered Saline (PBS; Invitrogen), and fusion media containing 1µM 4OH-tamoxifen was added (1:1 Ham's F-10:DMEM (phenol red free, high glucose), 2% Horse Serum, 2% Insulin-Transferrin-Selenium). On Day 7, cells were transfected with 50nM, 100nM or 200nM, 2-O-methyl AO targeting exon 51 (5'-UCAAGGAAGAUGGCAUUUCU-3') (MWG Operon) using the ExGen500 (Fermentas) transfection reagent at a ratio of 5.5µL:1µg of DNA. AO was removed on day 8, cells were washed with 1XPBS, and fresh fusion media containing 1µM 4OH-tamoxifen was added with titrating concentrations of drug and carrier controls. Forty-eight hours later, cell pellets were harvested and frozen for subsequent RNA isolation and exon skipping analysis [33].

A 5' FAM labeled 2'OMe AO targeting exon 51 (FAM-h51AON; 5'-FAM-UCAAGGAAGAUGGCAUUUCU-3', GenScript) was used for flow cytometry experiments assessing the efficiency of labeled AO uptake. FAM-h51AON was added on Day 7 to fusing iDRMs, removed, and cells were washed in 1XPBS. Forty-eight hours later each well was split in half; one half dedicated to RNA isolation and exon 51 skipping analysis, and the other half to

flow cytometry analysis. For flow cytometry, cells were gated on the live population and the percentage of FAM positive cells was analyzed using WinMDI software.

#### *RNA Isolation, PCR, and qPCR*

Cell pellets were collected, and total RNA isolated using the QIAGEN RNeasy Microkit. For exon 51 skipping analysis, 200ng of total RNA was reverse transcribed with an exon 54 gene specific primer [20]. A nested PCR was performed between *DMD* exons 43-52 using previously described primers, and the amplified product run on the Agilent 2100 Bioanalyzer for exon skipping quantification [20,33].

#### *Results*

##### *Correlation between AO uptake and exon skipping activity*

We explored the relationship between antisense oligonucleotide uptake and how it correlates to exon skipping activity in a cell culture system. To do this we used a 5' FAM labeled 2'OMe AO so that cellular uptake could be directly measured by flow cytometry and then related to *DMD* exon 51 skipping activity in iDRM5017. After plating and seven days of fusion, FAM-h51AON was added to the cells for 24 hours after which it was removed. Forty-eight hours later each well was harvested and split for analysis; one half designated for analysis by flow cytometry and the other half analyzed for exon 51 skipping activity by RT-PCR and capillary electrophoresis. We found that there was a dose dependent increase in the percentage of FAM positive cells (Fig. 1a). At the highest doses of 200nM and 300nM of FAM-h51AON the proportion of positive cells was nearing 100% of the entire population, and was almost indistinguishable from the positive control, the nuclear dye Quinacrine dihydrochloride. This trend was consistently observed when looking at a different measure, the mean fluorescence intensity (MFI) (Fig. 1b).

Although AO was added to cells with transfection reagent, the statistically significant increase in both FAM positive cells, and in the MFI, suggests that AO uptake was still to some extent dose dependent. From the conditions analyzed by flow cytometry we isolated total RNA and determined exon 51 skipping activity by a nested RT-PCR between *DMD* exons 43-52. There was a dose dependent increase in the proportion of *DMD* exon 51 skipping activity between 50-200nM FAM-h51AON (Fig. 1c). However, at 300nM FAM-h51AON there was a non-significant increase in the amount of observed exon skipping, indicating in this model a limitation of exon skipping capacity even with increased FAM-h51AON uptake (Fig. 1a, 1c). In parallel, an unlabeled h51AON 2'OMe was transfected into iDRM5017 and showed similar trends for *DMD* exon 51 skipping (Supplementary Fig. 1). These data suggest that the identification of independent molecular targets could further facilitate exon skipping activity.

#### *High-throughput screen to identify small molecule enhancers of AO mediated exon skipping*

To identify small molecules that synergize with antisense-based exon skipping strategies we performed a high-throughput screen of the Prestwick small molecule library ( $n=1120$  compounds). We utilized an Exon50-GFP reporter construct that has been previously described in which skipping *DMD* exon 50 restores the GFP reading frame, resulting in fluorescence [32]. This construct was stably transfected into C2C12 cells, a mouse myoblast line, and plated on 384 well plate formats for small molecule screening at a 10 $\mu$ M effective dose. Screens were performed in duplicate both in the presence of a sub-optimal dose of 300nM 2'OMe h50AON antisense oligonucleotide directed against human exon 50 or with compounds only. AO was added before incubation of the cells with the small molecules to identify those that facilitate AO-mediated exon skipping rather than AO delivery. Fluorescence readouts were measured using an automated quantitative fluorescent scanning system.

During analysis significant bias was observed between intra-plate row and column fluorescence values indicating the presence of systematic error (Supplementary Fig. 2a, 2e) [42].

Therefore, fluorescence values from plate rows and columns were normalized by mean polish in a step-wise fashion, first on a plate-by-plate basis and then across plates, which significantly reduced the observed variability (Methods, Equations 1-2; Supplementary Fig. 2b, 2f) [43]. Normalization was then performed across all four plates (Methods, Equations 3-4). Duplicate plates were normalized to each other to account for variability across screening days (Supplementary Fig. 2c, 2g). This resulted in a better approximation of a normal distribution when comparing pre and post-normalization raw fluorescence values (Supplementary Fig. 2d, 2h), as would be expected from an unbiased larger screen [43,44].

The Z score was calculated to differentiate compound performance in the screen, and represents the number of standard deviations away from the mean of the DMSO carrier controls (Methods, Equation 5). Z scores are plotted for all 1120 compounds in the ‘without’ and ‘with AO’ screen (Fig. 2a-b), with the distribution from each plate approximating normal (Supplementary Fig. 3a-b). Both of these screens identified several small molecules that increased observed fluorescence (Table 1). To eliminate artifacts such as autofluorescent compounds (see arrow in Fig. 2a-b), and to better discriminate small molecules that only had activity in the ‘Compound+AO’ screen the ratio was calculated for the ‘Compound+AO’/‘Compound only’ counterscreen (see Methods). The calculated ratio Z score is plotted for all 1120 compounds (Fig. 2c, Supplementary Fig. 3c). This approach effectively eliminated the presence of false positives, such as Quinacrine Dihydrochloride, which is a DNA intercalator and emits in the same channel as GFP (Fig. 2a-c; Table 1). In principle, compounds with the highest ratio Z scores exhibit exon skipping activity specifically in the presence of AO. After hierarchical clustering analysis of all Z scores from all three screens, the ratio Z score had higher similarity to the ‘with AO’ screen, as would be expected (Fig. 2d).

*Identification of screening hits by combining 2-D structural clustering, screen performance, and potential molecular targets*

We applied a 2-D structure-based clustering algorithm to the Prestwick library to determine if compounds with shared structural motifs exhibited comparable exon skipping activity [45]. The majority of compounds ( $n=751$ ) did not have structurally similar counterparts. However, there were still multiple clusters of varying sizes ranging from 2-18 compounds (Fig. 3a). The structural similarity present in the library was plotted for all clusters containing four or more compounds, and circled clusters were chosen for additional evaluation in iDRMs (Fig. 3b). Shared structures would be expected to have similar binding partners, increasing the likelihood that an intersection of activity and targets will identify conserved pathways responsible for the observed exon skipping effect [45]. Therefore, we expanded the structural clustering analysis to include over 4,000 small molecule ligands present in the Protein Data Bank (PDB), which contains well-defined crystal structures of ligands bound to their respective protein targets, as an unbiased means to determine potential protein targets for our screen. We found many compounds that both performed well in the screen and were structurally similar to ligands identified in PDB (Supplementary Table 1). Based on the PDB clustering results, exon skipping activity from the HTS, and the identification of additional compounds in the screen that possessed 2-D structural similarity, clusters of compounds were chosen for further evaluation in patient specific iDRMs.

#### *Assessment of compound synergy with AO in DMD patient iDRMs*

A subset of compounds was chosen to evaluate *DMD* exon skipping activity in iDRMs to determine if screening results were recapitulated in a relevant human model. iDRM5017 contains a *DMD* exon 45-50 deletion that is put back in-frame by the skipping of exon 51. Small molecules were assessed for synergy with doses of sub-optimal AO (50nM) targeting exon 51. Representative compounds were chosen for evaluation from the ‘Compound only’ screen, the ‘Compound+AO’ screen, and the ratio analysis of the two screens. First, from the ‘Compound only’ screen, menadione was chosen based on its Z score rank (#3 overall) as well as clustering

with a PDB molecular target, quinone reductase (Table 1, Fig. 4a-b). Previously, menadione was FDA approved as a dietary supplement. Menadione increased *DMD* exon 51 skipping moderately, approximately 2 fold at a 1 $\mu$ M concentration in combination with the sub-optimal 50nM h51AON dose (Fig. 4c). The 10 $\mu$ M dose proved to be toxic to cells. In addition, menadione possesses potential molecular targets with downstream effects including those that menadione binds directly, such as quinone reductase, or targets in which expression is indirectly regulated (Fig. 4d).

The subset of compounds chosen from the ‘Compound+AO’ screen was both highly ranked based on Z score and structurally similar. Cluster 394 was chosen based on these criteria and includes Rauwolscine hydrochloride (#3), Yohimbic acid monohydrate (#11) and additional structurally similar compounds, Yohimbine hydrochloride and Corynanthine hydrochloride (Table 1, Fig. 5a). These plant alkaloids and FDA approved drugs are known to bind  $\alpha$ 1 and  $\alpha$ 2 adrenergic receptors and are currently used in the treatment of erectile dysfunction [46]. Based on hierarchical clustering of their screen performance, these compounds were predicted to possess similar exon skipping activity (Fig. 5b). Indeed, both Rauwolscine HCl and Yohimbic Acid modestly increased *DMD* exon 51 skipping in iDRM5017 in a dose dependent manner, suggesting that they may be acting on a conserved molecular target (Fig. 5c). An analysis of their direct and indirect interactions includes an increase in expression of transcriptional regulators EGR1 and FOS, among other potential targets (Fig. 5d).

Analysis of the ratio Z scores found a compound cluster that matched all three of these criteria: screen activity, structural similarity, and a putative molecular target from PDB. Cluster 222 is composed of phenothiazines that have been used in the treatment of psychiatric disorders, and includes 6 structurally similar small molecules, one of which, Fluphenazine dihydrochloride, was ranked #2 based on its Z score from the HTS (Table 1, Fig. 6a). All 6 compounds are structurally similar at a cut-off of 0.65; however, at more stringent cutoffs three groups are delineated one of which includes Fluphenazine and Trifluoperazine (TFP).

Hierarchical clustering of screen performance indicates that Fluphenazine and Trifluoperazine are more closely related in terms of activity than the less structurally similar, Piperacetazine (Fig. 6b). These results were recapitulated when examining *DMD* exon 51 skipping in iDRM5017. Piperacetazine did not significantly increase antisense based exon skipping activity, which corroborates the high-throughput screening results. Trifluoperazine and Fluphenazine increase *DMD* exon 51 skipping in a dose dependent and statistically significant manner, ranging from a 3-5 fold increase (Fig. 6c), indicating that these structurally similar compounds have comparable exon skipping activity.

Trifluoperazine and Fluphenazine share five molecular targets including dopamine receptors, histamine receptors, neurotensin, Troponin C, and Calmodulin (Fig. 7) [38,39]. Trifluoperazine is a PDB ligand with a crystal structure bound to CaM, a calcium secondary messenger that is well documented to regulate downstream transcriptional targets including MEF2, SRF, CREB, PGC-1 $\alpha$ , among others [38,39,47]. TFP potently binds Ca<sup>2+</sup>-CaM, or activated CaM, and this binding induces 3-D conformational changes from an active ‘dumbbell’ form to an inactive ‘globular’ form. In the inactive ‘globular’ form the CaM hydrophobic pockets are unavailable for binding by target proteins, suggesting that CaM inhibition may be the relevant activity for this exon skipping effect [38,39].

### *Discussion and Conclusions*

DMD is one of the most common childhood forms of muscular dystrophy with no effective pharmacological therapies. Antisense oligonucleotides in clinical development target single exons for skipping, which restore the mRNA reading frame in a subset of *DMD* patients. To date, one of the main limitations with antisense based strategies is that the majority of systemically administered AO is cleared by the kidney instead of reaching the intended target, skeletal and cardiac muscle [48]. This has prompted studies focusing on improving AO efficacy, with strategies ranging from more efficient delivery methods to the identification of

independent molecular targets [30-33]. Another possibility for the observed inefficiencies is that even with the highest doses of AO in cells, all *DMD* mRNA transcripts are not efficiently skipped. These limitations are not mutually exclusive, and both can be addressed by the identification of distinct molecular targets that enhance exon skipping activity either: 1) in the presence of a sub-optimal dose of AO or 2) to increase the amount of maximum exon skipping that is observed with AO alone.

Our strategy was to perform a HTS and determine small molecules and by extension their molecular targets that could potentiate AOs and increase *DMD* exon skipping activity. We found that structurally similar compounds increased exon 51 skipping in iDRM5017, with the most active exon skipping drugs deriving from the ratio Z score analysis. In addition, these compounds contained plausible molecular targets identified from PDB ligands. Applying 2-D structure analysis distinguished biologically active from inactive compounds and gave insight into integral molecular pathways [37].

Previous work has identified small molecules from HTS that increase AO targeted exon skipping. In 2009, O'Leary *et al* screened ~10,000 small molecules in combination with AO to identify those that enhance *DMD* exon 72 skipping via a construct expressed in HEK 293 cells, a non-muscle cell line [31]. In their strategy and set-up exon skipping is only observed in the presence of both drug and AO. Hu *et al* performed a HTS using the Ex50GFP reporter construct without the addition of AO, indicating that compounds may exhibit non-specific effects [32]. Our screen was performed in a muscle cell lineage with an Ex50GFP reporter construct both without and with a sub-optimal AO concentration that increased baseline fluorescence, where drug enhancement of AO activity was observed over that baseline. In addition, we included a counterscreen of compounds only, and the ratio Z score analysis identified compounds with potent exon skipping activity specific to AOs.

Compounds identified in the screen and chosen for further evaluation synergized with two AOs; one targeting exon 50 in the high-throughput screen, and h51AON targeting exon 51, indicating the mechanism of action is likely not dictated by AO sequence specificity. Additional investigation is necessary to understand if exon skipping is enhanced in other *DMD* mutations, with AOs targeting different exons, and if this trend is observed with morpholino AOs. Small molecules are likely targeting distinct proteins and signaling pathways implying that exon skipping activity could be further induced by a combinatorial strategy of more than two drugs. For example, recently a small molecule, Retro-1, was found to potentiate exon skipping at the level of intracellular trafficking or processing and is correlated with increased AO accumulation in the nucleus [49]. The combination of multiple compounds could uniquely increase antisense efficacy, but first warrants an exact understanding of how these small molecules independently function.

Identified active drugs give insight into the link between affected molecular signaling pathways and how this translates into exon skipping. We identify Trifluoperazine and Fluphenazine as potent enhancers of AO exon skipping activity, with a well-documented molecular function of CaM inhibition [38,39]. CaM is the predominant cellular calcium sensor and is directly activated or inactivated by the concentration and spatiotemporal flux of calcium [50]. Typically, cytoplasmic Ca<sup>2+</sup> concentrations are 10<sup>3</sup> lower than Ca<sup>2+</sup> concentrations in the sarcoplasmic reticulum (SR). In response to a rise in cytoplasmic Ca<sup>2+</sup> concentrations, Ca<sup>2+</sup>-CaM will activate protein targets that redistribute from the cytosol to the nucleus and activate transcriptional targets or regulate alternative splicing processes [47,51,52]. Interestingly, O'Leary *et al* screened ~2000 kinase targeted siRNAs in a *DMD* exon 72 reporter construct, and found that knockdown of CaMK1 (a member of the Ca<sup>2+</sup>-Calmodulin dependent protein kinase family) and PKC, both downstream targets of CaM, increased AO targeted exon skipping 8 and 3 fold respectively, further supporting the observations described here [31].

Our previous work identified dantrolene inhibition of the RyR1 SR calcium channel, and modulation of intracellular calcium levels, as a mechanism for increasing AO exon skipping. Structurally distinct small molecule RyR1 inhibitors, ryanodine and S107, also increase AO based exon skipping, yet the mechanism by which RyR1 inhibition translates into exon skipping activity is unclear [53-55]. Trifluoperazine and Fluphenazine may provide insight into RyR1 downstream signaling events by indicating CaM as a relevant molecular target. Paradoxically, TFP has also been described in the activation of RyR2 mediated Ca<sup>2+</sup> release (RyR receptor in cardiac muscle), a biological activity that is independent of its reported calmodulin inhibition [56]. This supports the hypotheses that either 1) RyR1 antagonists are acting in the same pathway, but upstream of TFP/Fluphenazine CaM inhibition or 2) RyR1 antagonists and TFP/Fluphenazine are acting on completely distinct targets. The events downstream of CaM activated alternative splicing remain to be understood, yet its potent inhibition can increase exon skipping 3-5 fold, suggesting the importance of Ca<sup>2+</sup> regulation and its impact on Ca<sup>2+</sup>-binding proteins in directing exon skipping activity [38,39,53-55,57,58].

#### *Acknowledgments*

Viral packaging was performed at the UCLA Vector Core. Tamoxifen inducible MyoD-ER(T) construct was a kind gift from J. Chamberlain.

**Figure 1. Correlation of AO uptake and exon skipping activity in iDRM5017.** On the seventh day of iDRM5017 fusion, 5' FAM labeled h51AON targeting *DMD* exon 51 was transfected for 24 hours after which it was removed. After 48 hours each well was harvested for analysis, and split in half. **(A)** After gating on live cells, the percentage of FAM (or AO) positive cells was determined. Quinacrine dihydrochloride, a nuclear dye that emits at the same wavelength as FAM, was used as a positive control. **(B)** Mean fluorescence intensity of populations described in A. **(C)** The other half of each well was analyzed for *DMD* exon 51 skipping activity. Total RNA was isolated a nested RT-PCR performed between *DMD* exons 43-52. This experiment was repeated twice, with each condition being represented in triplicate. Error bars represent s.d. \* indicates  $P < 0.05$ .  $P$  values were determined using a two tailed student's t-test.

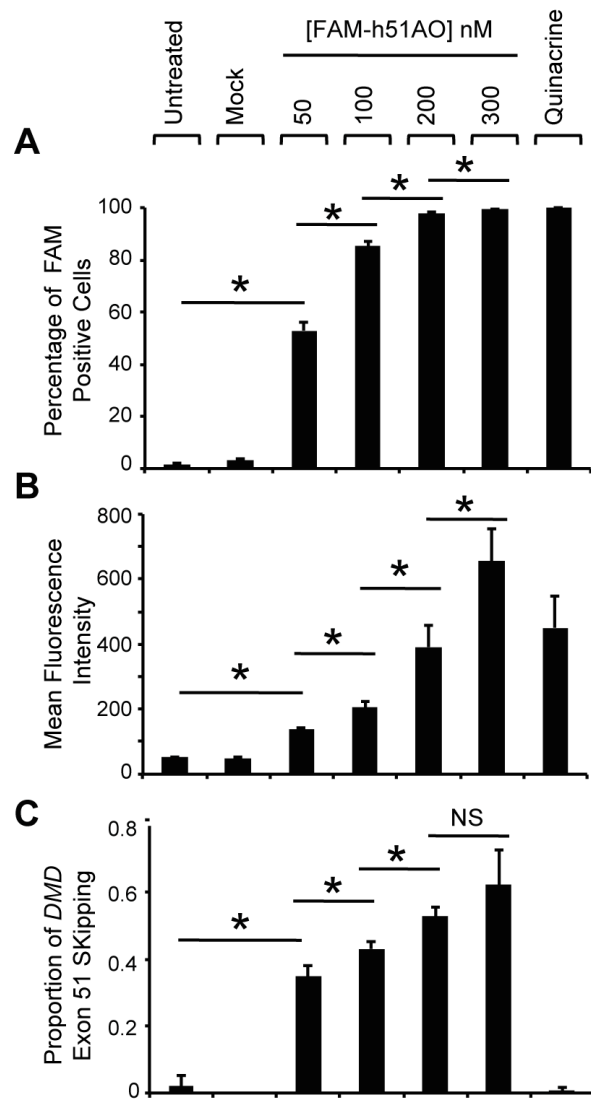


**Figure 2. High-throughput screening results and Z score determination.** The Z score was calculated from normalized fluorescence values for (A) 'Compound only' screen (B) 'Compound+AO' screen, done in the presence of a sub-optimal h50AON dose and (C) the ratio of the 'Compound+AO' divided by the 'Compound only' screen (+AO/C). Arrows indicate a DNA intercalator, Quinacrine dihydrochloride that was eliminated in the +AO/C analysis. (D) Hierarchical clustering of Z score values for the three screens. Arrows indicate locations of compounds that were chosen for further evaluation; the left arrow represents Cluster 222, the middle arrow represents Cluster 394, and the right arrow represents Menadione.

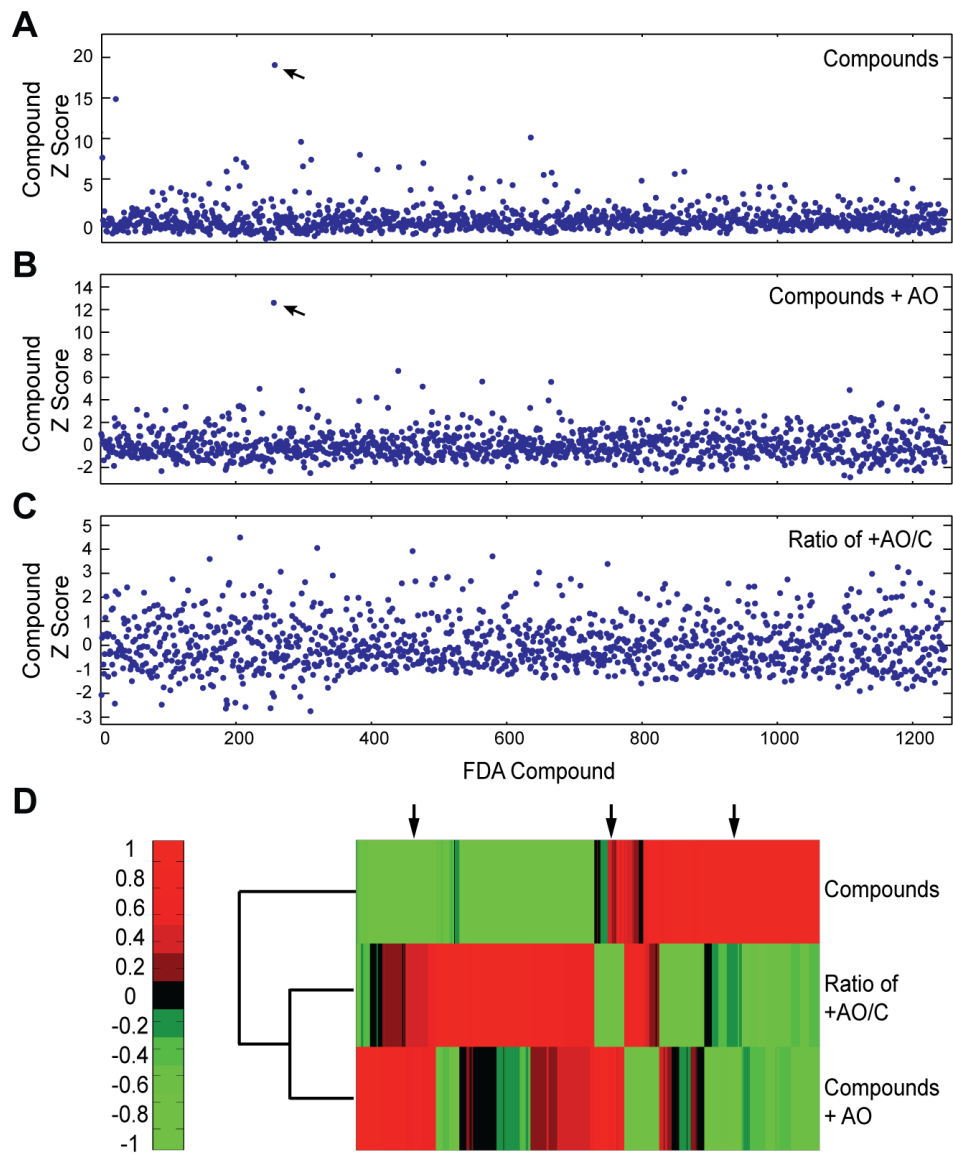


**Figure 3. 2-D structural clustering analysis of the Prestwick small molecule library.**

**(A)** Distribution of clusters present within the library as determined in ChemmineR. Similarity cutoff is 0.65. **(B)** Scatterplot of all of the clusters containing four or more compounds within the Prestwick small molecule library with a similarity cutoff of 0.65. Circled is Cluster 394 ( $n=4$ ), which was identified from the 'Compound+AO' screen, as well as Cluster 222 ( $n=6$ ), which was identified in the +AO/C ratio analysis.

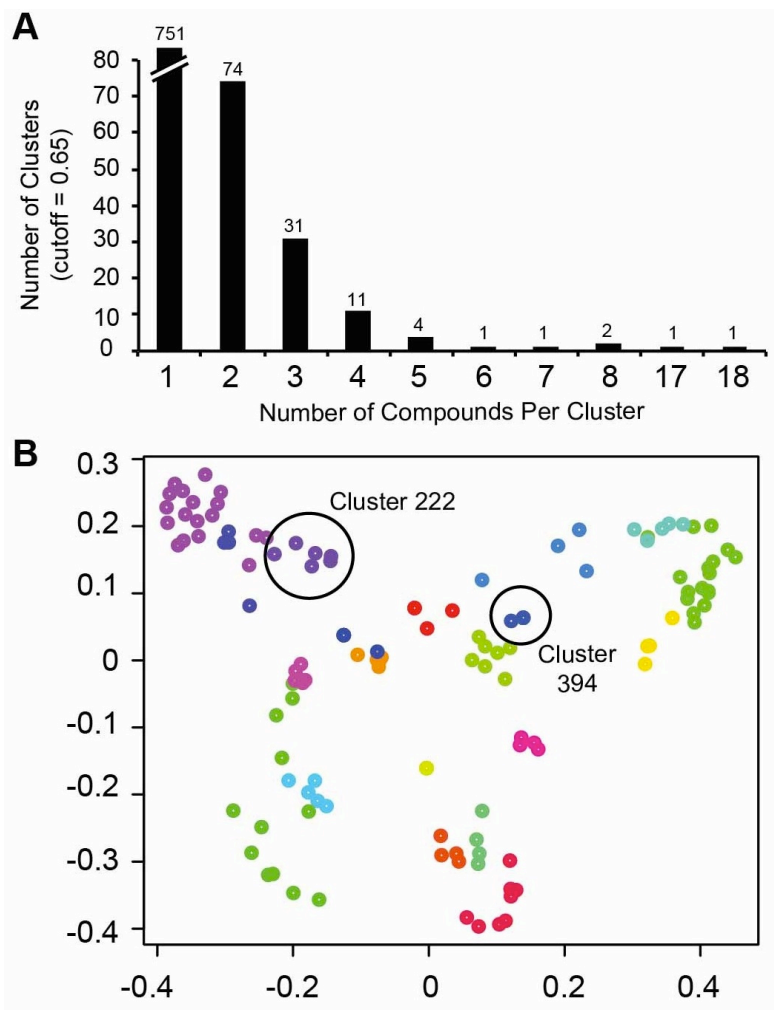


**Figure 4. Menadione as a potentiator of antisense-mediated exon skipping.**

Menadione was identified in the ‘Compound only’ screen. **(A)** Structure of Menadione, which **(B)** Clustered with VK3 in the Protein Data Bank, which has a known protein binding partner of quinone reductase. **(C)** Antisense-mediated *DMD* exon 51 skipping activity in iDRM5017. This experiment was repeated twice, with each condition being represented in triplicate. Error bars represent s.d. \* indicates  $P < 0.05$ .  $P$  values were determined using a two tailed student’s t-test. **(D)** Ingenuity interaction map of all known Menadione direct (solid line) or indirect (dotted line) protein interactions.

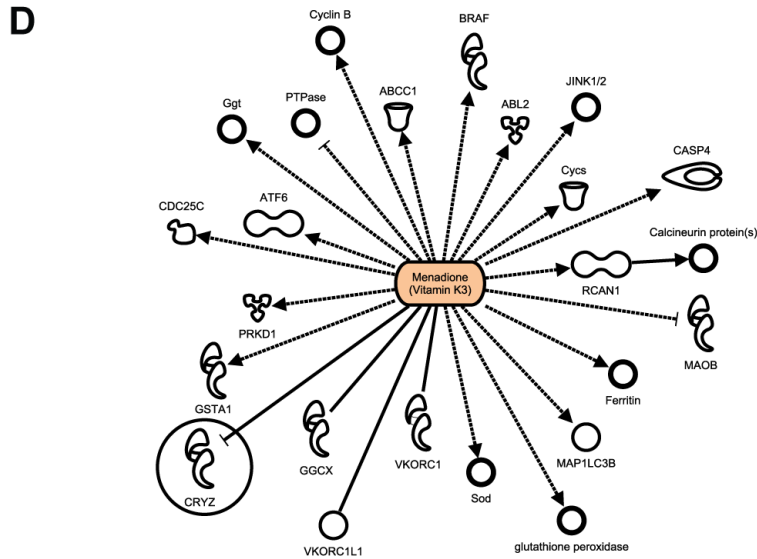
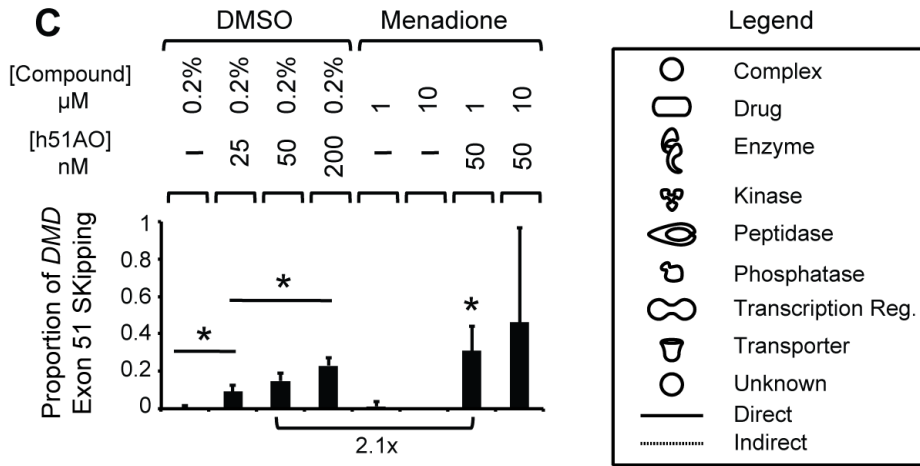
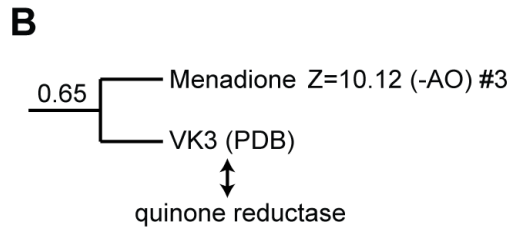
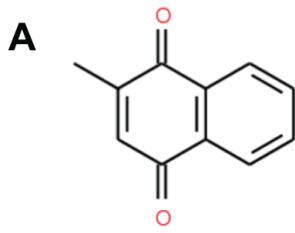


**Figure 5. Two structurally similar compounds from Cluster 394 increase antisense based exon skipping activity.** Structurally similar cluster 394 was identified in the ‘Compound+ AO’ screen, and consists of **(A)** Rauwolscine hydrochloride, Yohimbinic acid monohydrate, Yohimbine hydrochloride, and Corynanthine hydrochloride. **(B)** Hierarchical clustering of high-throughput screen performance for all four compounds. **(C)** *DMD* exon 51 skipping in iDRM5017. This experiment was repeated twice, with each condition being represented in triplicate. Error bars represent s.d. \* indicates  $P < 0.05$ .  $P$  values were determined using a two tailed student’s t-test. **(D)** Ingenuity interaction map of all known cluster 394 direct or indirect protein interactions.

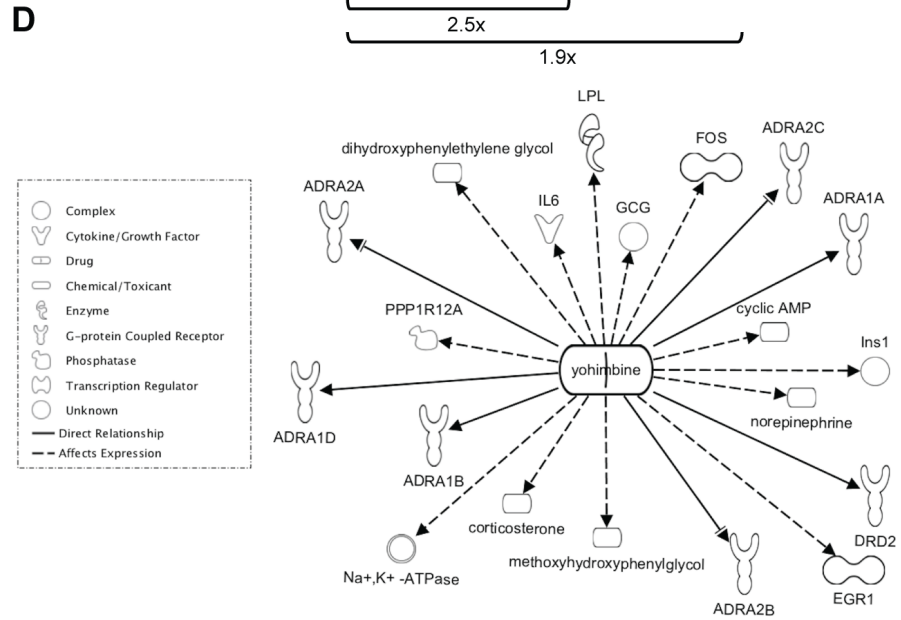
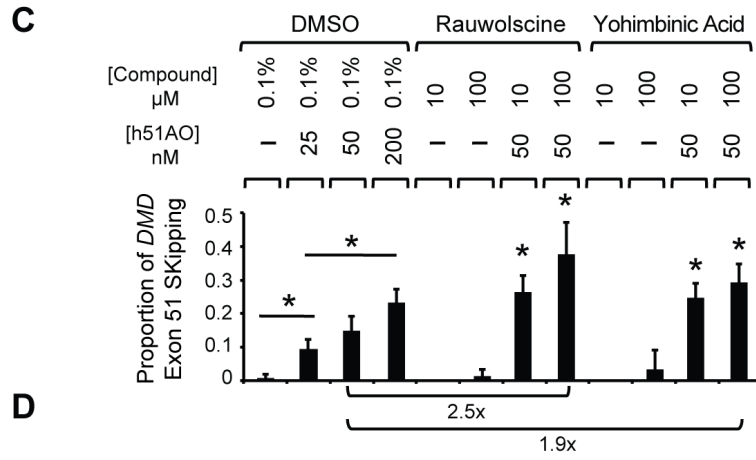
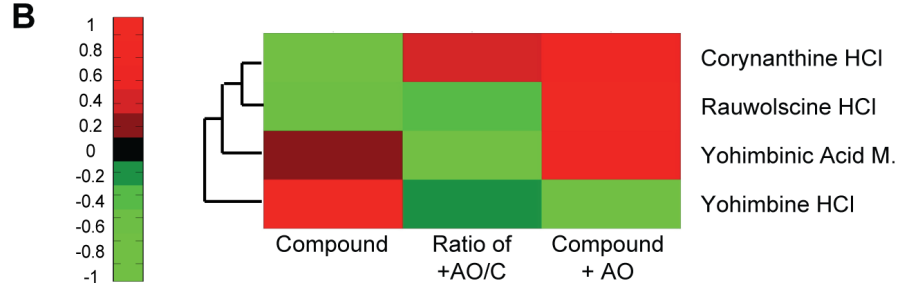
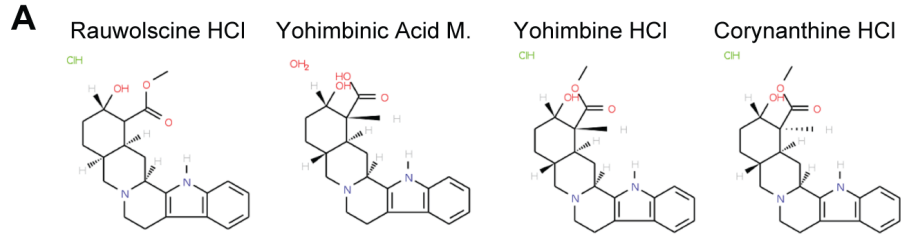


**Figure 6. Cluster 222, a calmodulin binding partner, modulates AO targeted exon skipping.** Structurally similar cluster 222 was identified in the ‘ratio’ analysis of high-throughput screening data and consists of **(A)** Fluphenazine hydrochloride, Trifluoperazine hydrochloride, Piperacetazine, Perphenazine, Flupentixol Dihydrochloride and Zuclopenthixol. To the right step-wise similarity cutoffs are displayed. **(B)** Hierarchical clustering of high-throughput screen performance for all compounds. **(C)** *DMD* exon 51 skipping in iDRM5017. This experiment was repeated twice, with each condition being represented in triplicate. Error bars represent s.d. \* indicates  $P < 0.05$ .  $P$  values were determined using a two tailed student’s t-test.

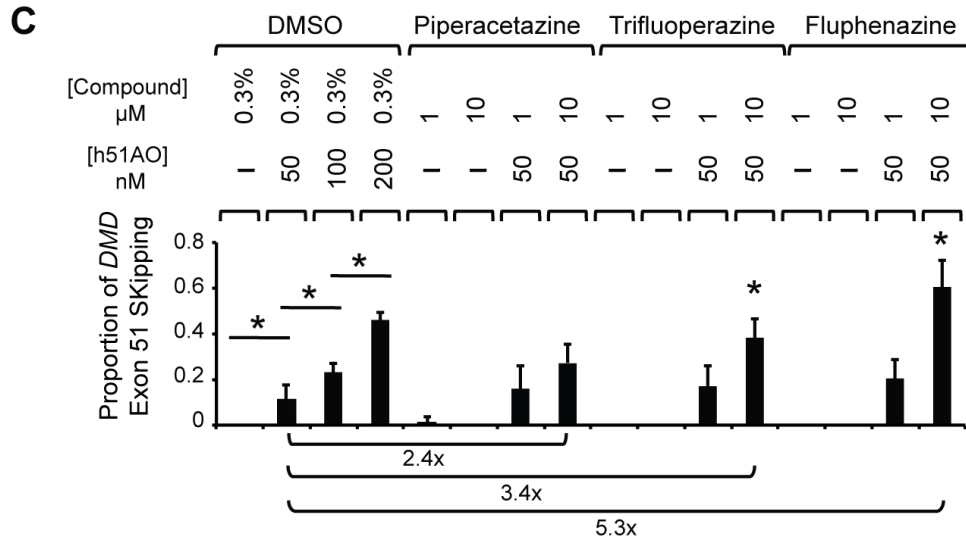
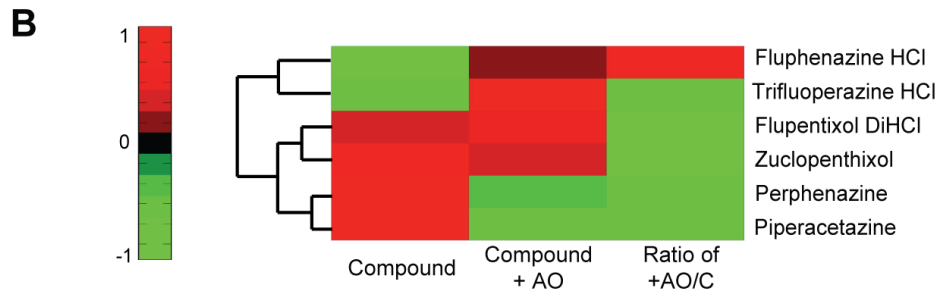
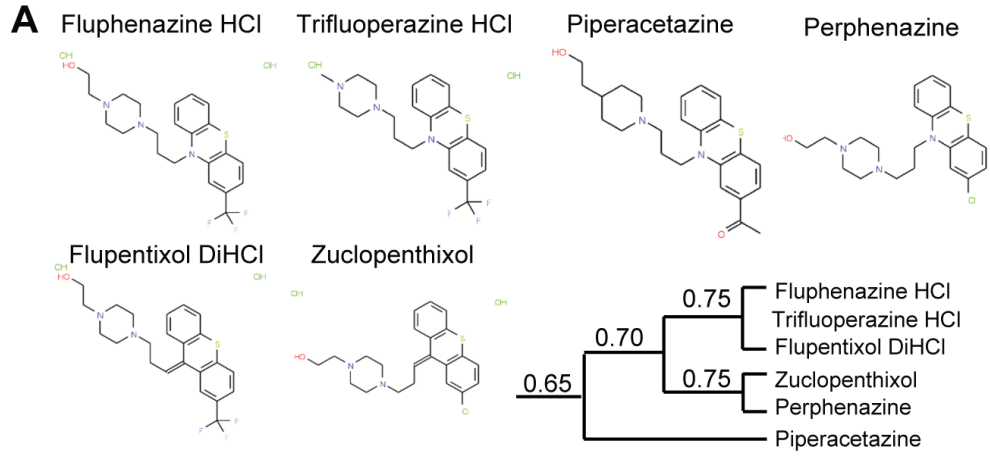
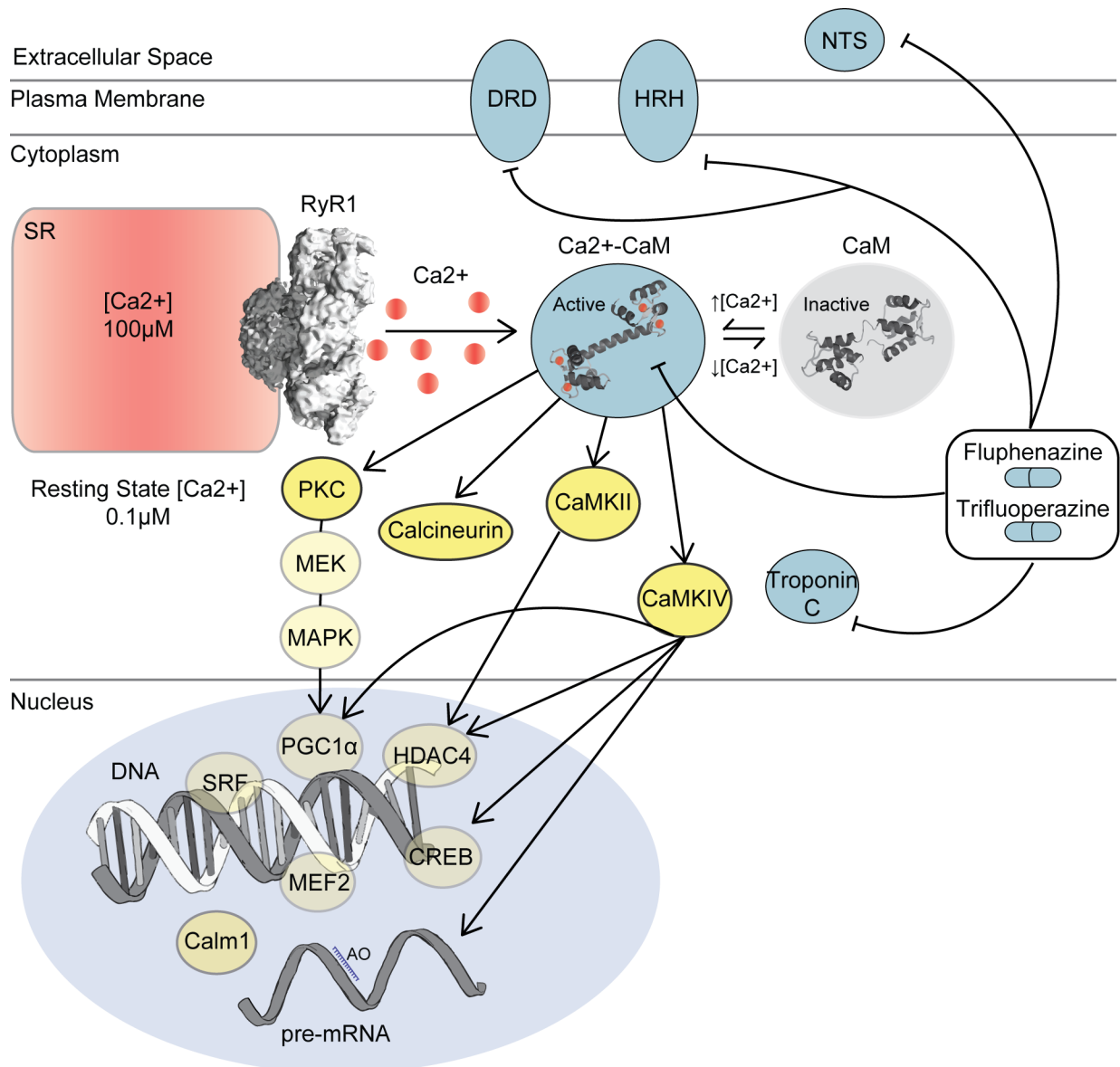
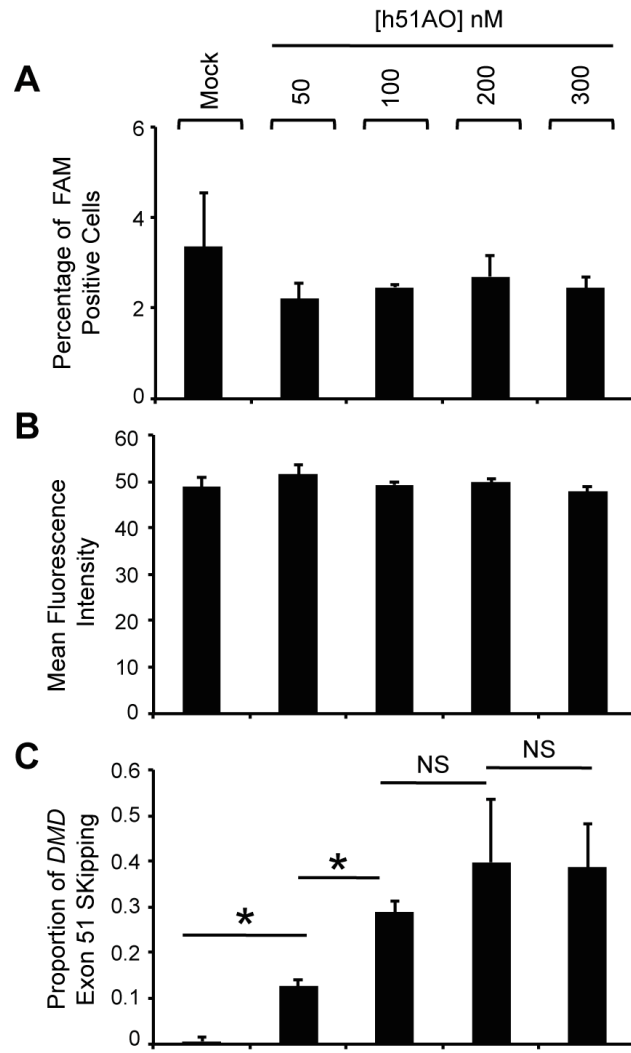


**Figure 7. A calcium mediated model of Cluster 222 directed exon skipping activity.**

Both Trifluoperazine and Fluphenazine exhibited an increase in exon skipping activity. All shared targets were determined by Ingenuity analysis and PDB analysis, and are displayed in their appropriate cellular compartments. Shared interactions between these two drugs and their direct and indirect affects are highlighted, as well as a sub-set of downstream signaling events that have been described in skeletal muscle.

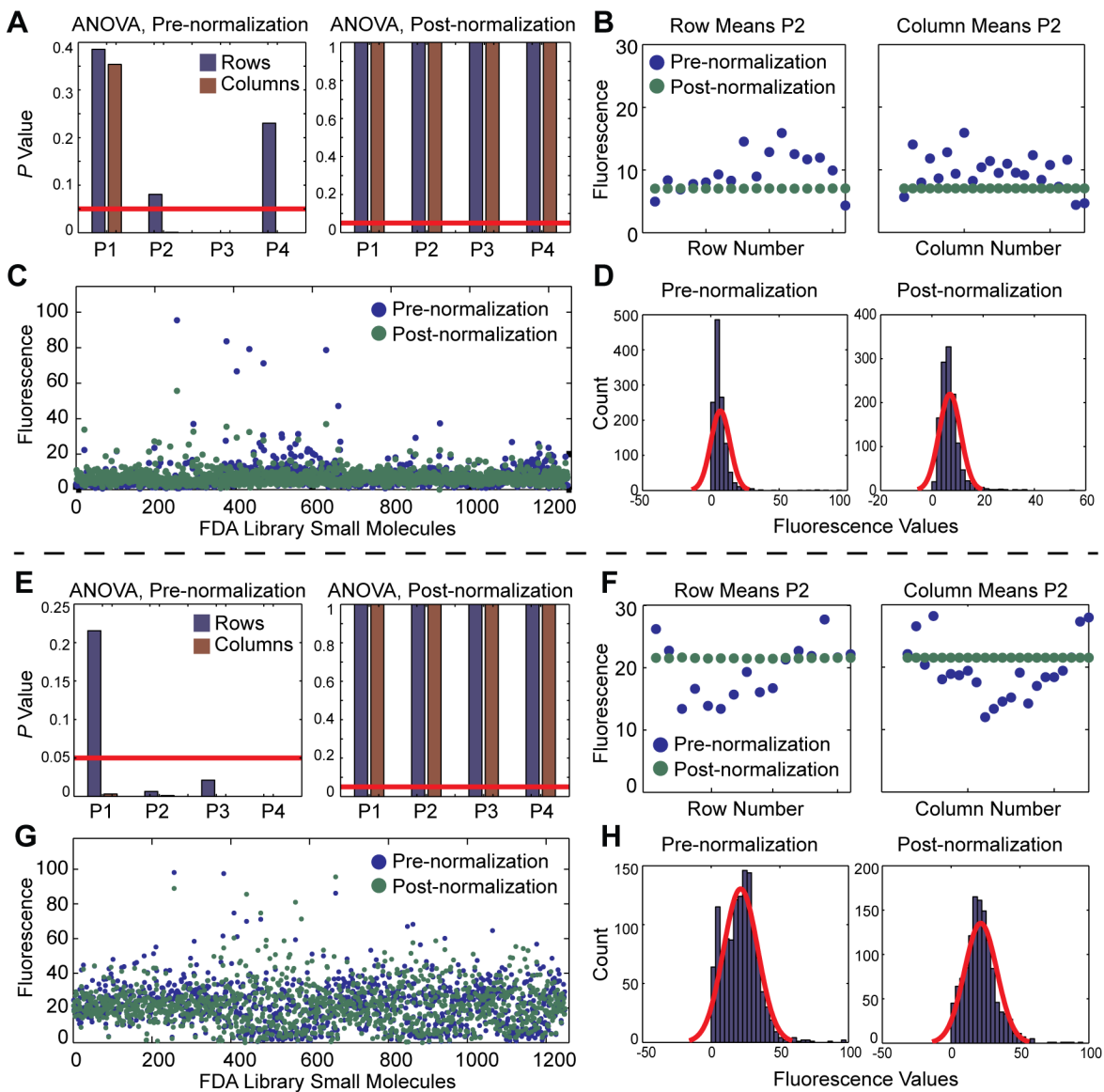


**Supplementary Figure 1. Unlabeled AO uptake and exon skipping activity in iDRM5017.** This experiment was performed in parallel to the FAM labeled AO experiment presented in Figure 1. On the seventh day of iDRM5017 fusion, h51AON targeting *DMD* exon 51 was transfected for 24 hours after which it was removed. After 48 hours each well was harvested for analysis, and split in half. **(A)** After gating on live cells, the percentage of FAM (or AO) positive cells was determined. **(B)** Mean fluorescence intensity of populations described in A. **(C)** The other half of each well was analyzed for *DMD* exon 51 skipping activity. Total RNA was isolated a nested RT-PCR performed between *DMD* exons 43-52. This experiment was repeated twice, with each condition being represented in triplicate. Error bars represent s.d. \* indicates  $P < 0.05$ .  $P$  values were determined using a two tailed student's t-test.



**Supplementary Figure 2. Normalization of high-throughput screening data. (A)**

Two-way ANOVA analysis of all Rows and Columns before and after fluorescence normalization for the ‘Compound only’ screen. P1-P4 indicates Plate 1, 2, 3, and 4. Blue represents fluorescence values before normalization and green represents fluorescence values after normalization. **(B)** Fluorescence values in the ‘Compound only’ screen for all Rows and Columns both before and after normalization for Plate 2 as an example. **(C)** Fluorescence values for all 1120 compounds both before and after normalization in the ‘Compound only’ screen. **(D)** Distribution of pre and post-normalized fluorescence values from the ‘Compound only’ screen. Red line indicates a normal distribution. **(E)** Panels E-H refer to the ‘Compound+AO’ analysis. Two-way ANOVA analysis of all Rows and Columns before and after fluorescence normalization in the ‘Compound+AO’ screen. P1-P4 indicates Plate 1, 2, 3, and 4. **(F)** Fluorescence values in the ‘Compound+AO’ screen for all Rows and Columns both before and after normalization for Plate 2 as an example. **(G)** Fluorescence values for all 1120 compounds both before and after normalization in the ‘Compound+AO’ screen. **(H)** Distribution of pre and post-normalized fluorescence values from the ‘Compound+AO’ screen. Red line indicates a normal distribution.



**Supplementary Figure 3. Distribution of Z scores is approximately normal. (A)**

‘Compound only’ Z score analysis and their distributions across all four plates. Red line indicates a normal distribution. **(B)** ‘Compound+AO’ Z score analysis and their distributions across all four plates. Red line indicates a normal distribution. **(C)** Ratio of +AO/C Z score analysis and their distributions across all four plates. Red line indicates a normal distribution.

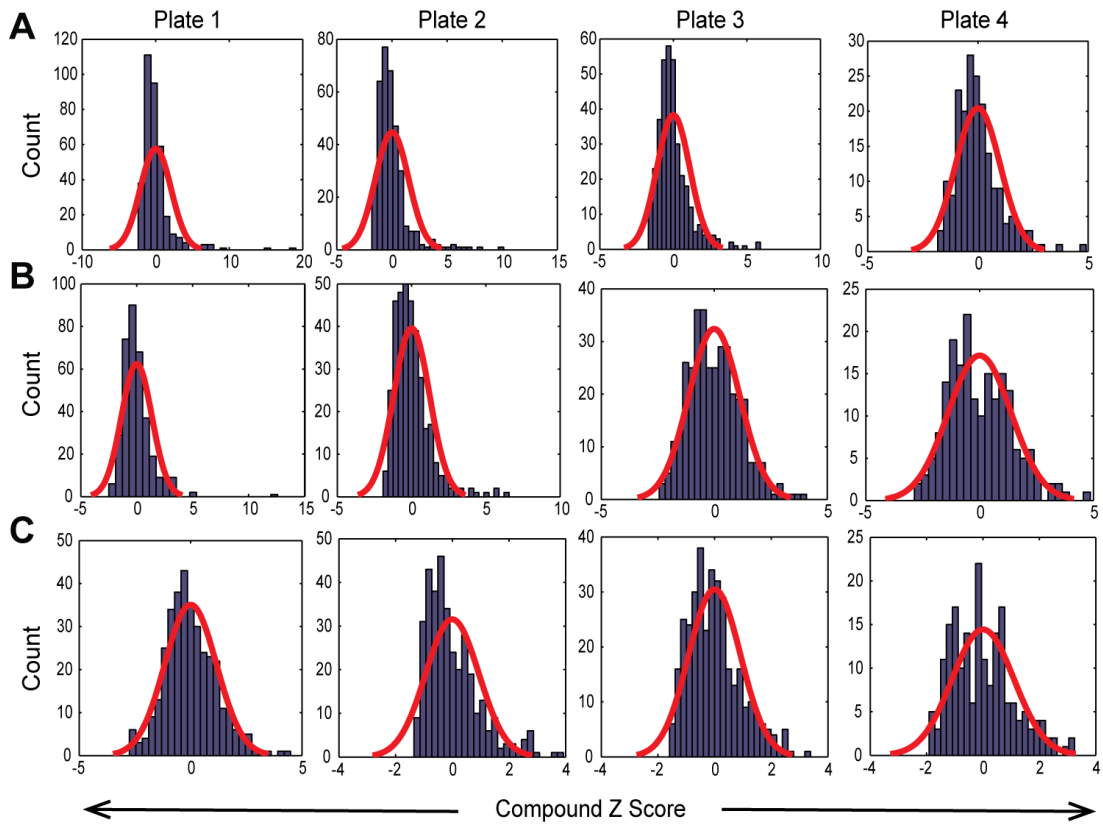


**Table 1. Z scores from the high-throughput screen for the ‘Compound only’ screen, ‘Compound+AO’ screen, and the analysis of the ratio of ‘Compound+AO’ compared to ‘Compound only’.**

Rank	Chemical name	Z Score	CLSZ_0.65	CLID_0.65
1	Quinacrine dihydrochloride dihydrate	19.06	1	518
2	Apomorphine hydrochloride hemihydrate	14.87	1	28
3	Menadione	10.12	1	300
4	Niclosamide	9.59	1	317
5	Methoxy-6-harmalan	7.98	3	248
6	Azaguanine-8	7.64	1	39
7	Pyrimethamine	7.44	1	400
8	Fendiline hydrochloride	7.39	2	449
9	Albendazole	7.00	2	540
10	Ellipticine	6.97	1	191
11	Fenbendazole	6.56	3	210
12	Clotrimazole	6.50	1	118
13	Tetrahydroalstonine	6.47	2	8
14	Ajmalicine hydrochloride	6.17	2	8
15	Mefloquine hydrochloride	5.92	1	429
16	S(+)-Terguride	5.92	3	418
17	Harmaline hydrochloride dihydrate	5.78	3	248
18	Reserpine	5.63	2	145
19	Parthenolide	5.51	1	717
20	Daunorubicin hydrochloride	5.14	2	185

Table 1. Compound only.

Rank	Chemical name	Z Score	CLSZ_0.65	CLID_0.65
1	Quinacrine dihydrochloride dihydrate	12.60	1	518
2	Tetrahydroalstonine	6.56	2	8
3	Rauwolfscine hydrochloride	5.62	4	394
4	Harmaline hydrochloride dihydrate	5.58	3	248
5	Ellipticine	5.17	1	191
6	Oxethazaine	4.98	1	620
7	Reserpine acid hydrochloride	4.86	1	918
8	Fenbendazole	4.83	3	210
9	Ajmalicine hydrochloride	4.20	2	8
10	S(+)-Terguride	4.08	3	418
11	Yohimbic acid monohydrate	3.95	4	394
12	Methoxy-6-harmalan	3.90	3	248
13	Zardaverine	3.69	1	285
14	Reserpine	3.66	2	145
15	Meropenem	3.56	1	1042
16	Clemizole hydrochloride	3.46	1	114
17	Mebendazole	3.43	3	210
18	Econazole nitrate	3.38	5	126
19	Niclosamide	3.37	1	317
20	Piperacetazine	3.35	6	222

Table 1. Compound + AO.

Rank	Chemical name	Z Score	CLSZ_0.65	CLID_0.65
1	Clemizole hydrochloride	4.49	1	114
2	Fluphenazine dihydrochloride	4.05	6	222
3	Probucol	3.92	1	343
4	N6-methyladenosine	3.70	3	309
5	Isoflupredone acetate	3.59	17	87
6	Succinylsulfathiazole	3.38	1	815
7	Ondansetron Hydrochloride	3.25	1	1059
8	Metoclopramide monohydrochloride	3.06	2	60
9	Propoxycaïne hydrochloride	3.05	1	1082
10	Sulfasalazine	3.04	1	693
11	Cefalonium	2.97	1	995
12	Methyldopa (L,-)	2.84	2	182
13	Hydroquinine hydrobromide hydrate	2.82	4	65
14	Tetramisole hydrochloride	2.77	2	289
15	Flumequine	2.75	1	481
16	Pipenzolate bromide	2.74	3	69
17	Procainamide hydrochloride	2.67	2	422
18	Tocopherol (R,S)	2.67	1	520
19	Phentolamine hydrochloride	2.63	1	330
20	Clemastine fumarate	2.60	1	545

Table 1. Ratio of +AO/C

**Supplementary Table 1. Compounds and their structurally similar ligands and protein targets identified from the Protein Data Bank.**

<b>Compound Only</b>	<b>PDB Target</b>
Menadione (Screen Hit)	
<a href="#">VK3 (PDB Ligand)</a>	human quinone reductase type 2
Pyrimethamine	
<a href="#">CP6</a>	plasmodium dihydrofolate reductase thymidylate synthase
Daunorubicin hydrochloride	
<a href="#">CMD</a>	DNA
<a href="#">DM1</a>	DNA
<a href="#">DM2</a>	DNA
<a href="#">DM3</a>	DNA
<a href="#">DM5</a>	DNA
<a href="#">DM6</a>	DNA
<a href="#">DM7</a>	DNA
<a href="#">DM8</a>	DNA
<a href="#">DM9</a>	DNA
<a href="#">DMM</a>	DNA
<a href="#">NOD</a>	DNA

---

<b>Compound + AO</b>	<b>PDB Target</b>
Zardaverine	
<a href="#">ZAR</a>	human phosphodiesterase 4d

---

<b>Ratio of +AO/C</b>	<b>PDB Target</b>
Fluphenazine dihydrochloride	
<a href="#">TFP</a>	human calmodulin human troponin c
N6-methyladenosine	
<a href="#">1DA</a>	pre-transition state enzyme mimic; mouse adenosine deaminase
<a href="#">3AD</a>	yeast poly(a) polymerase
<a href="#">9DI</a>	bovine purine nucleoside phosphorylase
<a href="#">AD3</a>	trypanosoma vivax inosine-adenosine-guanosine- preferring nucleoside hydrolase
<a href="#">ADY</a>	rattus S-adenosylhomocysteine hydrolase
<a href="#">FM1, FM2, FMB</a>	e coli purine nucleoside phosphorylase
Isoflupredone acetate	
<a href="#">AE2</a>	human dehydroepiandrosterone sulfotransferase
<a href="#">ANB</a>	enterobacter pentaerythritol tetranitrate reductase
<a href="#">AND</a>	brevibacterium cholesterol oxidase human dehydroepiandrosterone sulfotransferase
<a href="#">ANO</a>	mouse Igg1-kappa db3 fab
<a href="#">AOM</a>	human sex hormone-binding globulin
<a href="#">ASD</a>	Saccharopolyspora Cytochrome p450eryf
<a href="#">DEX</a>	human estrogenic 17beta-hydroxysteroid dehydrogenase
<a href="#">DHT</a>	human glucocorticoid receptor
<a href="#">PDN</a>	androgen receptor
<a href="#">STR</a>	corticosteroid-binding globulin
<a href="#">TES</a>	human mineralocorticoid receptor
<a href="#">ZK5</a>	androgen receptor human androgen receptor
Sulfasalazine	
<a href="#">SAS</a>	human glutathione s transferase
Methyldopa (L,-)	
<a href="#">DTY</a>	yeast tyrosine-regulated 3-deoxy-d-arabino-heptulosonate-7-phosphate synthase
<a href="#">IPO</a>	aeromonas proteolytica aminopeptidase
<a href="#">ISA</a>	pig calpain
<a href="#">IYR</a>	e coli tyrosyl-tryna synthetase
<a href="#">PHI</a>	streptomyces griseus aminopeptidase
<a href="#">TPQ</a>	pichia lysyl oxidase
Tocopherol (R,S)	
<a href="#">VIT</a>	daboia phospholipase a2 human alpha-tocopherol transfer protein

## References

1. Mendell JR, Shilling C, Leslie ND, Flanigan KM, al-Dahhak R, et al. (2012) Evidence-based path to newborn screening for Duchenne muscular dystrophy. *Ann Neurol* 71: 304-313.
2. Hoffman EP, Brown RH, Jr., Kunkel LM (1987) Dystrophin: the protein product of the Duchenne muscular dystrophy locus. *Cell* 51: 919-928.
3. Bonilla E, Samitt CE, Miranda AF, Hays AP, Salviati G, et al. (1988) Duchenne muscular dystrophy: deficiency of dystrophin at the muscle cell surface. *Cell* 54: 447-452.
4. Petrof BJ, Shrager JB, Stedman HH, Kelly AM, Sweeney HL (1993) Dystrophin protects the sarcolemma from stresses developed during muscle contraction. *Proc Natl Acad Sci U S A* 90: 3710-3714.
5. Monaco AP, Bertelson CJ, Middlesworth W, Colletti CA, Aldridge J, et al. (1985) Detection of deletions spanning the Duchenne muscular dystrophy locus using a tightly linked DNA segment. *Nature* 316: 842-845.
6. Charge SB, Rudnicki MA (2004) Cellular and molecular regulation of muscle regeneration. *Physiol Rev* 84: 209-238.
7. Jejurikar SS, Kuzon WM, Jr. (2003) Satellite cell depletion in degenerative skeletal muscle. *Apoptosis* 8: 573-578.
8. Vetrone SA, Montecino-Rodriguez E, Kudryashova E, Kramerova I, Hoffman EP, et al. (2009) Osteopontin promotes fibrosis in dystrophic mouse muscle by modulating immune cell subsets and intramuscular TGF-beta. *J Clin Invest* 119: 1583-1594.
9. Spencer MJ, Tidball JG (2001) Do immune cells promote the pathology of dystrophin-deficient myopathies? *Neuromuscul Disord* 11: 556-564.
10. Leroy-Willig A, Willig TN, Henry-Feugeas MC, Frouin V, Marinier E, et al. (1997) Body composition determined with MR in patients with Duchenne muscular dystrophy, spinal muscular atrophy, and normal subjects. *Magn Reson Imaging* 15: 737-744.
11. Klingler W, Jurkat-Rott K, Lehmann-Horn F, Schleip R (2012) The role of fibrosis in Duchenne muscular dystrophy. *Acta Myol* 31: 184-195.
12. Kohler M, Clarenbach CF, Bahler C, Brack T, Russi EW, et al. (2009) Disability and survival in Duchenne muscular dystrophy. *J Neurol Neurosurg Psychiatry* 80: 320-325.
13. Ishikawa Y, Miura T, Ishikawa Y, Aoyagi T, Ogata H, et al. (2011) Duchenne muscular dystrophy: survival by cardio-respiratory interventions. *Neuromuscul Disord* 21: 47-51.
14. Biggar WD, Harris VA, Eliasoph L, Alman B (2006) Long-term benefits of deflazacort treatment for boys with Duchenne muscular dystrophy in their second decade. *Neuromuscul Disord* 16: 249-255.

15. Fenichel GM, Florence JM, Pestronk A, Mendell JR, Moxley RT, 3rd, et al. (1991) Long-term benefit from prednisone therapy in Duchenne muscular dystrophy. *Neurology* 41: 1874-1877.
16. Tinsley J, Deconinck N, Fisher R, Kahn D, Phelps S, et al. (1998) Expression of full-length utrophin prevents muscular dystrophy in mdx mice. *Nat Med* 4: 1441-1444.
17. Bowles DE, McPhee SW, Li C, Gray SJ, Samulski JJ, et al. (2012) Phase 1 gene therapy for Duchenne muscular dystrophy using a translational optimized AAV vector. *Mol Ther* 20: 443-455.
18. Price FD, Kuroda K, Rudnicki MA (2007) Stem cell based therapies to treat muscular dystrophy. *Biochim Biophys Acta* 1772: 272-283.
19. Welch EM, Barton ER, Zhuo J, Tomizawa Y, Friesen WJ, et al. (2007) PTC124 targets genetic disorders caused by nonsense mutations. *Nature* 447: 87-91.
20. van Deutekom JC, Janson AA, Ginjaar IB, Frankhuizen WS, Aartsma-Rus A, et al. (2007) Local dystrophin restoration with antisense oligonucleotide PRO051. *N Engl J Med* 357: 2677-2686.
21. Goemans NM, Tulinius M, van den Akker JT, Burm BE, Ekhardt PF, et al. (2011) Systemic administration of PRO051 in Duchenne's muscular dystrophy. *N Engl J Med* 364: 1513-1522.
22. Kinali M, Arechavala-Gomez V, Feng L, Cirak S, Hunt D, et al. (2009) Local restoration of dystrophin expression with the morpholino oligomer AVI-4658 in Duchenne muscular dystrophy: a single-blind, placebo-controlled, dose-escalation, proof-of-concept study. *Lancet Neurol* 8: 918-928.
23. Cirak S, Arechavala-Gomez V, Guglieri M, Feng L, Torelli S, et al. (2011) Exon skipping and dystrophin restoration in patients with Duchenne muscular dystrophy after systemic phosphorodiamidate morpholino oligomer treatment: an open-label, phase 2, dose-escalation study. *Lancet* 378: 595-605.
24. Aartsma-Rus A, Fokkema I, Verschuuren J, Ginjaar I, van Deutekom J, et al. (2009) Theoretic applicability of antisense-mediated exon skipping for Duchenne muscular dystrophy mutations. *Hum Mutat* 30: 293-299.
25. Mendell JR (2013) Results at 74 Weeks of a Phase IIb Extension Study of the Exon-Skipping Drug Eteplirsen in Patients with Duchenne Muscular Dystrophy (DMD). Muscular Dystrophy Association Scientific Conference. Washington DC.
26. Anthony K, Cirak S, Torelli S, Tasca G, Feng L, et al. (2011) Dystrophin quantification and clinical correlations in Becker muscular dystrophy: implications for clinical trials. *Brain* 134: 3547-3559.
27. Neri M, Torelli S, Brown S, Ugo I, Sabatelli P, et al. (2007) Dystrophin levels as low as 30% are sufficient to avoid muscular dystrophy in the human. *Neuromuscul Disord* 17: 913-918.

28. Phelps SF, Hauser MA, Cole NM, Rafael JA, Hinkle RT, et al. (1995) Expression of full-length and truncated dystrophin mini-genes in transgenic mdx mice. *Hum Mol Genet* 4: 1251-1258.
29. Alter J, Lou F, Rabinowitz A, Yin H, Rosenfeld J, et al. (2006) Systemic delivery of morpholino oligonucleotide restores dystrophin expression bodywide and improves dystrophic pathology. *Nat Med* 12: 175-177.
30. Moulton HM, Moulton JD (2010) Morpholinos and their peptide conjugates: therapeutic promise and challenge for Duchenne muscular dystrophy. *Biochim Biophys Acta* 1798: 2296-2303.
31. O'Leary DA, Sharif O, Anderson P, Tu B, Welch G, et al. (2009) Identification of small molecule and genetic modulators of AON-induced dystrophin exon skipping by high-throughput screening. *PLoS One* 4: e8348.
32. Hu Y, Wu B, Zillmer A, Lu P, Benrashid E, et al. (2010) Guanine analogues enhance antisense oligonucleotide-induced exon skipping in dystrophin gene in vitro and in vivo. *Mol Ther* 18: 812-818.
33. Kendall GC, Mokhonova EI, Moran M, Sejbuk NE, Wang DW, et al. (2012) Dantrolene enhances antisense-mediated exon skipping in human and mouse models of Duchenne muscular dystrophy. *Sci Transl Med* 4: 164ra160.
34. Brown RD, Martin YC (1995) Use of Structure-Activity Data to Compare Structure-Based Clustering Methods and Descriptors for Use in Compound Selection. *J Chem Inf Comput Sci* 36: 572-584.
35. Noble ME, Endicott JA, Johnson LN (2004) Protein kinase inhibitors: insights into drug design from structure. *Science* 303: 1800-1805.
36. Johnson MA, Maggioria GM (1990) Concepts and Applications of Molecular Similarity. New York: John Wiley & Sons. 393 p.
37. Kubinyi H (1998) Similarity and Dissimilarity: A Medicinal Chemist's View. *Perspectives in Drug Discovery and Design*: 225-252.
38. Cook WJ, Walter LJ, Walter MR (1994) Drug binding by calmodulin: crystal structure of a calmodulin-trifluoperazine complex. *Biochemistry* 33: 15259-15265.
39. Vandonselaar M, Hickie RA, Quail JW, Delbaere LT (1994) Trifluoperazine-induced conformational change in Ca(2+)-calmodulin. *Nat Struct Biol* 1: 795-801.
40. Cao Y, Charisi A, Cheng LC, Jiang T, Girke T (2008) ChemmineR: a compound mining framework for R. *Bioinformatics* 24: 1733-1734.
41. Moors SL, Vos AM, Cummings MD, Van Vlijmen H, Ceulemans A (2011) Structure-based site of metabolism prediction for cytochrome P450 2D6. *J Med Chem* 54: 6098-6105.
42. Dragiev P, Nadon R, Makarenkov V (2011) Systematic error detection in experimental high-throughput screening. *BMC Bioinformatics* 12: 25.

43. Malo N, Hanley JA, Carlile G, Liu J, Pelletier J, et al. (2010) Experimental design and statistical methods for improved hit detection in high-throughput screening. *J Biomol Screen* 15: 990-1000.
44. Malo N, Hanley JA, Cerquozzi S, Pelletier J, Nadon R (2006) Statistical practice in high-throughput screening data analysis. *Nat Biotechnol* 24: 167-175.
45. Johnson M, Maggioria G (1990) *Concepts and Applications of Molecular Similarity*. New York: John Wiley & Sons.
46. Morales A (2000) Yohimbine in erectile dysfunction: the facts. *Int J Impot Res* 12 Suppl 1: S70-74.
47. Al-Shanti N, Stewart CE (2009) Ca<sup>2+</sup>/calmodulin-dependent transcriptional pathways: potential mediators of skeletal muscle growth and development. *Biol Rev Camb Philos Soc* 84: 637-652.
48. Lu QL, Wu B (2012) Systemic delivery of antisense oligomer in animal models and its implications for treating DMD. *Methods Mol Biol* 867: 393-405.
49. Ming X, Carver K, Fisher M, Noel R, Cintrat JC, et al. (2013) The small molecule Retro-1 enhances the pharmacological actions of antisense and splice switching oligonucleotides. *Nucleic Acids Res* 41: 3673-3687.
50. Chin D, Means AR (2000) Calmodulin: a prototypical calcium sensor. *Trends Cell Biol* 10: 322-328.
51. Luby-Phelps K, Hori M, Phelps JM, Won D (1995) Ca(2+)-regulated dynamic compartmentalization of calmodulin in living smooth muscle cells. *J Biol Chem* 270: 21532-21538.
52. Xie J, Black DL (2001) A CaMK IV responsive RNA element mediates depolarization-induced alternative splicing of ion channels. *Nature* 410: 936-939.
53. Bellinger AM, Reiken S, Carlson C, Mongillo M, Liu X, et al. (2009) Hypernitrosylated ryanodine receptor calcium release channels are leaky in dystrophic muscle. *Nat Med* 15: 325-330.
54. Kobayashi S, Bannister ML, Gangopadhyay JP, Hamada T, Parness J, et al. (2005) Dantrolene stabilizes domain interactions within the ryanodine receptor. *J Biol Chem* 280: 6580-6587.
55. Rousseau E, Smith JS, Meissner G (1987) Ryanodine modifies conductance and gating behavior of single Ca<sup>2+</sup> release channel. *Am J Physiol* 253: C364-368.
56. Qin J, Zima AV, Porta M, Blatter LA, Fill M (2009) Trifluoperazine: a ryanodine receptor agonist. *Pflugers Arch* 458: 643-651.
57. Andersson DC, Marks AR (2010) Fixing ryanodine receptor Ca leak - a novel therapeutic strategy for contractile failure in heart and skeletal muscle. *Drug Discov Today Dis Mech* 7: e151-e157.

58. Fill M, Copello JA (2002) Ryanodine receptor calcium release channels. *Physiol Rev* 82: 893-922.

## CHAPTER FIVE

### Conclusions

The *DMD* gene was discovered as the underlying genetic cause for Duchenne muscular dystrophy over 25 years ago, yet there are still no FDA approved pharmacological therapies addressing the underlying genetic defect [1-3]. Antisense oligonucleotide (AO) mediated exon skipping represents the most progressed therapy for DMD and is currently in Phase IIb and Phase III clinical trials. The FDA approval of exon skipping AOs would be a milestone in realizing both DMD therapies and personalized genetic therapies. Even so, there are still inherent inefficiencies in AO based exon skipping across patients, across mutations, and across different muscle types that need to be addressed [4-6].

The primary goal of the research presented here is to provide a well annotated DMD cell bank as a valuable resource for muscular dystrophy study, and second, to identify small molecules, and their molecular targets, that increase antisense exon skipping activity. We performed two independent high-throughput screens and found active drugs with shared downstream targets in conserved molecular pathways. One of these drugs, dantrolene, showed efficacy not only in mouse and human cell culture, but also when administered *in vivo* in *mdx* mice in an AO combinatorial therapy. This administration increased *Dmd* exon 23 skipping and dystrophin protein rescue 2-3 fold, which was sufficient to facilitate functional improvement in *mdx* mice after a month long treatment schedule [7]. Current work is focused on determining the optimal dosing combination of dantrolene and AO to induce exon skipping and rescue dystrophin protein in *mdx* mice. Long-term experiments with chronic administration of AO and dantrolene are planned to determine if this produces a sustained effect and if there is further amelioration or stabilization of the disease.

To identify potential molecular targets small molecules were tested in a patient specific mutational context. In the cell bank described in Chapter 2, there are 49 and counting DMD patient and control fibroblasts available, of which subsets with diverse DMD mutations have been reprogrammed into iDRMs. The reprogramming process is driven by the inducible

overexpression of MyoD and has been optimized so that iDRMs temporally express muscle specific genes and proteins during the fusion process making them viable for use in muscle based experiments. iDRM5017 contains a *DMD* exon 45-50 deletion that was tested in combination with AO and small molecules to identify those that potentiated exon 51 skipping to restore the mRNA reading frame. Dantrolene and additional RyR1 antagonists, Ryanodine and S107, were evaluated in iDRM5017 and all were found to significantly increase exon 51 skipping. These drugs directly inhibit RyR1 via distinct binding mechanisms; dantrolene by stabilization of domain interactions, ryanodine by binding the RyR pore and regulating Ca<sup>2+</sup> ion release, and S107 by allosteric modulation of accessory proteins [7-12]. Based on these results it was postulated that inhibition of the RyR1 and the likely decrease of intracellular calcium levels represented a key component to the exon skipping effect. An independent high-throughput screen identified a group of 2-D structurally similar small molecules that increased *DMD* exon 50 skipping and in iDRM5017 *DMD* exon 51 skipping. In these models, the most active compounds shared structural similarity and inhibition of a common target, calmodulin (CaM), which is a calcium binding protein that acts as an intermediate messenger and regulates downstream signal transduction pathways [13,14].

*Calcium as a regulator of alternative splicing: identifying signaling pathways that enhance antisense based DMD exon skipping activity*

Binding of spliceosomal sub-units to pre-mRNA sequences dictates the joining of specific splice sites and their adjacent exons. This process is dynamic and hierarchically ordered and binding of proteins to adjoining portions of the pre-mRNA can enhance inclusion or exclusion of exons by the spliceosome [15]. AOs used in our studies target a variety of splicing sequences including splice acceptor sites, splice donor sites, or exonic splicing enhancers (ESE) to dictate the exclusion of single exons from the mature mRNA transcript. We identified small molecules that enhanced exon skipping of AOs that were either 2'OMe or PMO chemistries, targeting

mouse or human ESE, splice acceptor, or splice donor sites indicating this activity is likely not sequence or chemistry dependent. Active drugs including dantrolene, ryanodine, S107, fluphenazine and trifluoperazine all bind and inhibit either calcium channels (RyR1) or calcium regulatory proteins (CaM) suggesting the importance of Ca<sup>2+</sup> regulation and its impact on Ca<sup>2+</sup>-binding proteins in directing exon skipping activity [8-12,16,17].

Calcium is a well-documented regulator and activator of gene expression [18]. Downstream Ca<sup>2+</sup>-CaM dependent events include the activation of the Ca<sup>2+</sup>-CaM dependent protein kinases, which activate transcription factors including CREB, CREM $\tau$ , ATF-1, SRF, ETS-1 [19-27]. Ca<sup>2+</sup>-CaM and Ca<sup>2+</sup>-CaM dependent protein kinases have been implicated in activating and regulating transcription factors through nuclear localization [27]. Ca<sup>2+</sup>-CaM and CAMKIV has also been directly linked to the regulation of alternative splicing. For example, in neuronal systems CAMKIV specifically modulates STREX exon splicing through the binding of a specific CaRRE sequence, functionally affecting the sensitivity of a Ca<sup>2+</sup>-activated potassium channel. Inclusion of the STREX exon in the mRNA transcript confers higher Ca<sup>2+</sup> sensitivity, providing a precedent for linking calcium regulation and a Ca<sup>2+</sup>-CaM dependent alternative splicing event [28].

Identified active drugs may delineate the connection between calcium dependent signal transduction and how this translates into exon skipping. Our previous work found that small molecule inhibition of RyR1 mediated calcium release is a potential molecular target for enacting this exon skipping effect. RyR1 is a calcium channel located on the sarcoplasmic reticulum (SR) that is responsible for releasing calcium into the cytoplasm during muscle contraction. Structurally distinct small molecules inhibit RyR1 through unique mechanisms, all ultimately functioning to inhibit the open state of the channel and prevent calcium flux from the sarcoplasmic reticulum. It remains unclear how RyR1 inhibition and a decrease in cytoplasmic calcium concentrations translates into exon skipping activity. Likely, RyR1 inhibition decreases

intracellular calcium levels resulting in downstream signal transduction events, and subsequent pre-mRNA exon skipping in the nucleus.

A commonality between these two screens is the potential targeting and inhibition of intracellular  $\text{Ca}^{2+}$  messenger calmodulin (CaM), which may represent a critical downstream signaling nexus for the observed exon skipping activity (Fig. 1). CaM is the predominant cellular calcium sensor and is directly activated or inactivated by the concentration and spatiotemporal flux of calcium [29]. At resting state cytoplasmic  $\text{Ca}^{2+}$  concentrations are  $10^3$  lower than  $\text{Ca}^{2+}$  concentrations in the SR. In response to a rise in cytoplasmic  $\text{Ca}^{2+}$ , activated  $\text{Ca}^{2+}$ -CaM, or its downstream targets, will redistribute from the cytosol to the nucleus and either directly or indirectly activate skeletal muscle transcriptional targets such as MEF2, CREB, SRF, and PGC- $1\alpha$  [27,30]. Structurally similar compounds, Fluphenazine and Trifluoperazine (TFP), were identified to have highly efficient exon skipping activity and also share known molecular targets including troponin C and calmodulin (CaM). Crystal structures of CaM complexed with TFP indicate that TFP binds  $\text{Ca}^{2+}$ -CaM, or activated CaM, and that this binding induces 3-D conformational changes from an active 'dumbbell' form to an inactive 'globular' form. In the inactive 'globular' form the CaM hydrophobic pockets are unavailable for binding by target proteins [16,17].

Paradoxically, TFP has also been described in the activation of RyR2 mediated  $\text{Ca}^{2+}$  release (RyR receptor in cardiac muscle), a biological activity that is independent of its reported calmodulin inhibition [31]. This supports the hypotheses that either 1) RyR1 antagonists are acting in the same pathway, but upstream of TFP/Fluphenazine CaM inhibition or 2) RyR1 antagonists and TFP/Fluphenazine are acting on completely distinct targets. Although TFP can act as a RyR agonist, there is still an observed increase in exon skipping activity, suggesting that CaM inhibition may be the relevant downstream effect of RyR1 inhibition. Dantrolene, Ryanodine and S107, function to decrease RyR1 mediated  $\text{Ca}^{2+}$  release into the cytoplasm,

likely preventing efficient Ca<sup>2+</sup> binding and activation of CaM [13,14]. However, the events downstream of CaM inhibition and its link to alternative splicing regulation remain to be understood.

Questions remain as to why exon skipping is only observed in the presence of AO, and not with drug alone. This effect suggests a level of specificity for enhancement of AO activity and that there are likely limited off-target alternative splicing effects. A complete understanding of this AO specificity requires mechanistic insights of the relevant small molecule modulated signaling pathways. This is currently being evaluated by RNA-seq for the combination of dantrolene and an AO targeting *DMD* exon 51 in iDRM5017, and will give insight into how dantrolene is potentiating AO activity and identify potential off-target effects.

#### *Therapeutic implications of improving exon skipping efficiencies*

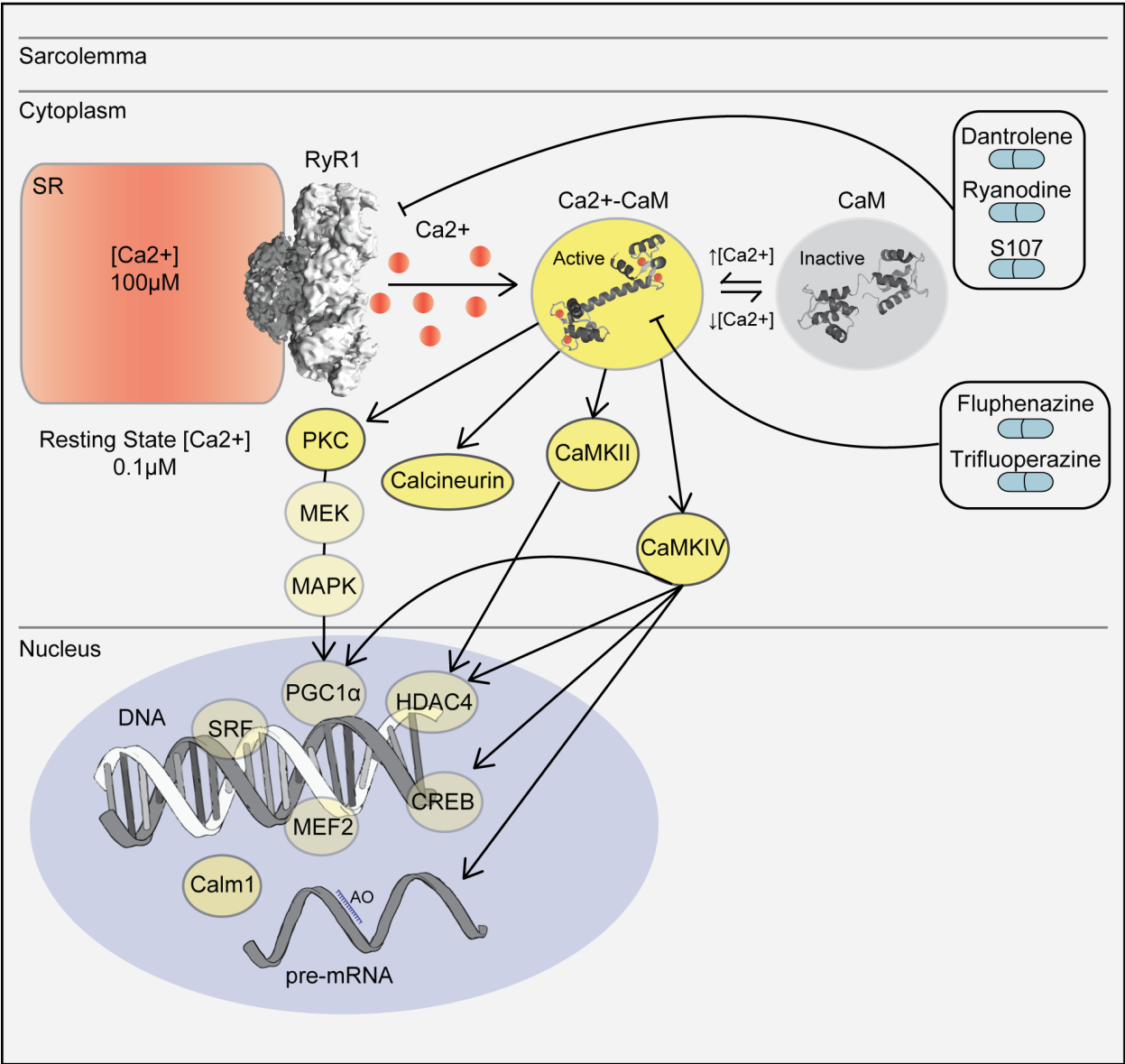
Exon skipping is sub-optimal in clinical trials indicating that an increase in exon skipping efficiency and ultimately the amount of dystrophin protein will improve the therapeutic benefit. For instance, with current dosing strategies 2'OMe and PMO AOs are likely not providing functional protection in cardiac muscle [4,32]. AO therapies would improve by enhancing target delivery, which has been the strategy for cell penetrating peptide tagged AOs [33]. In *mdx* mice, peptide tagged AOs enhanced skeletal and cardiac uptake and depending on the muscle facilitated dystrophin protein rescue from 10% - 100% of normal levels [34]. In humans there are significant off-target effects making them unlikely to be further pursued in clinic without addressing toxicity issues [33].

The strategy described here was to identify potential molecular targets that enhance the activity of AO based exon skipping strategies. These molecular targets could either benefit 1) sub-optimal levels of antisense-oligonucleotide or 2) further potentiate maximum antisense oligonucleotide doses. Both of these applications are plausible in a clinical setting, as uptake

between various muscles of PMO differs greatly [4,33]. For instance, the optimal systemic AO dose for the triceps may be sub-optimal in the quadriceps. Although the rationale may differ both muscles would benefit from a combination therapy. Indeed, after systemic administration of 2'OMe AO in *mdx* the measured skeletal muscle and tissues concentrations differ greatly [32]. Current experiments are evaluating the optimal *in vivo* dosing strategy for the combination of dantrolene and AO delivery in the *mdx* mouse. In addition, iDRMs with a variety of exon 51 skippable mutations are being evaluated for dantrolene synergy with AO. In the future it will be interesting to determine if dantrolene potentiates AOs targeting different exons, or even a cocktail of AOs designed for the multi-exon skip between *DMD* exons 45-55 that would treat 63% of patients [35]. Evaluating a range of mutations and exons will lend a better understanding to the mechanisms whereby perturbations in calcium signaling pathways regulate antisense exon skipping strategies.

**Figure 1. A model for Ca<sup>2+</sup> regulation of exon skipping activity.**

Intracellular calcium levels are critical regulators for the activation or inactivation of Ca<sup>2+</sup> dependent proteins. Resting state Ca<sup>2+</sup> levels are 10<sup>3</sup> times higher in the sarcoplasmic reticulum than in the cytoplasm. Following an action potential from a motor neuron signaling the muscle to contract, the Ryanodine Receptor (RyR1) opens allowing Ca<sup>2+</sup> ions into the cytoplasm. This increase in intracellular Ca<sup>2+</sup> concentration allows calmodulin (CaM) to bind 4 Ca<sup>2+</sup> ions, reorganizing its 3-D structure and exposing its hydrophobic pockets, which are critical for binding downstream target proteins. Also depicted is the structure of inactive CaM that is assumed with lower intracellular Ca<sup>2+</sup> levels and is not amenable for target interactions. Ca<sup>2+</sup> bound CaM is then free to activate downstream targets, such as the Ca<sup>2+</sup>/calmodulin-dependent kinases (CaMK). CaMKIV activates transcriptional factors such as CREB, which increases PGC-1 $\alpha$  transcription in both a CREB and MEF2 dependent manner. In addition, CAMKIV phosphorylates HDAC4, re-localizing it from the nucleus to the cytoplasm. CAMKII functions to phosphorylate HDACS that dissociate from MEF2 and SRF allowing them to become functionally active. In addition, an increase in intracellular Ca<sup>2+</sup> concentrations activates protein kinase C (PKC)-MEK-MAPK through Ca<sup>2+</sup>-calmodulin dependent pathways, which upregulates the transcription of PGC-1 $\alpha$ . Drugs that increase *DMD* exon skipping activity act in two critical steps of this pathway. Dantrolene, ryanodine and S107 inhibit the RyR, decrease intracellular Ca<sup>2+</sup> levels, and by extension likely inhibit the activation of CaM. In addition, specific CaM inhibitors, Fluphenazine and Trifluoperazine also have potent exon skipping activity, suggesting these drugs are acting in a potentially shared downstream pathway to produce the observed exon skipping effect.



## References

1. Monaco AP, Bertelson CJ, Middlesworth W, Colletti CA, Aldridge J, et al. (1985) Detection of deletions spanning the Duchenne muscular dystrophy locus using a tightly linked DNA segment. *Nature* 316: 842-845.
2. Bushby K, Finkel R, Birnkrant DJ, Case LE, Clemens PR, et al. (2010) Diagnosis and management of Duchenne muscular dystrophy, part 2: implementation of multidisciplinary care. *Lancet Neurol* 9: 177-189.
3. Bushby K, Finkel R, Birnkrant DJ, Case LE, Clemens PR, et al. (2010) Diagnosis and management of Duchenne muscular dystrophy, part 1: diagnosis, and pharmacological and psychosocial management. *Lancet Neurol* 9: 77-93.
4. Alter J, Lou F, Rabinowitz A, Yin H, Rosenfeld J, et al. (2006) Systemic delivery of morpholino oligonucleotide restores dystrophin expression bodywide and improves dystrophic pathology. *Nat Med* 12: 175-177.
5. Cirak S, Arechavala-Gomez V, Guglieri M, Feng L, Torelli S, et al. (2011) Exon skipping and dystrophin restoration in patients with Duchenne muscular dystrophy after systemic phosphorodiamidate morpholino oligomer treatment: an open-label, phase 2, dose-escalation study. *Lancet* 378: 595-605.
6. Goemans NM, Tulinius M, van den Akker JT, Burm BE, Ekhart PF, et al. (2011) Systemic administration of PRO051 in Duchenne's muscular dystrophy. *N Engl J Med* 364: 1513-1522.
7. Kendall GC, Mokhonova EI, Moran M, Sejbuk NE, Wang DW, et al. (2012) Dantrolene enhances antisense-mediated exon skipping in human and mouse models of Duchenne muscular dystrophy. *Sci Transl Med* 4: 164ra160.
8. Andersson DC, Marks AR (2010) Fixing ryanodine receptor Ca leak - a novel therapeutic strategy for contractile failure in heart and skeletal muscle. *Drug Discov Today Dis Mech* 7: e151-e157.
9. Bellinger AM, Reiken S, Carlson C, Mongillo M, Liu X, et al. (2009) Hypernitrosylated ryanodine receptor calcium release channels are leaky in dystrophic muscle. *Nat Med* 15: 325-330.
10. Fill M, Copello JA (2002) Ryanodine receptor calcium release channels. *Physiol Rev* 82: 893-922.
11. Kobayashi S, Bannister ML, Gangopadhyay JP, Hamada T, Parness J, et al. (2005) Dantrolene stabilizes domain interactions within the ryanodine receptor. *J Biol Chem* 280: 6580-6587.
12. Rousseau E, Smith JS, Meissner G (1987) Ryanodine modifies conductance and gating behavior of single Ca<sup>2+</sup> release channel. *Am J Physiol* 253: C364-368.
13. Alonso MT, Garcia-Sancho J (2011) Nuclear Ca(2+) signalling. *Cell Calcium* 49: 280-289.

14. Eldik LJV, Watterson DM (1998) *Calmodulin and Signal Transduction*. New York, New York: Academic Press. 482 p.
15. Black DL (2003) Mechanisms of alternative pre-messenger RNA splicing. *Annu Rev Biochem* 72: 291-336.
16. Cook WJ, Walter LJ, Walter MR (1994) Drug binding by calmodulin: crystal structure of a calmodulin-trifluoperazine complex. *Biochemistry* 33: 15259-15265.
17. Vandonselaar M, Hickie RA, Quail JW, Delbaere LT (1994) Trifluoperazine-induced conformational change in Ca(2+)-calmodulin. *Nat Struct Biol* 1: 795-801.
18. Berridge MJ, Bootman MD, Roderick HL (2003) Calcium signalling: dynamics, homeostasis and remodelling. *Nat Rev Mol Cell Biol* 4: 517-529.
19. Enslin H, Sun P, Brickey D, Soderling SH, Klamo E, et al. (1994) Characterization of Ca<sup>2+</sup>/calmodulin-dependent protein kinase IV. Role in transcriptional regulation. *J Biol Chem* 269: 15520-15527.
20. Fisher CL, Ghysdael J, Cambier JC (1991) Ligation of membrane Ig leads to calcium-mediated phosphorylation of the proto-oncogene product, Ets-1. *J Immunol* 146: 1743-1749.
21. Matthews RP, Guthrie CR, Wailes LM, Zhao X, Means AR, et al. (1994) Calcium/calmodulin-dependent protein kinase types II and IV differentially regulate CREB-dependent gene expression. *Mol Cell Biol* 14: 6107-6116.
22. Miranti CK, Ginty DD, Huang G, Chatila T, Greenberg ME (1995) Calcium activates serum response factor-dependent transcription by a Ras- and Elk-1-independent mechanism that involves a Ca<sup>2+</sup>/calmodulin-dependent kinase. *Mol Cell Biol* 15: 3672-3684.
23. Pognonec P, Boulukos KE, Gesquiere JC, Stehelin D, Ghysdael J (1988) Mitogenic stimulation of thymocytes results in the calcium-dependent phosphorylation of c-ets-1 proteins. *EMBO J* 7: 977-983.
24. Sheng M, Thompson MA, Greenberg ME (1991) CREB: a Ca(2+)-regulated transcription factor phosphorylated by calmodulin-dependent kinases. *Science* 252: 1427-1430.
25. Sun P, Lou L, Maurer RA (1996) Regulation of activating transcription factor-1 and the cAMP response element-binding protein by Ca<sup>2+</sup>/calmodulin-dependent protein kinases type I, II, and IV. *J Biol Chem* 271: 3066-3073.
26. Sun Z, Sassone-Corsi P, Means AR (1995) Calspermin gene transcription is regulated by two cyclic AMP response elements contained in an alternative promoter in the calmodulin kinase IV gene. *Mol Cell Biol* 15: 561-571.
27. Al-Shanti N, Stewart CE (2009) Ca<sup>2+</sup>/calmodulin-dependent transcriptional pathways: potential mediators of skeletal muscle growth and development. *Biol Rev Camb Philos Soc* 84: 637-652.

28. Xie J, Black DL (2001) A CaMK IV responsive RNA element mediates depolarization-induced alternative splicing of ion channels. *Nature* 410: 936-939.
29. Chin D, Means AR (2000) Calmodulin: a prototypical calcium sensor. *Trends Cell Biol* 10: 322-328.
30. Luby-Phelps K, Hori M, Phelps JM, Won D (1995) Ca(2+)-regulated dynamic compartmentalization of calmodulin in living smooth muscle cells. *J Biol Chem* 270: 21532-21538.
31. Qin J, Zima AV, Porta M, Blatter LA, Fill M (2009) Trifluoperazine: a ryanodine receptor agonist. *Pflugers Arch* 458: 643-651.
32. Heemskerk H, de Winter C, van Kuik P, Heuvelmans N, Sabatelli P, et al. (2010) Preclinical PK and PD studies on 2'-O-methyl-phosphorothioate RNA antisense oligonucleotides in the mdx mouse model. *Mol Ther* 18: 1210-1217.
33. Moulton HM, Moulton JD (2010) Morpholinos and their peptide conjugates: therapeutic promise and challenge for Duchenne muscular dystrophy. *Biochim Biophys Acta* 1798: 2296-2303.
34. Yin H, Moulton HM, Seow Y, Boyd C, Boutilier J, et al. (2008) Cell-penetrating peptide-conjugated antisense oligonucleotides restore systemic muscle and cardiac dystrophin expression and function. *Hum Mol Genet* 17: 3909-3918.
35. Beroud C, Tuffery-Giraud S, Matsuo M, Hamroun D, Humbertclaude V, et al. (2007) Multiexon skipping leading to an artificial DMD protein lacking amino acids from exons 45 through 55 could rescue up to 63% of patients with Duchenne muscular dystrophy. *Hum Mutat* 28: 196-202.